

**Universität für Bodenkultur Wien**



University of Natural Resources and Life Sciences, Vienna

**Functional characterization of affinity purified anti-  
ADAMTS13 IgG autoantibodies from patients with  
acquired thrombotic thrombocytopenic purpura and  
a healthy donor pool**

Dissertation

Rana Grillberger

Student Number: H0641036

Supervisor

Ao.Univ.Prof. Dipl.-Ing. Dr.nat.techn Florian Rümer

March 2014



*In the field of observation, chance favors only the prepared mind – Louis Pasteur*



## ACKNOWLEDGEMENTS

My first and sincere appreciation goes to *Friedrich Scheifflinger* for offering me an invaluable opportunity to grow as a research scientist at the Department of Research and Development, Baxter Bioscience, Austria.

I wish to express my deepest gratitude to my advisor, *Hanspeter Rottensteiner*, who guided me in selecting the final topic for my research. His insightful input throughout the research process and most importantly his relaxed working relationship has enabled me to effectively assemble and complete my PhD thesis. I very much appreciated his careful review of countless revisions of the manuscript.

I would also like to thank *Michael Dockal* in whose lab I worked for a short time. His constructive criticism helped me to rethink and focus my ideas.

Thanks go to lab technicians *Bernadette Gruber, Susanna Skalicky, and Christoph Redl*, who assisted me during my thesis work.

None of this would have been possible without the love and patience of *my husband and my son* throughout my studies.



## ABSTRACT

ADAMTS13-neutralizing IgG autoantibodies are the major cause of acquired idiopathic thrombotic thrombocytopenic purpura (TTP). My thesis presents the first characterization of affinity-purified anti-ADAMTS13 IgGs from plasma of patients with acquired TTP and a plasma pool of healthy donors (HD). All preparations contained IgG subclasses IgG1 to IgG4 with IgG2 as the most prevalent, then IgG1 and IgG3/4. For the IgGs from acquired TTP patients, binding to recombinant and plasma derived ADAMTS13, which was purified from a cold ethanol fractionated human plasma intermediate, revealed dissociation constants of ~1 nM resulting primarily from IgG1, IgG3, and IgG4. Routine static activity assays showed the TTP antibodies to have a neutralizing activity of 0.1-0.5 BU/ $\mu$ g and to interfere with the ADAMTS13-VWF interaction. In a newly established flow assay, ADAMTS13 activity was inhibited to a varying extent by two TTP antibody preparations when pre-adjusted to comparable FRETs-VWF73 based inhibitor titers. Anti-ADAMTS13 autoantibodies may thus exhibit inhibitory properties *in vivo* that are not consistent with the ADAMTS13 inhibitor levels determined in routine static assays. Therefore, in possible future treatment of acquired TTP with recombinant ADAMTS13, dosing should not be based on inhibitor titers obtained by routine assays alone. Similarly purified anti-ADAMTS13 IgGs from a HD plasma pool bound ADAMTS13 weakly and did not inhibit ADAMTS13 activity. Antibody epitope mapping studies revealed the IgGs to be polyclonal and elucidated the linear epitope profile of ADAMTS13 IgG autoantibodies. Despite being non-inhibitory, IgGs purified from pooled normal human plasma shared linear epitopes with the autoantibodies from patients with TTP suggesting that anti-ADAMTS13 IgG autoantibodies occurring in healthy individuals may provide the template for emergence of high affinity and pathogenic IgG autoantibodies in acquired TTP. This work sheds new light on the development of inhibitory antibodies in acquired autoimmune TTP and provides novel information on ADAMTS13-specific IgGs in healthy individuals.



# Table of contents

<b>I. INTRODUCTION.....</b>	<b>1</b>
I.1. History of thrombotic thrombocytopenic purpura (TTP).....	1
I.2. Von Willebrand Factor (VWF).....	2
I.2.1. Biosynthesis and secretion of VWF .....	2
I.2.2. Classical interactions of VWF .....	4
I.2.3. Clinical implication of VWF defects .....	6
I.2.4. VWF function in response to shear stress.....	6
I.3. ADAMTS13.....	9
I.3.1. Biosynthesis and secretion of ADAMTS13.....	9
I.3.2. ADAMTS13 Structure.....	9
I.3.3. ADAMTS13 glycosylation pattern.....	12
I.3.4. ADAMTS13 exosites and their corresponding binding sites on VWF .....	12
I.3.5. Acquired and congenital ADAMTS13 deficiency .....	15
I.3.6. ADAMTS13 testing.....	17
I.3.7. TTP treatment .....	24
<b>II. OBJECTIVE.....</b>	<b>26</b>
II.1. Isolation of plasma derived ADAMTS13 (pADAMTS13) .....	26
II.2. Functional characterization of anti-ADAMTS13 autoantibodies affinity-purified from plasma of acquired TTP patients and a healthy donor pool .....	27
II.3. Epitope mapping of affinity purified IgG autoantibodies from plasma of acquired TTP patients and healthy individuals .....	28
II.4. Assessment of the inhibitory activity of affinity purified ADAMTS13 autoantibodies from patients with TTP under flow conditions .....	28
<b>III. MATERIALS AND METHODS.....</b>	<b>30</b>
III.1. Sources of recombinant human ADAMTS13 and VWF and antibodies against ADAMTS13.....	30
III.2. Isolation of plasma derived ADAMTS13 .....	30
III.2.1. Screening of plasma fractionation intermediates for pADAMTS13 activity.....	30
III.2.2. Purification of pADAMTS13.....	32
III.2.3. Assessment of ADAMTS13 antigen by ELISA.....	34
III.2.4. Assessment of ADAMTS13 activity by the FRETS-VWF73 assay.....	34
III.2.5. N-terminal amino acid sequence analysis .....	35
III.2.6. Detection of ADAMTS13 by immunoblotting.....	35
III.2.7. Agarose gel electrophoresis and detection of ADAMTS13 and VWF .....	36

III.3. Functional characterization of anti-ADAMTS13 autoantibodies affinity-purified from plasma of acquired TTP patients and a healthy donor pool .....	37
III.3.1. ADAMTS13 related variables in patient's plasmas and HD's pooled plasma.....	37
III.3.2. Isolation of human anti-ADAMTS13 IgG antibodies and yields.....	38
III.3.3. Determination of total IgG subclasses by ELISA .....	38
III.3.4. Determination of IgG and subclasses of anti-ADAMTS13 antibodies by ELISA .....	39
III.3.5. Calculation of binding parameters for anti-ADAMTS13 IgG antibodies .....	40
III.3.6. Quantitation of ADAMTS13 inhibitory activity of anti-ADAMTS13 IgG antibodies .....	41
III.3.7. Influence of anti-ADAMTS13 IgG antibodies on the ADAMTS13-VWF interaction .....	42
III.3.8. Recovery of rADAMTS13 and pADAMTS13 activity in the TTP derived IgG preparations.....	43
III.4. Epitope mapping of affinity purified IgG autoantibodies from plasma of acquired TTP patients and healthy individuals .....	44
III.4.1. Epitope mapping using immunoprecipitation (IP) plus Western blotting.....	44
III.4.2. Epitope mapping using ADAMTS13 peptide arrays.....	44
III.4.3. Modeling of the ADAMTS13 metalloprotease domain .....	46
III.5. Assessment of the inhibitory activity of affinity purified ADAMTS13 autoantibodies from patients with TTP under flow conditions .....	46
III.5.1. Microchannels coating .....	46
III.5.2. Preparation of washed platelets and erythrocytes .....	47
III.5.3. Perfusion studies and image analysis.....	47
III.5.4. ADAMTS13 flow based activity assay .....	48
III.5.5. Inhibitor activity assessment under flow conditions.....	48
III.5.6. ADAMTS13 activity recovery under static and shear conditions in predefined inhibitor preparations adjusted with goat antiserum to ADAMTS13 .....	49

#### **IV. RESULTS ..... 50**

IV.1. Isolation of plasma derived ADAMTS13.....	50
IV.1.1. Identification of a cold ethanol-fractionated human plasma intermediate with a substantial amount of ADAMTS13 activity.....	50
IV.1.2. Affinity purification of pADAMTS13.....	52
IV.1.3. Identification of multimer species of pADAMTS13 using agarose gel electrophoresis .....	55
IV.2. Functional characterization of anti-ADAMTS13 autoantibodies affinity-purified from plasma of acquired TTP patients and a healthy donor pool .....	57
IV.2.1. Affinity purification of human anti-ADAMTS13 IgG antibodies .....	57
IV.2.2. Specificity and affinity of purified anti-ADAMTS13 IgG antibodies.....	58
IV.2.3. Subclass-specific affinities of purified anti-ADAMTS13 IgG antibodies .....	61
IV.2.4. Neutralizing activity of purified anti-ADAMTS13 IgG autoantibodies.....	63
IV.2.5. Influence of purified anti-ADAMTS13 IgG autoantibodies on the interaction between ADAMTS13 and VWF by ELISA.....	65
IV.2.6. Overriding of the inhibitory activity of the patients IgGs by rADAMTS13 and pADAMTS13 in vitro	67
IV.3. Epitope mapping of affinity purified IgG autoantibodies from plasma of acquired TTP patients and healthy individuals .....	69
IV.3.1. Binding of the anti-ADAMTS13 IgG preparations to ADAMTS13 variants .....	69
IV.3.2. Binding of the anti-ADAMTS13 IgG preparations to ADAMTS13 peptide arrays.....	71

IV.4. Assessment of the inhibitory activity of affinity purified ADAMTS13 autoantibodies from patients with TTP under flow conditions .....	75
IV.4.1. Establishment of an ADAMTS13 activity assay under flow .....	75
IV.4.2. Assessment of ADAMTS13 inhibitors using the ADAMTS13 activity assay under flow .....	80
IV.4.3. Inhibitory activity of purified anti-ADAMTS13 IgG autoantibodies under flow conditions .....	82
<b>V. DISCUSSION.....</b>	<b>84</b>
V.1. Isolation of plasma derived ADAMTS13.....	84
V.2. Functional characterization of anti-ADAMTS13 autoantibodies affinity-purified from plasma of acquired TTP patients and a healthy donor pool .....	86
V.3. Epitope mapping of affinity purified IgG autoantibodies from plasma of acquired TTP patients and healthy individuals .....	89
V.4. Assessment of the inhibitory activity of affinity purified ADAMTS13 autoantibodies from patients with TTP under flow conditions .....	91
<b>VI. CONCLUSION .....</b>	<b>96</b>
<b>REFERENCE LIST .....</b>	<b>97</b>
<b>APPENDED PUBLICATIONS .....</b>	<b>115</b>

## List of Tables

<b>Table 1.</b> Available ADAMTS13 activity assays under static conditions .....	20
<b>Table 2.</b> Available ADAMTS13 activity assays under flow conditions.....	22
<b>Table 3.</b> ADAMTS13-related variables measured in plasma samples from 3 acquired TTP patients and a HD pool .....	37
<b>Table 4.</b> Yield and subclass distribution of affinity-purified anti-ADAMTS13 IgG antibodies from Acquired TTP patients and a HD pool.....	58
<b>Table 5.</b> Calculated dissociation constants for the interaction of TTP-associated IgG autoantibodies with rADAMTS13 and pADAMTS13 using ELISA and/or Biacore.....	60
<b>Table 6.</b> Linear ADAMTS13 peptide epitopes detected with isolated antibodies from acquired TTP patients and a HD pool.....	73

## List of Figures

<b>Figure 1.</b> Domain structure of von Willebrand factor (VWF).....	3
<b>Figure 2.</b> Flow in a blood vessel. ....	7
<b>Figure 3.</b> Dynamic conformational change of VWF under shear. ....	8
<b>Figure 4.</b> ADAMTS13 domain structure. Mature ADAMTS13 consists of a metalloprotease domain..	10
<b>Figure 5.</b> Binding of VWF to ADAMTS13 followed by its proteolysis..	13
<b>Figure 6.</b> Flow chart of the plasma fractionation process up to Fraction II. ....	31
<b>Figure 7.</b> Identification of a Cohn fraction intermediate as a starting material for pADAMTS13 purification..	51
<b>Figure 8.</b> pADAMTS13 isolation using goat anti-ADAMTS13 affinity matrix.....	52
<b>Figure 9.</b> Removal of IgG impurities from pADAMTS13.....	53
<b>Figure 10.</b> Isolation of full-length pADAMTS13 with mAb257A2 recognizing the ADAMTS13 CUB domains. ....	54
<b>Figure 11.</b> Presence of ADAMTS13 oligomers in the final pADAMTS13 preparation..	56
<b>Figure 12.</b> Purity of the affinity-purified anti-ADAMTS13 IgG antibodies from acquired TTP patients and a HD pool..	57
<b>Figure 13.</b> Binding of affinity-purified anti-ADAMTS13 IgG antibodies from acquired TTP patients and a HD pool to ADAMTS13 using ELISA..	59
<b>Figure 14.</b> Binding of affinity-purified anti-ADAMTS13 IgG antibodies to rADAMTS13 using Biacore..	61
<b>Figure 15.</b> Subclass-specific binding of affinity-purified anti-ADAMTS13 IgG antibodies to ADAMTS13 using ELISA.....	62
<b>Figure 16.</b> Inhibitory activity of affinity-purified anti-ADAMTS13 IgG antibodies. ....	64
<b>Figure 17.</b> Interference of affinity-purified anti-ADAMTS13 IgG antibodies with the rADAMTS13-rVWF interaction. ....	65
<b>Figure 18.</b> Influence of the choice of the detection antibody in ADAMTS13-VWF binding ELISA on the apparent affinity of VWF to ADAMTS13..	67
<b>Figure 19.</b> ADAMTS13 recovery in the presence of IgG preparations from TTP patients with defined inhibitor titers.....	68
<b>Figure 20.</b> Relation between anti-ADAMTS13 inhibitor titer and EC50.....	69
<b>Figure 21.</b> Epitope mapping of affinity-purified anti-ADAMTS13 IgG antibodies by immunoprecipitation (IP) and Western blotting.....	70
<b>Figure 22.</b> Raw fluorescence images of representative peptide microarrays..	71
<b>Figure 23.</b> Epitope mapping of affinity-purified anti-ADAMTS13 IgG antibodies by peptides array....	72
<b>Figure 24.</b> Epitope mapping of affinity-purified anti-ADAMTS13 IgG antibodies using peptide arrays. ....	74
<b>Figure 25.</b> Homogeneous chain like structures of platelet aggregates on a layer of cellular fibronectin (cFN), collagen and VWF..	76
<b>Figure 26.</b> Influence of shear and time on VWF-mediated platelet aggregate accumulation in a novel flow-based assay..	77
<b>Figure 27.</b> VWF mediated platelet adhesion.....	78
<b>Figure 28.</b> Effect of ADAMTS13 on VWF-mediated platelet aggregate accumulation under flow conditions. Cell suspensions of fluorescently labeled platelets ( $2.5 \times 10^8$ platelets/ml),.....	79

**Figure 29.** Effect of goat ADAMTS13 antiserum on VWF-mediated platelet aggregate accumulation under flow conditions. .... 81

**Figure 30.** Inhibitory activity of affinity-purified human anti-ADAMTS13 IgG antibodies under flow conditions.. .... 83

## List of Abbreviations

ADAMTS13:	A Disintegrin-like And Metalloprotease with Thrombospondin-type I motif, member 13
AP:	Alkaline Phosphatase
BSA:	Bovine Serum Albumin
BU:	Bethesda Unit
CBA:	Collagen Binding Activity
cFN:	cellular Fibronectin
CHO:	Chinese Hamster Ovary
ECM:	Extra Cellular Matrix
ER:	Endoplasmic Reticulum
FF:	Fast Flow
FRET:	Fluorescence Resonance Energy Transfer
FRETS:	FRET Substrate
GP Iba:	Glycoprotein Iba
Hct:	Hematocrit
HD:	Healthy Donor
HEK:	Human Embryonic Kidney
HRP:	Horseradish Peroxidase
HSA:	Human Serum Albumin
IP:	Immunoprecipitation
$K_D$ :	Dissociation constant
NC:	Nitrocellulose
NHP:	Normal Human Plasma
NHS:	N-hydroxysuccinimide
OD:	Optical Density
pADAMTS13:	plasma derived ADAMTS13
PBS:	Phosphate Buffered Saline
PBST:	PBS containing 0.1% Tween-20

PVDF:	Polyvinylidene Fluoride
rADAMTS13:	recombinant ADAMTS13
rVWF:	recombinant VWF
SDS-PAGE:	Sodium Dodecyl Sulfate Polyacrylamide Gel Electrophoresis
TBS:	Tris Buffered Saline
TMB:	3,3',5,5'-Tetra-MethylBenzidine
TTP:	Thrombotic Thrombocytopenic Purpura
ULVWF:	Ultra Large VWF
VWF:	Von Willebrand Factor
VWD:	Von Willebrand Disease

# I. INTRODUCTION

## I.1. History of thrombotic thrombocytopenic purpura (TTP)

*In 1924*, Dr Moschcowitz described a case of a girl, aged 16 years old, who died suddenly of systemic microvascular thrombosis, a hitherto undescribed disease, today known as thrombotic thrombocytopenic purpura (TTP)<sup>1</sup>. For more than half a century after the report of the first patient, the mortality rate for this disorder exceeded 90%. During this period, TTP symptoms were defined and included thrombocytopenia resulting from platelet consumption by formation of innumerable platelet thrombi, and hemolysis with schistocytes or “split” red cells on blood smears due to intravascular thrombi encountering red cells at high shear stress in the partially occluded microvasculature. Together, these symptoms lead to microangiopathic hemolytic anemia<sup>2</sup>.

*In 1976*, the first report of successful treatment of TTP patients with whole blood exchange was published<sup>3</sup>. Shortly thereafter, infusion of normal fresh frozen plasma and plasmapheresis were shown to be the most effective therapy<sup>4</sup>.

*In 1982*, Moake et al<sup>5</sup> reported on the first association between unusually large or ultra-large Von Willebrand factor multimers (ULVWF), a protein which is synthesized and secreted by endothelial cells into the circulating blood, and TTP. The authors hypothesized that the ULVWF identified in the plasma of four patients with chronic relapsing forms of TTP were due to a lack of a VWF depolymerase that might be replaced during plasma exchange therapy<sup>5</sup>.

*In 1996*, two groups of investigators independently identified and partially purified the VWF cleaving protease from normal human plasma<sup>6,7</sup>. The authors showed that the cleaved peptide bond *in vivo* between residues Y1605 and M1606 of VWF<sup>8</sup> is also cleaved by the partially purified protease. The proteolytic activity was displayed when VWF multimers were subjected to high shear stress or denatured by guanidine<sup>7</sup> or urea<sup>6</sup> in the presence of low

ionic strength. Divalent metal ions such as  $Ba^{2+}$ ,  $Zn^{2+}$  and  $Ca^{2+}$  were also required for cleavage of VWF<sup>7;9</sup>.

*Between 1997 and 1998*, a pathophysiology of TTP was established. Furlan et al<sup>10</sup> reported a chronic deficiency of VWF cleaving protease in four patients with chronic relapsing TTP. Shortly thereafter, the presence of antibodies against the VWF-cleaving protease in plasma of patients with TTP was described<sup>11;12</sup>.

*In 2001*, the VWF cleaving protease was finally isolated to homogeneity and its partial amino-terminal sequence determined<sup>13;14</sup>. On the basis of this sequence, the full-length cDNA of the protease was cloned<sup>15-17</sup> and then designated ADAMTS13, a disintegrin-like and metalloprotease with thrombospondin-type I motif, as a new member of the ADAMTS family of metalloproteases.

## **I.2. Von Willebrand Factor (VWF)**

### **I.2.1. Biosynthesis and secretion of VWF**

VWF, a key component in the pathogenesis of TTP, is a multimeric blood glycoprotein that contains five kinds of structural domains: A, B, C, D, and CK (Figure 1). VWF is synthesized in endothelial cells<sup>18</sup> and megakaryocytes<sup>19</sup> where it is produced as a preproVWF precursor. The primary translation product consists of a 22-amino acid signal peptide that enables transport into the endoplasmic reticulum (ER), a 741-amino acid propeptide, and the 2050-amino acid mature subunit. After its synthesis, preproVWF is transported into the ER. Once the signal peptide is cleaved, proVWF dimerizes through C-terminal disulfide bonds between the CK domains. These dimers are then transported to the Golgi apparatus where the propeptide is cleaved by furin, and disulfide linkage of the dimers near the amino-termini between D3 domains occurs and produces hyperactive and gigantic multimers called ULVWF that may exceed 20 million Da in size. Up to 95% of VWF multimers are secreted

constitutively into the plasma; the remainder is condensed and packaged in tubular arrays within Weibel-Palade bodies in endothelial cells or in platelet alpha-granules<sup>20</sup>.

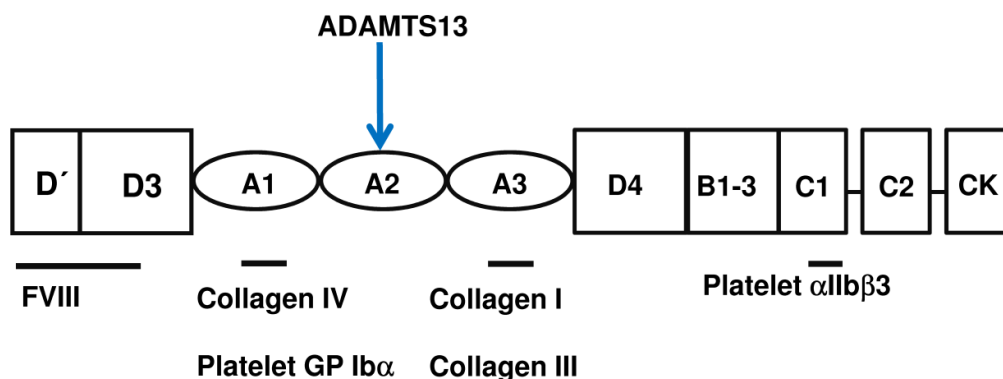


**Figure 1. Domain structure of von Willebrand factor (VWF).** The mature subunit of VWF contains five kinds of structural domains designated A, B, C, D, and CK, and arranged as indicated. The binding sites within the subunits have been identified for FVIII that interacts with D' and D3 domains, subendothelial collagen IV and platelet GP Ibα with the A1 domain, collagen I and III with the A3 domain, and finally platelet αIIbβ3 to C1 domain. The ADAMTS13 cleavage site is located in the A2 domain as indicated by the blue arrow.

In cultured endothelial cells, direct release of ULVWF is induced by several agonists including thrombin, histamine, and other mediators of inflammation and/or thrombosis<sup>21</sup>. ULVWF may also remain attached to the endothelial cell surface possibly via P selectin<sup>22</sup> and αvβ3<sup>23</sup>. A similar situation occurs *in vivo* as VWF levels are increased in plasma by thrombin, histamine, epinephrine, and vasopressin. The transition from ULVWF to plasma VWF results from partial proteolysis by ADAMTS13 at the Y1605-M1606 bond in the A2 domain. Unprocessed, these ULVWF multimers can spontaneously bind platelets, leading to widespread microthrombi in the circulation and thus to TTP.

## **I.2.2. Classical interactions of VWF**

### **I.2.2.1. Binding of platelets**

Platelets are anucleate cytoplasmic fragments derived from fragmentation of precursor megakaryocytes. They are discoid with a 2-3  $\mu\text{m}$  diameter and circulate in blood where they are involved in haemostasis and thrombosis. Upon vascular injury, VWF promotes the recruitment of platelets exposed to rapid blood flow through two receptors: The glycoprotein GP Ib $\alpha$  in the GPIb-IX-V complex and  $\alpha\text{IIb}\beta\text{3}$ , a member of the integrin family of cell surface receptors. GP Ib $\alpha$  is a single transmembrane receptor expressed in high copy numbers on the platelet surface<sup>24</sup> and its interactive site domain has been elucidated with VWF at the atomic level<sup>25</sup>. Binding of VWF to GP Ib $\alpha$  requires the A1 domain of VWF (Figure 1) to be exposed to high shear conditions generated by rapidly flowing blood. Such interaction is important in the formation of platelet-rich thrombi<sup>26</sup>.

The binding site of  $\alpha\text{IIb}\beta\text{3}$  is located in the C1 domain of VWF (Figure 1) at the classical RGDS recognition sequence of integrins. *In vitro* studies showed that such binding reinforces platelet to platelet interactions by contributing to platelet adhesion that is initiated through GP Ib $\alpha$  binding to VWF<sup>27</sup>.

### **I.2.2.2. Binding to collagen**

At sites of vascular damage, unfolded VWF attaches to subendothelial collagen through multiple binding sites under conditions of high shear stress. A dominant binding site for fibrillar collagen type I and III has been shown to be located in the VWF-A3 domain<sup>28</sup>, whereas collagen type VI was demonstrated to bind to the VWF-A1 domain<sup>29</sup>(Figure 1). Platelets have been also shown to directly bind collagen through the GPVI and integrin  $\alpha\text{II}\beta\text{1}$  receptors<sup>30</sup>. VWF-collagen interactions are therefore needed to facilitate recruitment of flowing platelets to collagen under high shear conditions<sup>31</sup>. From a structural point of view, once bound to collagen, VWF undergoes conformational shear induced changes that enable

its interaction with GP Ib $\alpha$  on platelets<sup>32</sup>. Thereby, VWF mediates platelet rolling on the subendothelium, which slows down the platelets and allows other platelet receptors such as GPVI and integrin  $\alpha$ IIb $\beta$ 1 to bind to collagen.

### **I.2.2.3. Binding to Factor VIII (FVIII)**

FVIII is a plasma glycoprotein that functions as an essential cofactor in the intrinsic coagulation pathway. It plays an important role in haemostasis, as its deficiency leads to a severe bleeding tendency as seen in haemophilia A. FVIII has a heterodimeric structure containing a metal ion-linked heavy (A1-a1-A2-a2-B region) and light (a3-A3-C1-C2 region) chain. Immediately after its release into the circulation, FVIII is caught into a non-covalent complex with its carrier protein VWF with a  $K_D$  of less than 1 nM<sup>33</sup>. The FVIII binding domain resides within the amino-terminal D'D3 region of VWF<sup>34</sup> (Figure 1). During blood coagulation, FVIII is released from VWF after proteolytic activation by thrombin and is then free to bind to membranes containing phosphatidylserine, where it may assemble as a cofactor with the serine protease factor IXa in the membrane-bound factor X-activating enzyme complex (known as tenase complex) to form an efficient procoagulant enzyme complex. The enzymatic product of this complex, activated factor X, activates prothrombin to thrombin. The activation and inactivation of FVIII is described in a review by Lenting and colleagues<sup>35</sup>. Activated FVIII may also be degraded by anticoagulant proteases such as activated protein C<sup>35</sup>. The necessity of FVIII-VWF complex formation is related to several protective roles of VWF including stabilization of FVIII structure<sup>36</sup>, FVIII protection from proteolytic degradation by phospholipid-binding proteases<sup>37</sup>, attenuation of the binding of FVIII to negatively charged phospholipid surfaces on activated platelets<sup>38</sup> and inhibition of the accessibility of FVIII to the FX-activating complex through blocking of the binding of FVIII to FIXa<sup>39</sup>. Binding of VWF to collagen was reported to reduce VWF affinity to FVIII<sup>40</sup> possibly making released FVIII more rapidly available for the coagulation cascade.

#### **I.2.2.4. Binding to ADAMTS13**

Binding of ADAMTS13 to VWF is described in detail in chapter I.3.4.

#### **I.2.3. Clinical implication of VWF defects**

A quantitative or a qualitative defect of VWF leads to von Willebrand disease (VWD), the most common inherited bleeding disorder, occurring in nearly 1% of the general population. VWD is generally classified by three types: Type 1, where the levels of VWF are partially reduced, type 2, where a qualitative deficiency of VWF impairs the protein function, and type 3, where VWF is undetectable. VWD type 2 patients are further categorized into four groups: A, B, M, and N. Patients with type 2A and 2M have a decreased VWF-dependent platelet adhesion but the presence (Type 2M) or selective deficiency of high molecular weight VWF multimers (Type 2A). Increased affinity for platelet GP Ib $\alpha$  receptors indicates type 2B; an inability of VWF to bind FVIII causes type 2N. Bleeding symptoms are mildest in patients with type 1 VWD and most severe in those with type 3 disease. The pathophysiology and classification of VWD are well described by Sadler and colleagues<sup>41</sup>.

#### **I.2.4. VWF function in response to shear stress**

##### **I.2.4.1. Rheological properties of blood**

Blood flow is caused by the heart's pumping action and can be described as an infinite number of adjacent laminae sliding across each-another at different velocities. As blood flows in a vessel, the velocity in the vessel's center is the highest falling to zero toward the wall, creating a parabolic velocity profile (Figure 2).

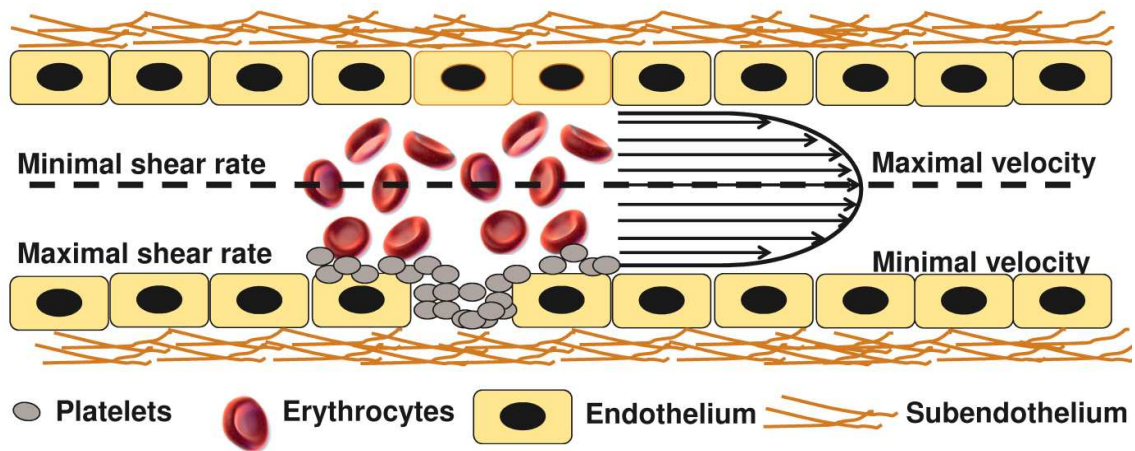


**Figure 2. Flow in a blood vessel.** In flowing blood, red blood cells occupy the greatest part of the lumen, pushing flowing platelets to the vessel wall where they are captured by the subendothelial components at sites of vascular injury, thereby creating a near wall platelets excess. Blood flows in a vessel with a parabolic velocity profile, i.e. the highest fluid velocity (arrows) in the center and the lowest toward the vessel wall, which results in high values of shear rates.

Differences in velocity between such fluid planes generate shear forces known as “shear stress”. Shear stress (commonly expressed in units of  $\text{dyn}/\text{cm}^2$ ) is defined as the force per unit area of contact between the fluid planes. Conversely, the gradient of velocity or “shear rate” (expressed in units of  $\text{cm}/\text{s}$  per  $\text{cm}$  or  $\text{s}^{-1}$ ) is dependent on the distance from the center of the lumen and is highest at the vessel wall and zero at the center (Figure 2).

Since blood is considered Newtonian, showing a fluid behavior with a constant viscosity at all shear rates, the relationship between shear stress and shear rate is linear where Shear rate ( $\text{cm}/\text{s}/\text{cm}$ ) = Shear stress ( $\text{dyn}/\text{cm}^2$ ) / Viscosity ( $\text{dyn}/\text{cm}^2 \cdot \text{s}$  which is equivalent to Poise or P). For example, in whole blood with a viscosity of 0.038 P, a shear stress of  $35 \text{ dyn}/\text{cm}^2$  results in a wall shear rate of approximately  $922 \text{ s}^{-1}$ . Wall shear rates are estimated to be  $20\text{-}200 \text{ s}^{-1}$  in veins and  $500\text{-}1600 \text{ s}^{-1}$  in large arteries, whereas those in stenotic vessels may reach  $10,000 \text{ s}^{-1}$ <sup>42</sup>. While red blood cells occupy the greatest part of the lumen, platelets oppose shear forces and move to the vessel wall where maximum shear rates occur. This in turn increases the likelihood of platelet-surface and vessel wall immobilized VWF interaction<sup>32</sup>.

### I.2.4.2. VWF- globular versus stretched conformation

Circulating VWF adopts a globular conformation until a critical shear stress of 35 dyn/cm<sup>2</sup> causes protein stretching which leads to an extended chain conformation toward the applied shear stress field<sup>43</sup>.

VWF multimers bound to the vessel wall or floating freely in the bloodstream are stretched up to 15 µm by the hydrodynamic forces in shear flow<sup>44</sup> (Figure 3). Such a globule-stretch transition was shown to be reversible as a drop in the shear forces is able to change VWF conformation from a stretched to a globular form<sup>44</sup> (Figure 3).

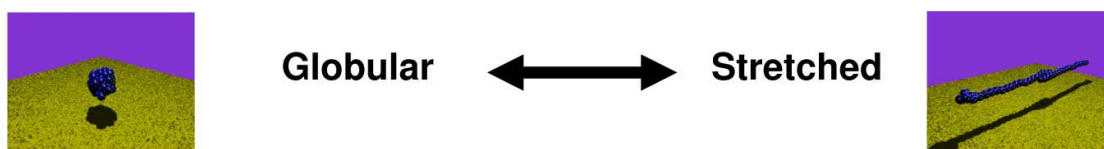


**Figure 3. Dynamic conformational change of VWF under shear.** Below a critical shear rate, VWF exhibits a globular conformation (left panel). In shear flow, hydrodynamic forces exceeding a critical shear rate stretch VWF by up to 15 µm. Image courtesy of Matthias Schneider<sup>44</sup>.

### I.2.4.3. Consequences of VWF elongated conformation

The elongated conformation of VWF contributes to several of its functions. This conformational change leads to the exposure of GP Ib binding site in the A1 domain<sup>32</sup>, thereby enabling the formation of a hemostatic platelet plug. It also unfolds the A2 domain to expose the Y1605-M1606 which allows VWF cleavage by ADAMTS13<sup>45</sup> and its conversion to smaller multimers with a wide range of size distributions. Furthermore, oxidation of M1606 in VWF A2 domain is accelerated rendering VWF resistant against ADAMTS13<sup>46</sup>. Finally, thiol-disulfide exchange is induced covalently associating ULVWF with VWF multimers in solution<sup>47</sup>.

### **I.3. ADAMTS13**

#### **I.3.1. Biosynthesis and secretion of ADAMTS13**

Human ADAMTS13 is a zinc metalloprotease consisting of 1427 amino acid residues and is synthesized with a molecular weight of 190 kDa instead of the predicted 145 kDa, indicating that the protein is extensively glycosylated. The mRNA encoding full-length ADAMTS13 (approximately 4.3 kb) is primarily detected in human liver where hepatic stellate cells have been shown to be the major ADAMTS13 producing cells<sup>48</sup>.

ADAMTS13 mRNA was also observed in vascular endothelial cells<sup>49:50</sup> and megakaryocytes or platelets<sup>51</sup>. Alternatively spliced mRNA forms may also occur in many tissues<sup>15-17</sup>. Various truncated forms of ADAMTS13 (150, 140, 130 and 110 kDa) have been reported to be present in plasma<sup>14</sup>. The protein is secreted into plasma as an already active enzyme. To date, it remains unknown whether spliced mRNA forms give rise to functional protein or whether the circulating variants of ADAMTS13 are due to proteolysis of full-length ADAMTS13 by serine proteases such as thrombin<sup>52</sup> or leucocyte elastase<sup>53</sup>. The concentration of ADAMTS13 in normal human plasma is 1 µg/ml<sup>14</sup> with a plasma half-life of 2-3 days<sup>54</sup>.

#### **I.3.2. ADAMTS13 Structure**

ADAMTS13 is the 13<sup>th</sup> member of the ADAMTS family of zinc-dependent metalloproteases which all share a signal peptide, a propeptide, a metalloprotease, a first thrombospondin-type 1 repeat, disintegrin-like, cysteine-rich, and spacer domains. Many ADAMTS proteases have additional thrombospondin-type 1 repeats after their spacer domain but ADAMTS13 has 7. ADAMTS13 also diverges from the ADAMTS family in that it has 2 CUB [complement C1r/C1s, Uegf (EGF-related sea urchin protein) and BMP-1 (bone morphogenic protein-1)] domains at its C-terminus (Figure 4).

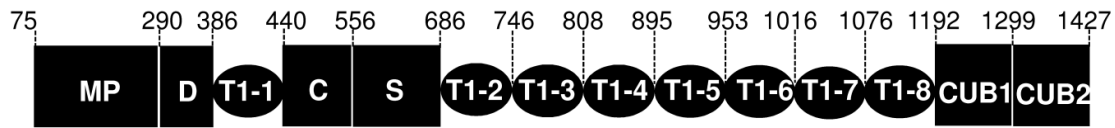


**Figure 4. ADAMTS13 domain structure.** Mature ADAMTS13 consists of a metalloprotease domain (MP), a disintegrin domain (D), a thrombospondin-type 1 repeat (T1-1), a cysteine-rich domain (C), a spacer domain (S), seven additional thrombospondin-type 1 repeats (T1-2/8), and two CUB domains (CUB1 and CUB2). ADAMTS13 domains are shown with the number of the first and last amino acid residue of each domain on top.

The precise contribution of each domain to ADAMTS13 function is detailed below.

**Propeptide.** At variance with other ADAMTS or ADAM family proteases, the ADAMTS13 propeptide is unusually short containing only 41 amino acid residues instead of the usual 200. The propeptide has been shown to have no distinct functional properties as it is dispensable for ADAMTS13 folding or secretion and not involved in maintaining enzyme latency<sup>55</sup>.

**Metalloprotease.** The metalloprotease of ADAMTS13 has a conserved reprotolysin-type zinc binding sequence “224HEXXHXXGXXHD235” where the  $Zn^{2+}$  ion is coordinated by three histidine residues. At position 225 of this sequence, a glutamate polarizing a water molecule stabilized by coordination with the  $Zn^{2+}$  ion is responsible for substrate proteolysis. The methionine 249 residue in ADAMTS13 constitutes a Met-turn known to play a crucial role in the structure of the  $Zn^{2+}$  binding motif in all ADAMTS metalloprotease domains.

In addition to  $Zn^{2+}$ ,  $Ca^{2+}$  is another divalent cation that plays an important role in ADAMTS13 function. Using homology modeling with ADAMTS1, -4 and -5, a candidate high affinity  $Ca^{2+}$  binding site predicted to include D187 and E212 with D182 or E184 was identified in the ADAMTS13 metalloprotease domain<sup>56</sup>.

**Disintegrin-like domain.** The metalloprotease domain of ADAMTS13 is followed by the disintegrin-like domain, a term attributed to this domain as it is similar to snake venom disintegrins despite lacking the canonical cysteine arrangement. The precise contribution of this domain in ADAMTS13 function remains uncertain.

**Cysteine-rich domain.** This domain is well conserved among the other ADAMTS family members as it contains a sequence enriched with 10 cysteine residues. Here, ADAMTS13 possesses an RGD sequence known as a potential cell adhesion sequence that recognizes integrins. A single point mutation of RGD to RGE revealed this sequence to be dispensable for the secretion or VWF cleaving protease activity<sup>57</sup>.

**Spacer domain.** Sequence analysis of the spacer domain among ADAMTS family members showed that the spacer domain is a cysteine-free region of highly variable length. The spacer domain of ADAMTS13 is globular with 10 anti-parallel  $\beta$ -strands organized in a jelly roll topology<sup>58</sup>. Experimental data show that ADAMTS13 variants lacking the disintegrin, the thrombospondin-type 1 repeat, or the cysteine-rich domains, are not able to cleave VWF and that adding the spacer domain to an ADAMTS13 variant truncated after the cysteine-rich domain restores ADAMTS13 proteolytic activity toward VWF<sup>57;59</sup>, indicating that this domain is essential for the enzyme's activity.

**Thrombospondin-type 1 repeat domains.** Like other ADAMTS proteases, ADAMTS13 possesses well conserved thrombospondin-type 1 repeats that are homologous to the type one repeats of thrombospondin 1 and 2. ADAMTS13 has eight thrombospondin-type 1 repeats, the first between the disintegrin-like domain and the cysteine-rich domain and the other seven between the spacer domain and the CUB1 domain. Thrombospondin-type 1 repeat domains in ADAMTS13 contain CD36-binding motifs including four CSVSCG and two CSASCG sequences possibly localizing ADAMTS13 on endothelial cells<sup>60;61</sup>.

**CUB domains.** The CUB domains are unique to ADAMTS13. These domains, by interacting with membrane lipids microdomains, have been shown to play a critical role in the apical sorting of ADAMTS13 protease toward the lumen of the vessel, as a mutation in the CUB1 domain that removes the C-terminal part of the CUB2 domain reverses the secretion polarity of ADAMTS13 in cell culture<sup>62</sup>. The function of ADAMTS13 CUB domains toward the proteolysis of VWF showed inconsistent results *in vitro* and *in vivo*.

### **I.3.3. ADAMTS13 glycosylation pattern**

Human ADAMTS13 contains glucose- $\beta$ 1,3-fucose, a disaccharide present on at least six of its thrombospondin-type I repeats<sup>63</sup>. It has also 10 putative N-linked glycans in the metalloprotease domain (N142, N146), the spacer domain (N552, N579, N614, N667), the 2<sup>nd</sup> and 4<sup>th</sup> thrombospondin-type 1 repeat (N707, N828) and in the CUB domains (N1235, N1354)<sup>64</sup>. Both O-fucosylation and N-glycosylation play a role in ADAMTS13 secretion<sup>63</sup>. While removal of N-glycans from VWF increases the susceptibility of the substrate to cleavage by ADAMTS13<sup>65</sup>, the N-linked glycans do not affect the proteolytic activity of the mature ADAMTS13<sup>64</sup>.

### **I.3.4. ADAMTS13 exosites and their corresponding binding sites on VWF**

ADAMTS13 has been shown to bind unfolded VWF with high affinity ( $K_D$  10-20 nM)<sup>66</sup>, and VWF proteolysis by ADAMTS13 occurs through multiple binding steps. Briefly, early interaction between globular VWF and C-terminal domains of ADAMTS13 takes place in a first step. Upon VWF unfolding, a step that reveals additional binding sites on VWF, multiple exosite interactions contribute to bring the ADAMTS13 metalloprotease domain close to the exposed Y1605-M1606 scissile bond in VWF. A critical step is the docking of the spacer domain onto the C-terminal end of the VWF A2 domain followed by the disintegrin domain interacting with low affinity with residues close to the cleavage site. In a final step, before proteolysis occurs, the metalloprotease domain subsites interact with VWF residues adjacent to the cleavage site thereby placing the Y1605-M1606 bond into the active site cleft (Figure 5)<sup>67</sup>.

## Shear exposed VWF

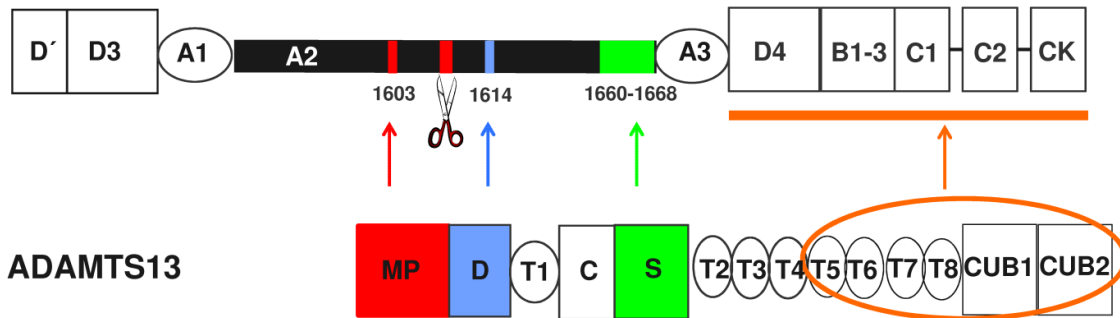


**Figure 5. Binding of VWF to ADAMTS13 followed by its proteolysis.** ADAMTS13 binds globular VWF via its C-terminal domains between the 5<sup>th</sup> thrombospondin-type 1 domain (T5) and the CUB2 domain. The complementary binding site in globular VWF occurs via its D4, B1-3, C1, C2 and CK domains. Under high shear forces, VWF unfolds exposing by this globular A2 domain which unravels several cryptic binding exosites (red, blue, green) enabling in a first step residues in the spacer domain (S) to bind the C-terminal sequence E1660-R1668 of VWF A2 domain. Thereafter, the disintegrin domain (D) interacts with D1614 in VWF. Finally, the metalloprotease domain (MP) interacts with L1603 in VWF. Together, these interactions engage the MP domain to cleave VWF at the Y1605-M1606 bond.

Each of ADAMTS13-VWF binding steps leading to VWF proteolysis is detailed.

### **Step 1: C-terminal thrombospondin-type 1 repeat and CUB domains binding to VWF.**

ADAMTS13 5<sup>th</sup> thrombospondin-type 1 repeat to CUB2 domains bind to the D4-CK domain of VWF which is constitutively exposed on the surface of globular VWF without flow<sup>68</sup>. Thereby 3% of ADAMTS13 circulate bound to globular VWF which may help to localize VWF and ADAMTS13 to the site of a vessel damage<sup>69</sup>.

### **Step 2: VWF unfolding, a prerequisite for exosite interaction.**

The unfolding of VWF is a prerequisite to reveal binding sites on VWF and expose the Y1605-M1606 scissile bond to ADAMTS13. Without unfolding, VWF cleavage does not occur. Since cleavage sites in globular VWF are exposed *in vitro* only by flow or denaturing agents, short substrates of the VWF A2 domain were used to identify the binding sites of ADAMTS13 domains within the VWF A2 domain. Using a series of partial deletions in the A2 domains, Kokame et al demonstrated that a region comprising 73 amino acids (designated as VWF73 1596-1668)

consisting of 10 amino acids before and 63 amino acids after the scissile bond within the central A2 domain of VWF is the minimum substrate for ADAMTS13<sup>70</sup>. Deletion of the last 9 C-terminal residues (1660-1668) of this fragment completely eliminated cleavage by ADAMTS13. This substrate or others such as VWF76 (1593-1668) and VWF115 (1554-1668) contributed to identification of ADAMTS13 binding sites on VWF.

**Step 3: Spacer domain binding to VWF.** The spacer domain binds to an exosite at the C-terminus of the VWF A2 domain that is far from the scissile bond and includes residues E1660-R1668<sup>71</sup>. This exosite is cryptic in native VWF, suggesting that shear-induced unfolding of the VWF A2 domain unravels not only the Y1605-M1606 scissile bond but also exposes the E1660-R1668 exosite for interaction with the spacer domain of ADAMTS13.

The exact amino acid residues that contribute to the interaction of ADAMTS13 spacer domain and VWF A2 domain were delineated by Pos et al<sup>72</sup> who showed that an interactive surface comprising R660, Y661, and Y665 plays a role in binding to and cleavage of VWF. Using a triple mutant variant of the spacer domain of ADAMTS13 “ADAMTS13-R660A/Y661A/Y665A”, the investigators demonstrated that this variant displayed an approximately 12-fold reduced conversion of VWF115 but not of the shorter substrate VWF106 that lacked residues E1660-R1668<sup>72</sup>.

**Step 4: Disintegrin-like domain binding to VWF.** Targeted mutagenesis of a nonconserved region among ADAMTS family members within this domain (R349A, L350G) revealed a 20-fold reduction in proteolytic activity of ADAMTS13 toward VWF115 and multimeric VWF<sup>73</sup>. These two amino acids are adjacent to the metalloprotease domain and were shown to define a functional exosite that interacts with a complementary exosite on VWF involving D1614. This interaction ideally positions the R349 and L350 residues to interact directly with the VWF A2 domain.

**Step 5: Metalloprotease domain binding to VWF.** Xiang and colleagues demonstrated that L1603, Y1605, and D1614 in the VWF A2 domain directly interact with L198, V195, and

R349 in the metalloprotease domain of ADAMTS13<sup>74</sup>, respectively, thereby ensuring that the cleavage site in VWF is engaged over the active center of ADAMTS13.

### **I.3.5. Acquired and congenital ADAMTS13 deficiency**

ADAMTS13 activity is strongly reduced in most patients with TTP. Today, two forms of ADAMTS13 deficiency are recognized: Acquired and congenital. Acquired ADAMTS13 deficiency is caused by the presence of autoantibodies against ADAMTS13 while the congenital form is due to an inherited deficiency of ADAMTS13.

#### **I.3.5.1. Congenital TTP**

Congenital TTP (also known as Upshaw-Schulman syndrome) has an autosomal recessive inheritance. ADAMTS13 deficiency results from homozygous or compound heterozygous mutations of the ADAMTS13 gene, which spans 29 exons and ~37 kb and is located at chromosome 9q34. More than 140 different aberrations have been identified in the ADAMTS13 gene and include missense, nonsense, frame shift insertion, or deletion and splicing site mutations. The mutated sites in ADAMTS13 are distributed across the entire length of the ADAMTS13 gene without an apparent hot spot. The mutants may cause impaired ADAMTS13 synthesis, secretion, or proteolytic activity.

The clinical presentation of this form of TTP is variable; patients may experience their first disease episode during the neonatal period or childhood, in adulthood with one single episode, or as a chronic-relapsing form. A review by Lotta et al<sup>75</sup> describes mutations and polymorphisms in congenital TTP.

#### **I.3.5.2. Acquired TTP**

Acquired TTP patients are described as having idiopathic TTP if no other condition causing thrombotic microangiopathy is apparent or as having secondary TTP if other conditions are

identified that may cause TTP such as hematopoietic stem cell transplantation, pregnancy, drug association, other autoimmune diseases, HIV infection, or cancer. The annual incidence of acquired TTP with severe ADAMTS13 deficiency is 1.74 cases per million per year<sup>76</sup> predominantly in females.

The etiology of acquired TTP is unknown. A genetic predisposition linked to the MHC class II allele HLA DRB1\*11 has been identified as a risk factor for developing acquired TTP<sup>77</sup>. TTP was also reported to occur concomitantly with other clinical conditions including pregnancy or autoimmune disease (e.g. systemic lupus erythematosus)<sup>78</sup>. A number of case reports suggest that viral or bacterial infections such as Influenza A, HIV, parovirus, Helicobacter pilori, hepatitis C, brucella, or legionella play a role in the onset of acquired TTP. Hyperactive immune reactions commonly associated with such microbial agents may be the causative trigger of autoimmune ADAMTS13 inhibitors and TTP. Finally, drugs such as the antiplatelet agent ticlopidine, used in patients with coronary artery disease or stroke, may induce TTP<sup>79</sup>.

#### **I.3.5.2.1. Targeted ADAMTS13 epitopes in acquired TTP**

Antibodies from TTP patients have been studied using various epitope mapping techniques including direct immunoblotting<sup>57;80</sup>, immunoprecipitation with ADAMTS13 domain fragments plus immunoblotting<sup>81-84</sup>, and phage display expressing various peptides of ADAMTS13<sup>85</sup>. These studies revealed that nearly all anti-ADAMTS13 IgGs bind the cysteine-rich and spacer domains. The antigenicity of the spacer domain is dictated by amino acid regions T572-N579; regions V657-G666 contribute to its antigenicity<sup>82</sup>. By site-directed mutagenesis, Pos et al<sup>72;86</sup> finally demonstrated that residues R568, F592, R660, Y661, and Y665, present on the outer surface of the spacer domain, are targeted by the majority of anti-ADAMTS13 antibodies in the plasma of TTP patients. Screening of the phage display libraries of individuals with acquired TTP revealed most of the autoantibodies to incorporate variable heavy chain gene segment VH1-69<sup>87</sup> suggesting complementarity between VH1-69 encoded

variable domain residues of the autoantibodies and the exposed exosite residues on the spacer domain<sup>72</sup>.

Autoantibodies reactive with the metalloprotease, CUB and thrombospondin-type 1 repeat 2-8 domains have been also detected in patient plasma samples<sup>57;80;84;87</sup>. It is not clear whether antibodies directed against the CUB and the thrombospondin-type 1 repeat 2-8 domains of ADAMTS13 interfere with the processing of VWF by ADAMTS13.

### **I.3.6. ADAMTS13 testing**

#### **I.3.6.1. ADAMTS13 activity assays**

ADAMTS13 activity in normal human plasma is reported to be 50 to 178%<sup>88</sup>. In TTP, severe deficiency of ADAMTS13 activity in plasma is typically < 5% of normal.

Since 1998, various laboratory assays measuring the activity of ADAMTS13 in plasma have been developed. The assays can be categorized into static and flow based assays. Tables 1 and 2 list all reported ADAMTS13 activity assays under static and flow conditions, respectively.

##### **I.3.6.1.1. Static assays**

The first two assays to measure ADAMTS13 activity in plasma under static conditions were based on measurement of the loss of high VWF multimers by sodium dodecyl sulfate (SDS) - agarose gel electrophoresis followed by immunoblotting<sup>11</sup> and the generation of VWF cleaved fragments by SDS polyacrylamide gel electrophoresis (SDS-PAGE) followed by immunoblotting<sup>12</sup> (Table 1). ADAMTS13 activity has been also estimated using either the decrease in residual VWF activity reflected by a decrease in collagen binding<sup>89</sup>, ristocetin cofactor activity<sup>90</sup>, or the absence of specific epitopes in VWF due to reduction in VWF multimer size using immunological methods (i.e. Two sites immunoradiometric assay<sup>91</sup>). A second generation of tests evolved using synthetic or recombinant derivative substrates of

the VWF A2 domain (rVWF A2) tagged with distinct markers to facilitate quantitation by distinct methods including ELISA<sup>92-94</sup>, horseradish-peroxidase (HRP) activity assay<sup>95</sup>, Western blotting<sup>96</sup>, fluorescence resonance energy transfer (FRET)<sup>97</sup>, and surface enhanced laser/ desorption/ ionization time-of-flight mass spectrometry (SELDI-TOF-MS)<sup>98</sup> (Table 1). A multicenter study showed that assays based on VWF peptides displayed excellent performance characteristics compared with assays based on multimeric VWF<sup>99</sup>.

Although static assays have provided remarkable insights into the pathogenesis of acquired TTP, each has its limitations. On one hand, the use of denaturing agents (urea or guanidine) to unfold full-length VWF may inactivate ADAMTS13 and dissociate antibody-antigen complexes leading to artifactual overestimation of ADAMTS13 activity. On the other hand, the short derivative fluorescent peptide is a non-natural substrate as it lacks the ancillary binding domains reported to be critical for interaction with C-terminal domains of ADAMTS13. Another concern is that elevated plasma levels of bilirubin and hemoglobin in TTP patients may quench the fluorescent signal, resulting in falsely low ADAMTS13 activity. To overcome the latter limitation, an optimized FRET-VWF71 substrate with brighter dyes with improved spectral properties was recently designed<sup>100</sup>.

#### **1.3.6.1.2. Flow assays**

Four publications report using flow conditions to measure ADAMTS13 activity (Table 2). Dong et al described an activity assay based on evaluation of the extent of cleavage of endothelial cell - derived ULVWF string-like structures in a parallel flow chamber in the presence of patients plasma and platelets<sup>101</sup>. Another shear based assay used a cone and plate analyzer to measure the decrease of platelet adhesion and aggregation in a mixture of test plasma and citrated normal whole blood on a polystyrene surface under arterial flow conditions<sup>102</sup>. A cone and plate viscometer was used to subject reaction mixtures containing ADAMTS13, VWF and platelets to various shear stresses for varying periods<sup>103</sup>. Finally, mixtures of VWF and citrated plasma were subjected to constant vortexing<sup>104</sup>. In the last two

assays, proteolysis of VWF was analyzed by SDS-PAGE<sup>103</sup> or 2.5% agarose gel electrophoresis<sup>104</sup> and immunoblotting.

Among these flow assays, only the assay described by Dong et al closely mimics the situation *in vivo*, simulating endothelial ULVWF release following endothelial activation<sup>101</sup>. In a multicenter study, this assay was shown to only discriminate ADAMTS13 levels higher or lower than 20% without measuring a precise value of ADAMTS13 activity<sup>99</sup>. Furthermore, the assay is technically challenging, not easily reproducible and time consuming in term of preparation of endothelial cells.

**Table 1. Available ADAMTS13 activity assays under static conditions**

<b>VWF Substrate</b>	<b>Denaturing agent</b>	<b>Activator</b>	<b>Digestion time</b>	<b>Detection method</b>	<b>Indication of VWF proteolysis</b>	<b>Reference</b>
Purified plasma derived VWF	1.5 M Urea	10 mM BaCl <sub>2</sub>	Overnight	SDS-1% agarose electrophoresis and Western blotting	Decreased VWF multimer size	11
Purified plasma derived VWF	0.15 M Guanidine	None	1 h	SDS-PAGE and Western blotting	Generation of VWF 176 kDa dimers	12
EDTA treated and dialyzed plasma VWF	1.5 M Urea	3 mM BaCl <sub>2</sub>	Overnight	Collagen binding	Decreased collagen binding	89
Wild type rVWF	1.5 M Urea	3 mM BaCl <sub>2</sub>	Overnight	Two site immuno-radiometric assay (IRMA)	Decreased VWF antigen	91
Purified plasma derived VWF	1.6 M Urea	6.25 mM BaCl <sub>2</sub>	Overnight	Ristocetin cofactor activity (RCo)	Decrease VWF:RCo activity	90
Double tagged rVWF A2 peptide (His tag at N-terminus and Tag-100 at C-terminus)	None	None	2 h	ELISA using Ni <sup>2+</sup> coated plate and monoclonal antibody against Tag-100	Decrease of intact bound VWF A2 peptide containing the Tag-100 epitope	92
rVWF A2 peptide with a His tag at N-terminus	None	None	1 h	SDS-PAGE and Western blotting	Generation of cleaved peptide band at 16 kDa	96
Double tagged rVWF A2 peptide (HRP at N-terminus and biotin at C-terminus)	None	None	30 min	Peptide adsorption on streptavidin-agarose and quantification of HRP activity	Increase of the amount of unadsorbed HRP activity	95
FRETs-synthetic VWF73	None	25 mM CaCl <sub>2</sub>	1 h	Fluorescence resonance energy transfer (FRET)	Increase of fluorescence	97

**Table 1. Available ADAMTS13 activity assays under static conditions (continued)**

<b>VWF Substrate</b>	<b>Denaturing agent</b>	<b>Activator</b>	<b>Digestion time</b>	<b>Detection method</b>	<b>Indication of VWF proteolysis</b>	<b>Reference</b>
Double tagged rVWF A2 peptide with GST at N-terminus and His tag at C-terminus (GST-VWF73-His)	None	None	3 h	ELISA using an antibody to GST for peptide immobilization and anti-His tag for peptide detection	Decrease of intact bound VWF peptide	93
GST-VWF73-His	None	5 mM MgCl <sub>2</sub>	1 h	ELISA using an antibody to GST for peptide immobilization and an antibody to 10 amino acids before the cleavage site for peptide detection	Increase of cleaved bound VWF peptide	94
GST-VWF73-His	None	1 mM BaCl <sub>2</sub>	16 h	Capture of His tagged cleaved VWF peptide on a metal affinity protein chip and quantification by SELDI-TOF-MS	Detection of cleaved VWF peptide	98
FRETS-rVWF71	None	10 mM CaCl <sub>2</sub>	1 h	Fluorescence resonance energy transfer (FRET)	Increase of fluorescence	100

**Table 2. Available ADAMTS13 activity assays under flow conditions**

Principle	VWF substrate	Activator	Time and shear parameters	Detection method	Indication of VWF proteolysis	Reference
Decrease by normal human plasma of platelets deposition on a polystyrene surface from normal whole blood under flow conditions using a cone and plate analyzer	Sodium citrate anti-coagulated normal blood	None	2 min at 1800s <sup>-1</sup>	Calculation of the total area covered with platelets and average size of surface bound objects	Decrease in % of surface coverage by platelets, and in average size of surface bound objects	102
Breakdown by normal human plasma of ULVWF-platelet strings under flow using a parallel-plate flow chamber	ULVWF released by histamine-stimulated human umbilical vein endothelial cells	None	10 min at 2.5 dyn/cm <sup>2</sup>	Quantification of individual ULVWF-platelet strings attached to endothelial cells in 20 continuous view fields.	Breakdown of ULVWF-platelet strings attached to endothelial cells	101
Cleavage of soluble VWF by ADAMTS13 in the presence of human platelets under flow using a cone and plate viscosimeter	Purified plasma VWF	0.1 μM ZnCl <sub>2</sub> 5 mM CaCl <sub>2</sub>	Various fluid shear stress (up to 50 dyn/cm <sup>2</sup> ) for different times (up to 10 min)	SDS-PAGE and Western blotting	Generation of VWF 176 kDa dimers	103
Cleavage of soluble VWF by ADAMTS13 under constant vortexing using a bench vortexer	Purified plasma VWF	1.7 μM ZnCl <sub>2</sub> 5 mM CaCl <sub>2</sub>	2500 rpm (~32 dyn/cm <sup>2</sup> ) for 60 min	SDS-2.5% agarose gel electrophoresis and Western blotting	Decreased VWF multimer size	104

### **I.3.6.2. ADAMTS13 antigen**

Together with ADAMTS13 activity assays, ADAMTS13 antigen measurements help to assess disease severity and response to plasma exchange therapy. For this purpose, several assays using ELISA techniques have been developed with monoclonal<sup>105</sup> or polyclonal antibodies<sup>106</sup> directed against ADAMTS13. ADAMTS13 antigen levels in plasma from healthy subjects (n=99) span 740-1420 ng/ml, while levels in plasma from acquired TTP patients during acute episodes are found to vary from very low or undetectable to within the reference range. A severe reduction in ADAMTS13 antigen levels was found to be statistically associated with disease mortality<sup>107</sup>.

### **I.3.6.3. Anti-ADAMTS13 autoantibodies**

Anti-ADAMTS13 autoantibodies can be determined by functional activity or immunological assay. The former detects inhibitory anti-ADAMTS13 autoantibodies, while the latter identifies both inhibitory and non-inhibitory autoantibodies.

#### **I.3.6.3.1. Detection of inhibitory autoantibodies under static conditions**

The inhibitory effect of autoantibodies on ADAMTS13 can be analyzed in normal human plasma. ADAMTS13 inhibitors are titrated *in vitro* using classical mixing studies of heat inactivated plasma and normal plasma<sup>11;12</sup>, the patient's plasma being heated at 56°C to eliminate endogenous ADAMTS13 activity. Heat-treated patient plasma is then mixed 1:1 or at serial dilutions with normal human plasma and the mixtures incubated at 37°C for 120 min to allow for antibody-antigen interactions. ADAMTS13 residual activity is measured by any of the functional assays described in Table 1, the two most commonly used methods being the residual collagen binding activity and FRETs-VWF73 static assay. Inhibitor levels are expressed in Bethesda units per ml (BU/ml), one BU referring to the decrease in ADAMTS13 activity in normal plasma by 50%. Although a severe deficiency of ADAMTS13 activity is not found in all patients diagnosed with acquired TTP, determining the presence of neutralizing

ADAMTS13 autoantibodies is a specific method to diagnose acquired TTP. Furthermore, inhibitor detection helps clinicians to identify patients at risk and give them guidelines for combining immune therapy with plasma exchange therapy.

#### **I.3.6.3.2. Detection of inhibitory autoantibodies under flow conditions**

Inhibitor testing under flow conditions has not yet been implemented for routine testing. Two reports describe comparative measurements of patient plasma samples under static and shear conditions. In one study, the vortex-based shear assay led to inhibitor titers that were in good agreement with those obtained with the FRETs-VWF73 assay<sup>104</sup>. Another group of investigators described for longitudinal samples from one patient with acquired TTP who experienced multiple acute episodes of the disease discrepancies in ADAMTS13 activity levels when measured with static activity assays and the endothelial cell-based flow assay<sup>108</sup>.

#### **I.3.6.3.3. Detection of inhibitory and non-inhibitory autoantibodies by immunological assays**

Autoantibodies to ADAMTS13 are usually measured by ELISA where recombinant ADAMTS13 (rADAMTS13) is immobilized on solid phase<sup>109</sup>. Thereby, these autoantibodies were found to be primarily IgG (97% of acute TTP cases)<sup>109</sup> and mainly of subclasses IgG1 and IgG4<sup>86;110</sup>. IgM and IgA classes have been also observed, however to a lesser extent<sup>78;86;109</sup>.

#### **I.3.7. TTP treatment**

Plasma exchange of at least one plasma volume is the treatment of choice in acquired TTP. This therapy works by replacing ADAMTS13 and removing ADAMTS13 neutralizing autoantibodies. The response to plasma exchange is judged by the platelet count and anticipated after the second or third daily treatment. In conjunction to plasma exchange, patients with severe ADAMTS13 deficiency may begin corticosteroid therapy to suppress the

immune response or monoclonal anti-CD20 therapy to deplete autoantibody-producing B cells. If all of these treatments are insufficient, various immunosuppressive agents such as cyclophosphamide, vincristine, or cyclosporine may be used. Congenital TTP is treated by fresh frozen plasma infusion until remission is achieved; relapses may be prevented by regular prophylactic infusions<sup>111</sup>. Despite advances in treatment, the mortality rate is still high, with 10-20% of patients with either form of TTP succumbing to the acute disease episode<sup>112</sup>.

## **II. OBJECTIVE**

Anti-ADAMTS13 antibodies are usually characterized using plasma from patients with acquired TTP or less frequently by isolated IgG fractions. So far, a single brief description of affinity-purified anti-ADAMTS13 IgGs from one acquired TTP patient exist<sup>113</sup>. To elucidate the human anti-ADAMTS13 antibody response in acquired TTP, I sought to functionally characterize affinity-purified anti-ADAMTS13 IgG autoantibodies from acquired TTP patients with positive IgG titers and known inhibitors. The research was carried out in four distinct steps as described below.

### **II.1. Isolation of plasma derived ADAMTS13 (pADAMTS13)**

In 1996, two groups of investigators independently identified and partially purified ADAMTS13 from normal human plasma<sup>6,7</sup>. The authors reported on a protease with a high molecular weight of 300 kDa as judged by gel filtration. Four years later, the protease was isolated to homogeneity from normal human plasma using immunoabsorbent columns coupled to anti-ADAMTS13 polyclonal IgG from plasma of patients with acquired TTP. Thereby, pADAMTS13 was shown to contain species with a common N-terminal amino acid sequence<sup>14</sup>. Almost simultaneously, Fujikawa et al<sup>13</sup> isolated pADAMTS13 with a molecular weight of 150 kDa before and 190 kDa after reduction on SDS-PAGE from a commercial preparation of factor VIII/VWF. Lastly, in 2010, Hiura et al<sup>114</sup> used a cryosupernatant as a starting material to isolate ADAMTS13 using an anti-ADAMTS13 monoclonal antibody directed towards the disintegrin-like domain. Despite these published purification procedures, plasma derived ADAMTS13 is not yet commercially available for research purposes.

pADAMTS13 is the native autoantigen targeted by IgG autoantibodies in the plasma of acquired TTP patients, I therefore developed a method to purify ~1 mg of pADAMTS13 to serve as reference material to rADAMTS13 to characterize patients' derived IgGs.

As Baxter operates a commercial plasma fractionation facility, I screened different plasma fractionation intermediates for ADAMTS13 activity and identified one fraction free of major plasma protein contaminants with 0.5 U/ml of ADAMTS13 activity. Using this fraction as a starting material, ADAMTS13 was isolated by hydrophobic interaction chromatography followed by sequential affinity purification by means of a polyclonal goat anti-human ADAMTS13 antibody and a monoclonal antibody recognizing the C-terminal CUB domains of ADAMTS13. The present work describes the purification process and comprehensively characterizes the final pADAMTS13 preparation obtained.

## **II.2. Functional characterization of anti-ADAMTS13 autoantibodies affinity-purified from plasma of acquired TTP patients and a healthy donor pool**

In a second step, using immuno-adsorption on an ADAMTS13 affinity matrix followed by protein G, IgG ADAMTS13 autoantibodies were affinity-purified from three acquired TTP patients with positive IgG titers and known inhibitors. A plasma pool of 45 randomly selected healthy donors (HD) subjected to the same procedure served as control. The following properties of this IgG fraction were studied: The distribution of isotypes, affinity toward rADAMTS13 and pADAMTS13, inhibitory activity under static conditions and competitive inhibition of ADAMTS13 binding to VWF. I also compared recombinant ADAMTS13 versus pADAMTS13 for its ability to normalize von Willebrand factor-cleaving activity in the TTP derived IgGs preparations by overriding their inhibitory activity under static conditions. Here, I discuss the subclass differences in concentrations and affinities toward ADAMTS13, the required units of ADAMTS13 to overcome the threshold of the inhibitory autoantibodies titers under static conditions and the relevance of ADAMTS13-binding IgG autoantibodies in HD that lack inhibitor activity.

### **II.3. Epitope mapping of affinity purified IgG autoantibodies from plasma of acquired TTP patients and healthy individuals**

Antibodies from TTP patients have previously been studied using various epitope mapping techniques<sup>80;82;84;85</sup>. Applying patient-derived monoclonal antibodies and point mutated variants of ADAMTS13, these studies revealed that IgG autoantibodies target a major binding site on the surface of the spacer domain of ADAMTS13<sup>72;81;82;86;115</sup>, and identified additional epitopes located in other domains of the protease. By contrast, ADAMTS13-specific autoantibodies from healthy individuals remain ill-defined and their binding specificities are unknown.

Using a novel method based on peptide arrays displaying the entire sequence of ADAMTS13 as well as a previously described immunoprecipitation plus Western blotting (IP+WB) method, the binding specificity of anti-ADAMTS13 IgG antibodies derived from the plasmas of TTP patients as well as the pool of HD was elucidated.

### **II.4. Assessment of the inhibitory activity of affinity purified ADAMTS13 autoantibodies from patients with TTP under flow conditions**

The two most commonly used assays to test plasma samples for ADAMTS13 inhibitors in clinical practice are of the Bethesda type and employ the FRETs-VWF73 assay<sup>97</sup> or collagen binding assay (CBA)<sup>89</sup> (Table 1). Both assays are performed under static conditions without the vascular shear stress known to make the peptide bond in the VWF A2 domain accessible for cleavage by ADAMTS13 under physiological conditions. In the FRETs-VWF73 assay, cleavage is enabled using a short peptide substrate, whereas in the CBA, a denaturing agent is used to expose the cleavage site in full-length VWF. To circumvent the potential pitfalls of such assays, various shear-based systems for determining ADAMTS13 activity have been developed (Table 2), including one that measures the cleavage of multimeric VWF upon simulation of fluid shear conditions by a vortexer<sup>104</sup>, and one that evaluates in a parallel flow chamber the extent of cleavage of ULVWF when attached to endothelial cells<sup>101</sup>.

Although such assays are unlikely to be implemented for routine inhibitor testing, comparative measurements of patient plasma samples under static and shear conditions have been reported. In one study, the vortex-based shear assay yielded inhibitor titers that were consistent with those obtained by FRETs-VWF73 assay<sup>104</sup>. Another research group described for longitudinal samples from one acquired TTP patient experiencing multiple acute episodes of the disease discrepancies in ADAMTS13 activity levels when measured with static activity assays and the endothelial cell-based flow assay<sup>108</sup>.

In this last step, I investigated whether flow-based assays that more closely mimic the *in vivo* situation might more accurately predict the pathogenicity of autoantibodies in acquired TTP patients than conventional static assays. For this purpose, I developed a flow assay based on perfusion of a platelet-, erythrocyte-, VWF- and ADAMTS13-containing suspension over a surface coated with extracellular matrix (ECM) components. The ability of this assay to quantify inhibitors was demonstrated with a goat ADAMTS13 antiserum and further investigated using affinity-purified IgG antibodies from TTP patients. The results of this study are discussed in terms of discrepancies in inhibitor assessment when determined by a static and a flow-based assay. I also consider possible molecular mechanisms underlying these observations and their potential clinical implications.

### **III. MATERIALS AND METHODS**

#### **III.1. Sources of recombinant human ADAMTS13 and VWF and antibodies against ADAMTS13**

Wild-type rADAMTS13 (Baxter Bioscience, Vienna, Austria) was expressed by stably transfected chinese hamster ovary (CHO) cell lines in serum free medium as described<sup>116</sup> then purified by applying a conventional multi step chromatography and formulated in a physiological protein-free buffer.

rVWF (Baxter Bioscience) was co-expressed with the recombinant FVIII in CHO cells used to produce the recombinant FVIII product Advate then purified by a series of chromatographic steps and formulated in a physiological protein-free buffer as described<sup>117</sup>.

Monoclonal antibodies mAb257C2, mAb257A2-2, mAb242H2 referring to clone 257C2, 257A2-2, and 242H2, respectively were generated by standard hybridoma techniques by immunizing mice with HEK derived rADAMTS13 (Baxter Bioscience). Polyclonal goat ADAMTS13 antiserum (Baxter Bioscience) and a rabbit anti-ADAMTS13 total IgG fraction or affinity purified IgGs (as indicated) were obtained as described previously<sup>109</sup>. Using epitope mapping, mAb257C2 and mAb257A2-2 were found to bind the CUB domains of ADAMTS13 while mAb242H2 recognized the metalloprotease domain of ADAMTS13.

#### **III.2. Isolation of plasma derived ADAMTS13**

##### **III.2.1. Screening of plasma fractionation intermediates for pADAMTS13 activity**

Different plasma fractionation intermediates (Baxter plasma center, Vienna, Austria) were analyzed for ADAMTS13 activity in order to find a suitable starting material for the purification process of pADAMTS13. A summary of the fractionation process up to Fraction II is briefly described below and summarized in Figure 6.

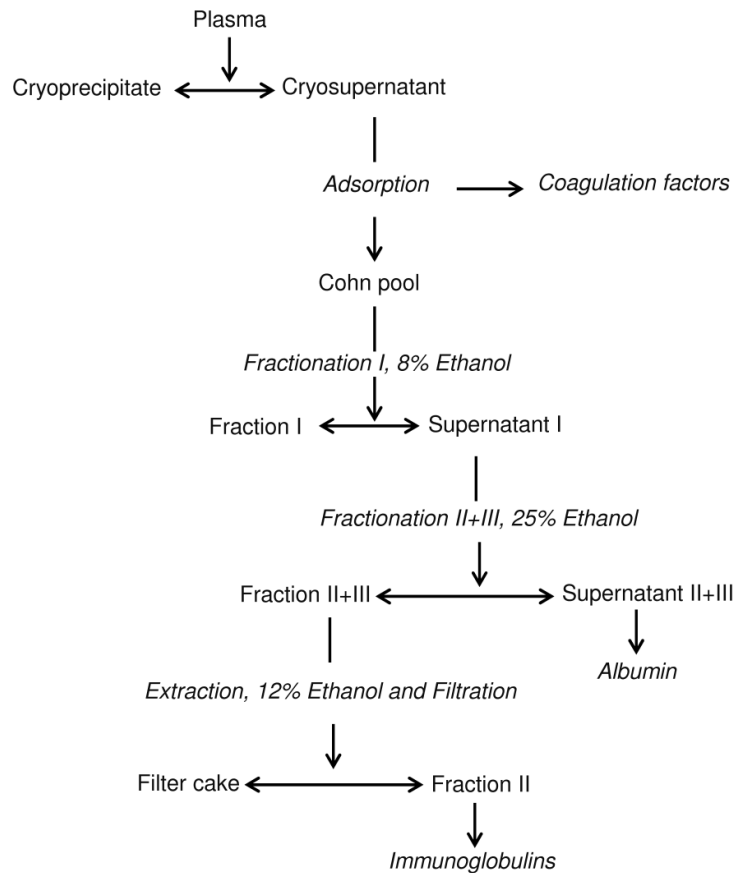


**Figure 6. Flow chart of the plasma fractionation process up to Fraction II.** The plasma fractionation process consists of thawing frozen plasma in cold conditions to produce cryoprecipitate. The cryoprecipitate is rich in fibrinogen and factor VIII. Several other coagulation factors such as FEIBA, factor IX-complex, VIII-concentrate, antithrombin III-complex, C1 esterase inhibitor are separated from cryosupernatant plasma by adsorptive technologies before it is processed by alcohol fractionation. Ethanol is added to the cryosupernatant plasma pool to a final concentration of 8 % (v/v). This latter step is designed "Fractionation I". By lowering the temperature and adjusting the pH, the precipitate "Fraction I" is prepared and collected. Supernatant I is further processed. Ethanol is added to Supernatant I to give a final concentration of 25 % (v/v). After reducing the temperature and adjusting the pH, the suspension is allowed to stand for at least 8 hours to complete the precipitation. Subsequently, the precipitate is collected in cooled centrifuges. Supernatant II+III is used for the production of human albumin. Fraction II+III is harvested from the rotors of the centrifuges then resuspended in a buffer solution and stirred for 2 hours. Ethanol is added to give a final concentration of 12 % (v/v). After lowering the temperature and adjusting the pH, the suspension is allowed to stand for at least 3 hours to complete the precipitation. The precipitate of the resuspended Fraction II+III is separated by filtration. The filter cake obtained from this last step is collected and further processed to give Fraction II that allows the separation of immunoglobulins.

Compared to the original plasma pool, Fraction I, Fraction II+III, the resuspended filter cake and Fraction II have a concentration factor of 100 (w/v), 22 (w/v), 22 (w/v), 77 (w/v), respectively. Therefore, 1 g of each fraction was resuspended in 25 mM Tris, 5 mM NaCl at

pH 7.40 to a volume equivalent to the original plasma pool (1:100 for Fraction I, 1:22 for Fraction II+III, 1:22 for the filter cake and 1:77 for Fraction II). The dissolved fractions were mixed on an overhead rotor then centrifuged at 4°C for 20 min at 21300xg. The resulting supernatants were screened for ADAMTS13 activity as described in chapter III.2.4 then diluted 1:10 with 25 mM Tris, 5 mM NaCl at pH 7.40 and subjected to SDS-PAGE using 4-20% Tris-Glycine gels (Cambrex Bio Science; Rockland, USA) under reducing conditions. Gels were stained with Biosafe Coomassie blue (Bio-Rad, Hercules, CA, USA).

### **III.2.2. Purification of pADAMTS13**

1.5 kg of the filter cake obtained from approximately 22 l of plasma was resuspended at 4°C in 19 l of a buffer containing 25 mM Tris-HCl, 5 mM NaCl, 0.5M  $(\text{NH}_4)_2\text{SO}_4$ , 1 mM PMSF, 10 mM benzamidine, pH 7.4. The resuspended filter cake was filtered through 0.22- $\mu\text{m}$  membrane filter. The filtrate (15 l) containing 9 mg of pADAMTS13 with a specific activity of 0.8 active unit per  $\mu\text{g}$  (U/ $\mu\text{g}$ ) as assessed by ADAMTS13 antigen ELISA and the FRET-S-VWF73 activity assay was subjected to hydrophobic interaction chromatography on a column (5x25 cm) of Phenyl Sepharose HP (GE Healthcare, Uppsala, Sweden). Stepwise elution was performed using 25 mM Tris-HCl, 5 mM NaCl, pH 7.4 (step A) followed by 25 mM Tris-HCl, 5 mM NaCl, 50% Ethylene Glycol, pH 7.4 (step B) in the presence of a protease inhibitor cocktail composed of 10 mM benzamidine (Sigma, St. Louis, MO), 1 mM PMSF (Sigma), 5  $\mu\text{M}$  E64 (Sigma) and 21  $\mu\text{M}$  Leupeptin (Sigma). ADAMTS13 activity recovery was 20% in the elution fractions of step A and 80% in step B. Elution pools originating from step A and B after 3 consecutive runs were collected and mixed. Following ethylene glycol removal by diafiltration, ammonium sulfate was added to 38% saturation. The precipitates obtained were isolated by centrifugation and resuspended with Tris buffered saline (TBS) in a volume equivalent to one-eighth of the original elution fraction volume. The resuspended pellet (350 ml) was treated for one h with the protease inhibitor cocktail described above, dialyzed

overnight against TBS containing 20 mM CaCl<sub>2</sub> and 2% sorbitol as a protein stabilizer. Recovery of ADAMTS13 antigen in the dialyzed solution was approximately 90% (~8 mg) of the initial protease amount before addition of ammonium sulfate. No significant change of the specific activity was observed indicating that the protease was not inactivated under the conditions applied. pADAMTS13 was further purified by immunoaffinity chromatography. The column was prepared by coupling 200 mg of goat polyclonal IgG antibody recognizing human ADAMTS13 to 20 ml of N-hydroxysuccinimide (NHS)-activated Sepharose matrix 4 fast flow (4FF) (GE Healthcare). Concentrated pADAMTS13 was loaded onto the equilibrated column and eluted with 0.1 M glycine-HCl, pH 2.7 in the presence of 2% sorbitol and the protease inhibitor cocktail. The elution pool was immediately neutralized with a one-tenth volume of 1 M Tris-HCl (pH 9.0) and dialyzed against 25 mM Tris-HCl, 5 mM CaCl<sub>2</sub>, 2% sorbitol, pH 8.0. 70% of ADAMTS13 antigen recovered in the elution pool (~5 mg) with a specific activity of 0.8 U/μg. As immunoglobulins were the major contaminants, affinity purified pADAMTS13 was applied onto a protein G Sepharose TM 4FF (0.7x 2.5 cm) column (GE Healthcare) using 0.1 M glycine-HCl, pH 2.7 for elution. 50% of purified pADAMTS13 antigen recovered in the flow through with a specific activity of 0.9 U/μg. To remove truncated variants 2 mg of this fraction were applied to an immunoaffinity column prepared by coupling 4 mg of mAb257A2 recognizing specifically the C-terminal CUB domains of ADAMTS13 to a 1 ml NHS-activated Sepharose column (0.7x 2.5 cm) (GE Healthcare). ADAMTS13 was eluted with 0.1M glycine-HCl, pH 2.7 containing 2% sorbitol. The eluate was immediately neutralized and dialyzed against 25 mM Tris-HCl, 5 mM CaCl<sub>2</sub>, 2% sorbitol, pH 8. Approximately 70% (~1.4 mg) of purified pADAMTS13 antigen recovered in the elution pool with a specific activity of 0.6 U/μg. Purity of samples was assessed by reducing SDS-PAGE on 4-12% gels (Invitrogen, Carlsbad, CA) followed by coomassie staining.

### **III.2.3. Assessment of ADAMTS13 antigen by ELISA**

ADAMTS13 antigen levels were analyzed by ELISA as described<sup>106</sup>. Briefly, microtiter plates (Nunc-Immuno Maxisorp, Roskilde, Denmark) were coated for 5 h at room temperature with a polyclonal rabbit anti-human ADAMTS13 IgG (2 µg/ml) diluted in 0.1 M bicarbonate solution, pH 9.6. After blocking with phosphate-buffered saline (PBS) containing 0.5% non-fat dry milk (Blotting Grade Blocker Non-Fat Dry Milk; Bio-Rad), the plate was washed three times with PBS containing 0.1% Tween-20. Samples diluted in blocking solution (100 µl/well) were added to the plate. After overnight incubation at room temperature, the plate was washed and bound ADAMTS13 was detected using HRP-conjugated purified polyclonal rabbit anti-human ADAMTS13 IgG preparation<sup>109</sup> (20 ng/ml) diluted in blocking solution followed by the addition of the chromogenic substrate (3,3',5,5'-tetra-methylbenzidine) (Sure Blue™ TMB Microwell Peroxidase Substrate, KPL, Maryland, USA). Color development was stopped with 1 N hydrochloric acid and the absorbance was read at 450 nm on an iEMS microplate reader (Labsystems, Helsinki, Finland). rADAMTS13 (0.5 ng/ml to 20 ng/ml) spiked into diluted ADAMTS13-depleted human plasma (Baxter Bioscience) prediluted 1:100 in blocking solution served as a calibration curve.

### **III.2.4. Assessment of ADAMTS13 activity by the FRET-VWF73 assay**

ADAMTS13 activity levels were analyzed by the FRET-VWF73 assay as described<sup>97</sup>. Briefly, assay calibration was obtained by using serial dilutions of normal human plasma (NHP; George King Bio-Medical, Overland Park, USA) of 1:25 (100%); 3:4 (75%); 1:2 (50%); 1:4 (25%); 1:10 (10%) and 1:20 (5%) in assay buffer (5 mmol/l Bis-Tris, 25 mmol/l CaCl<sub>2</sub>, 0.005% Tween-20, pH 6.0) containing 1mM Pefabloc SC (Boehringer, Mannheim, Germany) as a protease inhibitor and 1% of heat inactivated plasma to correct for a plasma matrix effect in the lower activity range of the standard curve. All test samples were subsequently diluted 1:25 in assay buffer. 100 µl of diluted standard or test sample were added to a 96-well

Nunc plate (Nunc-Immuno Maxisorp) then 100  $\mu$ l of 4  $\mu$ M FRETs-VWF73 substrate (Peptanova GmbH, Sandhausen, Germany) diluted in 5 mM Bis-Tris, 25 mM CaCl<sub>2</sub>, 0.005% Tween-20, pH 6.0 were added to each well. Fluorescence was measured at 30°C every 5 min in a fluorometer (Spectrafluor Plus, Tecan, Durham, NC) equipped with a 340 nm excitation filter and a 450 nm emission filter. The reaction rate was calculated by linear regression analysis of fluorescence over time from 5 to 60 min.

### **III.2.5. N-terminal amino acid sequence analysis**

ADAMTS13 variants copurified with full-length ADAMTS13 were separated by reducing 4-12% SDS-PAGE (Invitrogen) and electrotransferred to a polyvinylidene fluoride (PVDF) membrane (Invitrogen) for N-terminal amino acid sequence analysis. After transfer, the membrane was stained for one minute with Biosafe Coomassie blue (Bio-Rad) and destained with 40% methanol, 10% acetic acid, and air dried. N-terminal amino acid sequence analysis of the excised protein bands was carried out at Toplab (Martinsried, Germany) using standard Edman chemistry with a Procise 492A Protein Sequencer (Applied Biosystems, Forster City, CA, USA).

### **III.2.6. Detection of ADAMTS13 by immunoblotting**

Elution pools from the purification were subjected to 4-12% SDS PAGE and transferred to a nitrocellulose (NC) membrane (Invitrogen). The NC membrane was blocked for 1 h at room temperature with 3% non-fat dry milk (Bio-Rad) in TBS, 0.1% Tween-20 and incubated with polyclonal rabbit anti-ADAMTS13 followed by alkaline phosphatase (AP)-labeled goat anti-rabbit antibodies (Bio-Rad) or with mAb257C2 or mAb242H2 followed by AP-labeled rabbit anti-mouse antibodies (Bio-Rad) and colorimetric detection using 5-bromo-4-chloro-3'-indolyphosphate p-toluidine / nitro-blue tetrazolium chloride (BCIP/NBT; Bio-Rad).

### **III.2.7. Agarose gel electrophoresis and detection of ADAMTS13 and VWF**

To test for the presence of ADAMTS13 multimers, ADAMTS13 was separated on a 2.5% agarose gel by vertical electrophoresis using SE-600 gel electrophoresis unit (GE Healthcare) and the discontinuous buffer system as described<sup>118</sup> with minor modifications. Briefly gels were poured between glassplates of 18 x 16 cm size. Before casting the separating gel, a base of 2-2.5 cm 10% acrylamidgel (Bio-Rad) was poured to prevent the agarose gel from slipping out of the glass plates during electrophoresis. The buffer used for preparing the running gel had a final concentration of 200 mM Tris/ 100 mM Glycin/ 0.4% SDS, pH 9.2. Agarose gels were prepared using 2.5% agarose (SeaKem HGT(P)-Agarose; Biozym Diagnostics, Oldenburg, Germany). The stacking gel contained 0.8% agarose in 70 mM Tris, 4 mM Na<sub>2</sub>EDTA, 0.1% SDS, pH 8.5. The electrophoresis buffer was composed of 100 mM Tris, 150 mM glycine, 0.1% SDS, pH 8.5. Samples to be analyzed were diluted in the absence or presence of 50 mM DTT in 70 mM Tris-HCl, 4 mM Na<sub>2</sub>EDTA, pH 6.7, 2.4% SDS, 0.005% Bromophenol blue and 9 M urea. After incubation at 90°C for 5min, 30 µl samples were applied to each well and electrophoresis was started at a constant voltage of 30 V at 10°C for 16 h.

pADAMTS13 subjected to SDS-2.5% agarose under reducing and non-reducing conditions was transferred to a PVDF membrane. The membrane was blocked using casein blocking buffer (Sigma) for 1 h at room temperature. ADAMTS13 was visualized with polyclonal rabbit anti-ADAMTS13 antibodies followed by HRP-labeled rabbit anti-goat IgG secondary antibody (Pierce, Rockford, IL) and supersignal west femto maximum sensitivity substrate (Pierce).

Such gels were also used to test for VWF eventually copurified with pADAMTS13. VWF was visualized on PVDF membrane by probing with polyclonal goat anti-human VWF antibody (Dako, Glostrup, Denmark), HRP-labeled rabbit anti-goat IgG secondary antibody, and supersignal west femto maximum sensitivity substrate.

### III.3. Functional characterization of anti-ADAMTS13 autoantibodies affinity-purified from plasma of acquired TTP patients and a healthy donor pool

#### III.3.1. ADAMTS13 related variables in patient's plasmas and HD's pooled plasma

ADAMTS13 related variables in HD's pooled plasma and patient's plasmas are summarized in table 3. All plasma samples were tested for ADAMTS13 antigen (ADAMTS13: Ag)<sup>106</sup>, ADAMTS13 activity (ADAMTS13: Ac)<sup>97</sup>, functional ADAMTS13 inhibitors using the FRETSS-VWF73 assay<sup>97</sup>, total IgG and subclasses, IgM, IgA anti-ADAMTS13 antibodies<sup>119;120</sup> and ADAMTS13-specific IgG subclasses immune complexes as described<sup>120</sup>.

**Table 3. ADAMTS13-related variables measured in plasma samples from 3 acquired TTP patients and a HD pool**

	Patient 1	Patient 2	Patient 3	HD pool	
<b>ADAMTS13 antigen (µg/ml)</b>	0.21	0.04	0.03	0.61	
<b>ADAMTS13 activity (U/ml)</b>	<0.05	<0.05	<0.05	0.95	
<b>Functional inhibitors (BU/ml)</b>	1.60	1.75	1.33	Non detectable	
<b>Anti-ADAMTS13 Immunoglobulins (Titer)</b>	<b>Total IgG</b>	1:50	1:50	1:200	-
	<b>IgG1</b>	1:25	1:25	1:400	-
	<b>IgG2</b>	-	-	-	-
	<b>IgG3</b>	-	-	1:200	-
	<b>IgG4</b>	1:400	1:800	1:50	-
	<b>IgA</b>	-	-	-	-
	<b>IgM</b>	-	-	-	-
<b>ADAMTS13-specific immune complexes (Titer)</b>	<b>IgG1</b>	1:50	-	1:50	-
	<b>IgG2</b>	1:25	-	-	-
	<b>IgG3</b>	-	-	1:50	-
	<b>IgG4</b>	1:200	1:100	-	-

HD: Healthy donor pool  
A minus sign denotes a negative result.

### **III.3.2. Isolation of human anti-ADAMTS13 IgG antibodies and yields**

Two to three liters of plasma obtained during plasma exchange therapy from one patient diagnosed with acquired TTP secondary to Sibutramine (patient 1) and two patients with idiopathic acquired TTP (patients 2 and 3) were used as starting material to purify anti-ADAMTS13 IgG autoantibodies. Each participant provided informed consent according to the Declaration of Helsinki. Pooled NHP was obtained from 45 healthy donors (HD; Baxter plasma center) and pooled. Plasma samples were loaded onto an affinity matrix generated by coupling of 2 mg of rADAMTS13 to 1 ml of NHS-activated Sepharose 4FF (GE Healthcare) according to the manufacturer's instructions. Bound antibodies were eluted with 0.1 M glycine-HCl at pH 2.7 or 3.7 (as indicated). After neutralization, the elution pool was applied onto a 1 ml protein G Sepharose 4FF column (GE Healthcare). The IgG fraction was eluted with 0.1 M glycine-HCl at pH 2.7, then immediately neutralized and dialyzed against Tris-buffered saline at pH 7.4. The purity of the isolated IgG was assessed by SDS-PAGE under reducing conditions on Novex 4-20% Tris-glycine gels (Invitrogen) that were silver stained using the SilverQuest Silver Staining Kit (Invitrogen). Elution pools were analyzed for total human IgG levels using a commercial ELISA kit (Bethyl Laboratories, Montgomery, TX).

### **III.3.3. Determination of total IgG subclasses by ELISA**

Total IgG subclasses in the obtained HD or TTP derived IgG preparations were determined with an in-house quantitative IgG subclass specific ELISA developed on the basis of the single incubation multilayer immune technique<sup>121</sup> using paired-polyclonal sheep anti-human IgG subclass specific antibodies and the corresponding peroxidases. The ELISA was calibrated using the international certified reference material 470<sup>122</sup>, for which the IgG subclass distribution is known<sup>123</sup>. For each subclass ELISA, a linear dose-response range was established. Assays were done in 96-well Nunc Maxisorp F-96 polystyrene plates (Nunc-Immuno Maxisorp), incubated overnight at 4°C with 100 µl/well of non-conjugated

antibody at a protein concentration of 10 µg/ml in 0.1 M NaHCO<sub>2</sub>, 0.1 M Na<sub>2</sub>CO<sub>3</sub> at a pH of 9.5. Plates were washed with PBS containing Tween-20 and blocked by incubation with 200 µl/well dilution buffer (0.8% NaCl, 0.02% KCl, 0.02% KH<sub>2</sub>PO<sub>4</sub>, 0.126% Na<sub>2</sub>HPO<sub>4</sub>, pH 7.2-7.4, 0.05% Tween-20, 2 mM benzamidine and 1 mg/ml gelatin) at 37°C for 60 min. Plates were washed once and 100 µl/well of serially diluted standards or samples were added. After incubation at room temperature for 15 min, 100 µl/well of the respective peroxidase conjugate (at a concentration of 2 µg/ml in dilution buffer) were added. The plates were further incubated for 60 min at room temperature and the reaction stopped by washing. The bound peroxidase was visualized with 100 µl/well of TMB; the reaction was stopped with 100 µl/well of 1.5 M sulfuric acid and activity measured on a EL 808 microplate autoreader (Bio-Tek, Winooski, VT) at 450 nm. A calibration curve was established by correlating the logarithms of the blank-corrected mean optical densities for the standard dilutions with the logarithms of the known IgG subclass concentrations. The IgG subclass concentrations of the samples were extrapolated according to optical density measurements and using values that were within the previously determined dose-response range.

### **III.3.4. Determination of IgG and subclasses of anti-ADAMTS13 antibodies by ELISA**

IgG class and subclasses anti-ADAMTS13 antibodies were determined as described<sup>119;120</sup> with minor modifications. 100 µl rADAMTS13 (2 µg/ml) was directly coated onto ELISA microplates (Nunc-Immuno Maxisorp) overnight at 4°C. After blocking the non-specific binding sites with 200 µl of Protein-Free T20 (Pierce) containing 500 mM NaCl, the plates were incubated for 3 h at RT with with diluted plasma or increasing concentrations of the purified IgG. Bound anti-ADAMTS13 antibodies were detected with HRP-conjugated goat anti-human IgG (1:30000) (AbD Serotec, Martinsried, Germany) or HRP-conjugated mouse monoclonal anti-human IgG1 (1:2000) (Zymed Laboratories, Inc., San Francisco, CA); HRP-conjugated mouse monoclonal anti-human IgG2 (1:500) (Southern Biotech, Birmingham,

AL); HRP-conjugated mouse monoclonal anti-human IgG3 (1:3000) (Zymed) and HRP-conjugated mouse monoclonal anti-human IgG4 (1:3000) (Zymed) antibodies. Finally, the enzyme substrate TMB was added. Color development was stopped with 1.9 M H<sub>2</sub>SO<sub>4</sub> and the absorbance was read at 450 nm on an iEMS microplate reader (Labsystems, Helsinki, Finland). Between each step, the plates were washed with PBS containing 0.1% (v/v) Tween-20 (pH 7.4).

To determine whether rADAMTS13 in solution competes with the immobilized rADAMTS13 in the ELISA system for binding with the purified IgG anti-ADAMTS13 antibodies, rADAMTS13 (4-250 µg/ml) or 5% human serum albumin (HSA; Sigma) were incubated with a fixed concentration (1 µg/ml) of IgGs from the acquired TTP patients or the HD pool for 2 h at 37°C. The mixture was then analyzed by anti-ADAMTS13 IgG ELISA. By using the total IgG anti-ADAMTS13 antibodies ELISA, the competitive binding was assessed by comparing the optical densities (OD) values of each preparation before and after addition of rADAMTS13 or HSA in solution. Binding of IgGs in the absence of soluble rADAMTS13 was set to 100%.

### **III.3.5. Calculation of binding parameters for anti-ADAMTS13 IgG antibodies**

Assuming that the final absorbance values for ADAMTS13-specific IgG and subclasses by ELISA reflected the quantity of antibodies bound to rADAMTS13, dissociation constants ( $K_D$ ) was calculated using the equation  $A = A_{\max} \left\{ \frac{[L]}{(K_D + [L])} \right\}$ , where A is the absorbance at 450 nm,  $A_{\max}$  the maximum A at saturation and [L] the molar concentration of the purified antibody. Data were analyzed using SigmaPlot software 12.0 (Systat Software, San Jose, CA, USA) and  $K_D$  values were obtained by fitting the data to a one-binding-site model.

Affinities of the purified antibodies to rADAMTS13 were also determined by surface plasmon resonance technology using Biacore T200 (GE Healthcare). Purified autoantibodies were captured on a CM5 sensor chip via monoclonal mouse anti-human IgG (Fc) antibodies

(Human antibody capture kit, GE Healthcare). A series of dilutions of rADAMTS13 (5-160 nM) diluted in HEPES buffered saline containing 3 mM EDTA and 0.05% v/v surfactant P20 at pH 7.4 as running buffer was applied to the chip. The  $K_D$  was calculated assuming a homogeneous 1:1 interaction between the antibodies and rADAMTS13. The binding parameters of the anti-ADAMTS13 IgG antibodies for pADAMTS13 at 40 nM were determined in a similar fashion.

### **III.3.6. Quantitation of ADAMTS13 inhibitory activity of anti-ADAMTS13 IgG antibodies**

Purified IgG antibodies were tested for ADAMTS13 neutralizing activity by two common Bethesda-like methods using the minimal FRETs-VWF73 peptide<sup>97</sup> or full-length VWF as substrate<sup>89</sup> and by VWF multimer analysis<sup>118;124</sup>.

In the FRETs-VWF73 assay, equal volumes of NHP and the respective antibody solutions in 25 mM HEPES, 175 mM NaCl pH 7.4 containing 0.5% bovine serum albumin (BSA; Sigma) were mixed 1:1 or in serial dilutions. The mixtures were then incubated for 2 h at 37°C, were measured for ADAMTS13 residual activity as described<sup>97</sup>.

Collagen-binding activity was measured by the CBA assay as described<sup>89</sup> with minor modifications. Equal volumes of rADAMTS13 (2 U/ml) and various dilutions of the respective antibody solutions in 0.9% (w/v) NaCl containing 0.1% BSA were mixed and incubated for 2 h at 37°C. Samples were then diluted (1:10) in 1.5 M urea, 5 mM Tris, pH 8.0 and mixed with 9.3 mM BaCl<sub>2</sub> and 2 U/ml of (rVWF). After 2.5 h incubation at 37°C, the reactions were stopped by adding Na<sub>2</sub>SO<sub>4</sub> (8.25 mM) and ADAMTS13 residual activity was assessed using a commercial kit (TECHNOZYM® vWF:CBA ELISA; Technoclone, Vienna, Austria). In the FRETs-VWF73 and CBA assays, purified human IgG (Calbiochem, La Jolla, CA, USA) and goat IgG antiserum (Total IgGs) to ADAMTS13 were used as negative and positive control, respectively.

The purified antibodies' inhibitory activity (designed also as inhibitor titer) was calculated using one BU as the inhibitory activity that lowers the ADAMTS13 activity of plasma by 50%. ADAMTS13-neutralizing specific activity (BU/ $\mu$ g purified IgG) was calculated by dividing the inhibitor titer (BU/ml) of the IgG preparation by its concentration ( $\mu$ g/ml).

Finally, the antibodies' neutralizing activity was qualitatively assessed by VWF multimer analysis. The samples used for the CBA assay were analyzed by low-density horizontal SDS 1% agarose gel electrophoresis and immunostaining with a polyclonal rabbit anti-human VWF as described<sup>118;124</sup>.

### **III.3.7. Influence of anti-ADAMTS13 IgG antibodies on the ADAMTS13-VWF interaction**

Binding of ADAMTS13 to VWF was performed using a modified version of a previously described equilibrium plate-binding assay<sup>66</sup>. rVWF (7.5  $\mu$ g/ml) was coated onto a 96-well ELISA microplate in PBS overnight at room temperature. Unbound VWF was removed and stored at -80°C to further estimate the amount of immobilized VWF by means of a commercial ELISA (Asserachrom VWF, Boehringer). The plate was washed and blocked with 2% BSA in 0.1% Tween-20-PBS (PBST) for 1 h. After washing, rADAMTS13 diluted from 0 to 10 nM in PBST containing 1% BSA and 10 mM EDTA was added to the plate and incubated for 2 h. Bound ADAMTS13 was detected using 512 ng/ml of polyclonal rabbit anti-ADAMTS13 antibody that was affinity purified on ADAMTS13 columns followed by a combination of biotinylated goat anti-rabbit IgG (1:400 000) (Sigma) and HRP-conjugated streptavidin (Sigma). The binding curve was generated using SigmaPlot software 12.0. The data were fitted to the one binding site equation.

Competitive binding of the antibodies was assessed by incubating 5 nM rADAMTS13 with increasing amounts of the respective purified IgGs for 2 h at 37°C. A goat IgG antiserum to ADAMTS13 (Baxter Bioscience) served as positive control. Results were expressed as the

percentage of binding obtained in the absence of the added antibody. The apparent inhibition constants ( $K_i$ ) of the purified TTP-associated antibodies were calculated using the equation  $IC_{50} = (1 + [\text{immobilized VWF}]/K_D) \times K_i$ , where  $K_D$  was determined from the binding experiments.

Since the calculated apparent  $K_D$  significantly differed from that reported in the literature, such difference was investigated by two distinct ELISA set-ups. In the first one, either His-tagged human embryonic kidney cells (HEK) derived rADAMTS13 prepared as described<sup>109</sup> or CHO derived rADAMTS13 diluted from 0 to 5.1 nM in PBST containing 1% BSA and 10 mM EDTA were added to the plate and incubated for 2h. Bound ADAMTS13 was detected using the polyclonal rabbit anti-ADAMTS13 IgG antibody followed by the biotinylated goat anti-rabbit IgG as described above. In the second set-up, His-tagged HEK derived rADAMTS13 diluted from 0 to 328 nM in PBST containing 1% BSA and 10 mM EDTA was added to the plate and incubated for 2 h. Bound ADAMTS13 was detected using HRP-conjugated polyclonal rabbit anti-His IgG antibody (1:50000) (Bethyl Laboratories). In both set-ups, the binding curve was generated using SigmaPlot software 12.0. The data were fitted to the one binding site equation.

### **III.3.8. Recovery of rADAMTS13 and pADAMTS13 activity in the TTP derived IgG preparations**

Using the FRET-S-VWF73 assay, ADAMTS13 activity restoration in the presence of preadjusted inhibitor titers derived from patients 2 and 3 IgG preparations were analyzed; sufficient amounts of IgGs from patient 1 were not anymore available for this experiment. Predefined inhibitor titers (1, 2 and 4 BU/ml) of patient 2 and patient 3 preparations were preincubated at 37°C for 2 h with increasing activity increments of rADAMTS13 or pADAMTS13 (250-2500 mU/ml). ADAMTS13 recovered activity was assessed in the ADAMTS13-IgG antibody mixtures according to the FRET-S-VWF73 assay<sup>97</sup>. Reconstituted activity was plotted against the added ADAMTS13 activity and the required concentration of

rADAMTS13 to recover 500 mU/ml of ADAMTS13 activity was estimated by manual extrapolation for each inhibitor titer. The relation between anti-ADAMTS13 inhibitor titer (BU/ml) and estimated ADAMTS13 concentration necessary for a recovery of 500 mU/ml was assessed by linear regression analysis.

### **III.4. Epitope mapping of affinity purified IgG autoantibodies from plasma of acquired TTP patients and healthy individuals**

#### **III.4.1. Epitope mapping using immunoprecipitation (IP) plus Western blotting**

A modified IP plus Western blotting protocol was used to detect the antigen-antibody interaction in solution as described previously<sup>84;115</sup>. This experiment was performed by Veronica C. Casina under the supervision of Dr. X. Long Zheng at the Department of Pathology and Laboratory Medicine in the Children's Hospital of Philadelphia. 50 ng of wild type (WT) and ADAMTS13 variants with a V5-His epitope tagged at their C-termini were incubated with 250 ng of purified IgG (25  $\mu$ l) and 40  $\mu$ l of protein A Sepharose 4B (Invitrogen) in binding buffer (50 mM Tris-HCl, pH 7.6 containing 0.15 M NaCl, 1% BSA, 1% Triton X-100, and 0.1% Tween-20) at 4°C overnight. After being washed with the same buffer, bound recombinant WT and ADAMTS13 variants were eluted from the beads with 1xSDS-PAGE sample buffer (heated for 5 min at 100°C). The bound ADAMTS13 and variants were determined by Western blotting with anti-V5 IgG (Invitrogen) (1:5000) in 20 mM Tris-HCl, 150 mM NaCl, pH 7.5 containing 0.05% Tween-20, followed by infra-red Dye 800CW-labeled goat anti-mouse IgG (1:20,000) (LI-COR Bioscience, Lincoln, Nebraska) as previously described.

#### **III.4.2. Epitope mapping using ADAMTS13 peptide arrays**

Linear peptide epitope mapping was performed utilizing PEPperMAP® technology (PEPperPRINT GmbH, Heidelberg, Germany). The human IgG anti-ADAMTS13

autoantibodies purified either from the TTP patients plasma or the HD plasma pool were used to probe the peptide microarrays. The C- and N-termini of ADAMTS13 were first elongated by neutral GSGSGSG sequences to avoid truncated peptides. The protein sequence was then translated into 13mer peptides with a peptide-peptide overlap of 12 amino acids. Four arrays of 2710 peptides each were printed in duplicates. Each array was framed by a fusion tag (Flag) peptide (DYKDDDDKGG, 110 spots) and influenza virus hemagglutinin (HA) epitope tag peptide (YPYDVDPYAG, 110 spots) as controls. After pre-swelling the arrays for 10 min in PBST and 60 min in blocking buffer (Rockland Immunochemicals, Inc., Gilbertsville, PA), the peptide microarrays were initially incubated with the secondary F(ab')<sub>2</sub> goat anti-human IgG (H+L) antibody conjugated with DyLight680 (KPL) at a dilution of 1:5000 for 60 min at room temperature to verify that no significant background interactions occurred with the peptide arrays. The microarrays were washed twice, and incubated for an additional 30 min in PBST. The peptide arrays were then incubated overnight at 4°C with the TTP or HD derived purified IgG preparations at a final concentration of 10 µg/ml. Control incubation was performed with a monoclonal anti-ADAMTS13 antibody prepared in house and directed against the metalloprotease domain. After multiple washes in PBST, the slides were incubated for 30 min with the secondary antibody described above at a dilution of 1:5000 at room temperature. After two additional washes in PBST, the microarrays were rinsed with ultrapure water and dried in a stream of air. Green/red fluorescence intensities were acquired on an Odyssey Imager (Lincoln) at a spatial resolution of 21 µm. The staining of Flag and HA control peptides that frame the arrays gave rise to high and homogeneous spot intensities. For each spot, the fluorescence intensity was obtained by subtracting the background intensity from the foreground intensity. Intensity maps were generated based on the corrected foreground intensities which were averaged over the double spots. Epitopes were considered positive for peptides with a spot to spot deviation equal to or less than 50%. The averaged foreground fluorescence spot intensities were classified in three ranges: weak, medium and high.

### **III.4.3. Modeling of the ADAMTS13 metalloprotease domain**

The metalloprotease domain of ADAMTS13 was modeled via Swiss-model workspace by Dr. X. Long Zheng. The modeled residues (33-244) of the metalloprotease were based on the crystal structure of human ADAMTS4/5<sup>125</sup>. The modeled metalloprotease domain and the DTCS fragment<sup>58</sup> of ADAMTS13 were used to paint the antibody binding epitopes using Pymol software.

### **III.5. Assessment of the inhibitory activity of affinity purified ADAMTS13 autoantibodies from patients with TTP under flow conditions**

#### **III.5.1. Microchannels coating**

The Cellix VenaFlux platform (Cellix, Dublin, Ireland) was used to study ADAMTS13 activity under shear conditions. The system consists of a PC-controlled syringe pump with biochips (Vena8 Biochip; Cellix) enclosing eight parallel microchannels and an image analysis software. Each channel was first coated with cellular fibronectin (cFN) (except when indicated) from human fibroblasts at a concentration of 100 µg/ml at 4°C. After blocking with 4% BSA in PBS, the channels were washed and additionally coated with 160 µg/ml Horn collagen provided as a suspension of type I fibers from equine tendon (Nycomed, Linz, Austria) for 4 h at 4°C. Following another washing step, 100 µg/ml of rVWF was coated overnight at 4°C to the fibronectin-collagen coated channel surface. Prior to use, coated channels were washed with HEPES/NaCl buffer. Using phase contrast microscopy, the density and the homogeneity of the fibrillar collagen surface was checked on each channel before the perfusion experiments.

### **III.5.2. Preparation of washed platelets and erythrocytes**

A cell suspension of platelet and erythrocyte concentrates (Red Cross, Vienna, Austria) was used for the perfusion experiments. Upon reception, platelet concentrates were washed (1:1) with calcium free Krebs Ringer buffer (107 mM NaCl, 20 mM NaHCO<sub>3</sub>, 4 mM KCl, 2 mM Na<sub>2</sub>SO<sub>4</sub>, 19 mM Tri Na Citrate x 2H<sub>2</sub>O, 0.5% D+glucose pH 7.35) containing 10 mM acetylsalicylic acid (Sigma) to inhibit platelet activation. Following centrifugation at 1300xg for 10 min at 10°C, the pellets were resuspended with Krebs Ringer buffer containing 2.5 mM CaCl<sub>2</sub> in a volume equivalent to the supernatant then centrifuged as described above to prepare a final platelets stock suspension of 10<sup>9</sup> platelets/ml. In parallel, the erythrocyte concentrates were washed (1:1) with 10 mM HEPES and 150 mM NaCl pH 7.35 then centrifuged at 1300xg for 10 min at 10°C. The supernatant was discarded and the erythrocytes were washed with calcium containing Krebs Ringer buffer to generate an erythrocytes stock suspension of 80% hematocrite (Hct). A final suspension was prepared with the washed platelets and erythrocytes adjusted to their original value in blood of 2.5x10<sup>8</sup> platelets/ml and 40% Hct. The blood cells suspension was then treated with DiOC<sub>6</sub> (2 μM) (Invitrogen) to render platelets fluorescent.

### **III.5.3. Perfusion studies and image analysis**

The reconstituted blood cells suspension was aspirated with a PC-controlled syringe pump through each of the eight channels enclosed in the biochip that was mounted on the stage of a Zeiss Axiovert 40 CFL inverted Epi-Fluorescence microscope. The flow was adjusted to obtain distinct wall shear rates as indicated. During the experiment and after 5 min, images of seven fields along each channel reflecting the platelets adhesion profile were acquired via a cooled high-resolution Hamamatsu ORCA-03 digital camera connected to the microscope. The area covered with platelet-aggregates was estimated in pixel at each of the seven images using the Image-Pro Plus Analysis Software. A threshold value above background

was selected to obtain the total area of aggregates covering the channel per image. Platelet accumulation was measured as the percentage of platelet coverage on the coated surface and calculated following the formula: % coverage =  $\text{Sum} \times 100 / (\text{Image width} \times \text{Image Height})$  where Sum refers to the mean of the seven total areas of coverage (in pixels). Image width and height are also expressed in pixels.

To examine platelets binding to rVWF, a purified mouse monoclonal anti-human CD42b (50  $\mu\text{g/ml}$ ) (eBioscience, San Diego, CA) or an isotype control (50  $\mu\text{g/ml}$ ) (mouse IgG1, kappa, DakoCytomation, US) were added to the cell suspension containing  $2.5 \times 10^8$  platelets/ml, 40% Hct and 10  $\mu\text{g/ml}$  rVWF. Following 15 min of incubation time, the mixture was perfused at a wall shear rate of  $1500 \text{ s}^{-1}$  over a surface coated with cFN, collagen and rVWF.

#### **III.5.4. ADAMTS13 flow based activity assay**

The ADAMTS13 activity assay is based on preventing VWF-dependent platelet aggregate formation by ADAMTS13 under flow. For this, rADAMTS13 or pADAMTS13 (1-4 U/ml) were added concurrently to rVWF (10  $\mu\text{g/ml}$ ) to the cell suspension and perfused at a shear rate of  $2500 \text{ s}^{-1}$ . After 5 min of perfusion, the mean surface area covered with platelet-aggregates in seven continuous positions was calculated. The surface coverage of platelet aggregates obtained without addition of ADAMTS13 was set to 100%. By plotting platelet surface coverage (%) against ADAMTS13 activity, a standard curve was generated using the SigmaPlot software 12.0. Data were fitted by a 4 parameter logistic function.

#### **III.5.5. Inhibitor activity assessment under flow conditions**

The ability of the established ADAMTS13 activity flow assay to measure ADAMTS13 inhibitors was assessed with a goat antiserum to ADAMTS13 (Z797). In one set of experiments, the serum was adjusted to various FRETs-VWF73-based inhibitor titers (2-8 BU/ml), mixed with a fixed amount of rADAMTS13 or pADAMTS13 (4 U/ml end

concentration), and incubated for 2 h at 37°C. The ADAMTS13-IgG antibody-containing solutions were then added to the cell suspension containing rVWF (10 µg/ml) and immediately perfused over the rVWF-coated microchannels at a shear rate of 2500 s<sup>-1</sup>. The increase as a percentage of surface coverage by platelet aggregates after 5 min of continuous flow was plotted against the added FRET5-VWF73-based inhibitor titer of the antibody.

Affinity purified anti-ADAMTS13 IgG autoantibodies obtained from acquired idiopathic TTP patient 2 and 3 plasmas were adjusted to predefined FRET5-VWF73-based inhibitor titers (0.3-12 BU/ml end titer) and analyzed as described above.

### **III.5.6. ADAMTS13 activity recovery under static and shear conditions in predefined inhibitor preparations adjusted with goat antiserum to ADAMTS13**

Predefined inhibitor titers (1, 2 and 4 BU/ml) of the goat antiserum to ADAMTS13 were preincubated at 37°C for 2 h with increasing activity increments of rADAMTS13 (1-16 U/ml). ADAMTS13 activity recovery was assessed by testing the mixture under static conditions using the FRET5-VWF73 assay or under flow conditions. For the latter condition, the cell suspension containing rVWF (10 µg/ml) was first spiked with the ADAMTS13-IgG antibodies mixture described above then perfused over the coated channels for 5 min at a shear rate of 2500 s<sup>-1</sup>. A range of 80 to 30% of surface coverage (equivalent to 0.5 U/ml to 4 U/ml) was selected to evaluate the recovery of ADAMTS13 activity in the presence of a known FRET5 based inhibitor titer. The reconstituted activity was plotted against the added rADAMTS13 activity and the required concentration of rADAMTS13 to recover 2 U/ml ADAMTS13 activity was estimated by manual extrapolation for each inhibitor titer and each assay condition.

## **IV. RESULTS**

### **IV.1. Isolation of plasma derived ADAMTS13**

#### **IV.1.1. Identification of a cold ethanol-fractionated human plasma intermediate with a substantial amount of ADAMTS13 activity**

Cold ethanol-fractionated human plasma intermediates were screened for ADAMTS13 activity. The filter cake, equivalent to the filtration step in the processing of Fraction II+III precipitate to Fraction II was found to contain a substantial amount of the protease activity. ADAMTS13 activity was measured in each intermediate of the plasma fractionation process up to Fraction II (Figure 7A). Following fractionation I with 8% ethanol (v/v), ADAMTS13 remained in the supernatant I (0.81 U/ml) then precipitated in Fraction II+III (0.92 U/ml) when 25% ethanol (v/v) was added to the supernatant I. After resuspension of Fraction II+III with 12% ethanol and filtration, ADAMTS13 activity remained in the filter cake (0.56 U/ml) with a specific activity of 0.8 U/ $\mu$ g.

Compared to the other intermediates, the filter cake was free of the predominant HSA (band at ~67 kDa) and free of the immunoglobulins heavy and light chains (Figure 7B). Consequently, this intermediate was selected as a starting material for the purification of pADAMTS13.

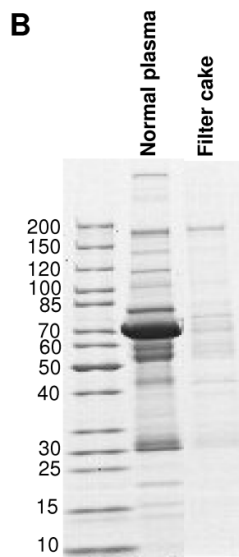
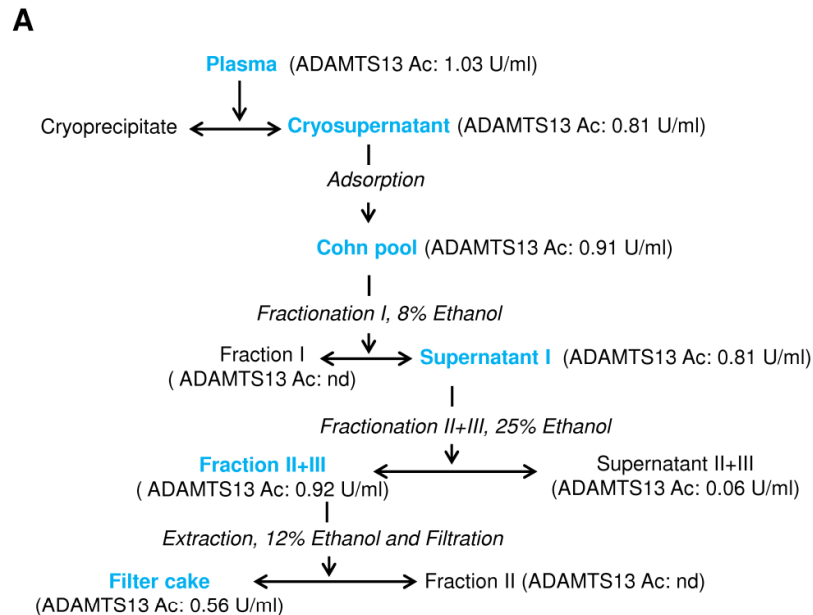


**Figure 7. Identification of a Cohn fraction intermediate as a starting material for pADAMTS13 purification.** **A)** Screening for ADAMTS13 activity in the plasma fractionation intermediates. ADAMTS13 activity (ADAMTS13 Ac) in plasma is approximately 1 U/ml. Following fractionation I, ADAMTS13 remains in the supernatant I (0.90 U/ml) then precipitates in Fraction II+III (0.92 U/ml). After resuspension of Fraction II+III with 12% ethanol and filtration, ADAMTS13 activity remained in the filter cake. nd denotes non-detectable. Blue color refers to the fractions containing ADAMTS13 activity. **B)** SDS-PAGE and total protein staining of the selected Cohn fraction intermediate with reference to normal plasma. Normal plasma and the “filter cake” resuspended in a volume equivalent to the original plasma were diluted 1:20 in TBS and subjected to SDS-PAGE (4-20%) under reducing conditions. Protein bands are stained with Coomassie blue. Molecular weights of marker proteins (MBI Fermentas, USA) are indicated on the left. The filter cake selected as a starting material to purify ADAMTS13 contained ~0.6 U/ml of ADAMTS13 activity and was devoid of human albumin (~65 kDa) and immunoglobulines heavy (50 kDa) and light chains (25 kDa).

#### IV.1.2. Affinity purification of pADAMTS13

The resuspended and filtered filter cake was subjected to hydrophobic interaction chromatography followed by ammonium sulfate precipitation and a first step of affinity purification using a goat polyclonal anti-ADAMTS13 antibody. At this step, the specific activity in the elution pool was  $\sim 0.8$  U/ $\mu$ g indicating that the protease was not inactivated by the applied elution conditions (Figure 8A). Total protein staining revealed the elution pool to be significantly depleted of several contaminants that were present in the load (Figure 8A); however human IgGs were apparently co-purified with pADAMTS13. Western blot analysis with rabbit polyclonal anti-ADAMTS13 antibody showed heterogeneous sizes of ADAMTS13 indicating the presence of ADAMTS13 variants in the elution pool (Figure 8B). The approximate molecular masses of the immunopositive variants deduced from electrophoretic mobility were 190, 170, 130 and 80 kDa (Figure 8B).

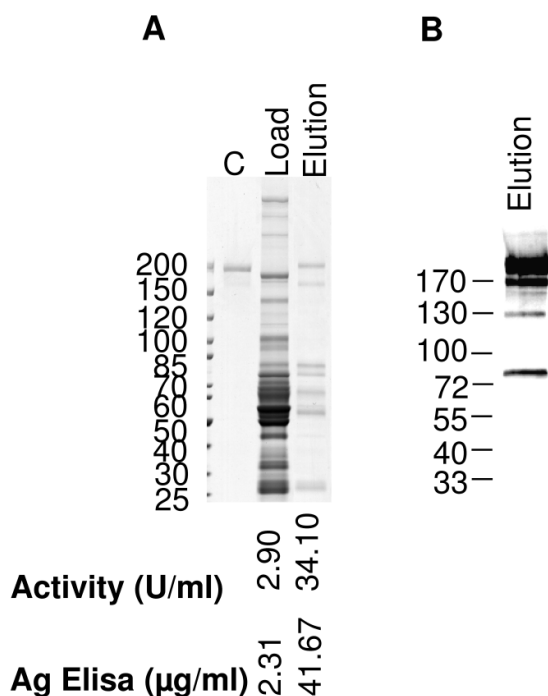


**Figure 8. pADAMTS13 isolation using goat anti-ADAMTS13 affinity matrix.** The resuspended pellet resulting from the ammonium sulfate precipitation step was processed by affinity purification using polyclonal goat anti-ADAMTS13 antibody. The load and the elution pool were subjected to SDS-PAGE (4-12%) under reducing conditions. **A)** Total protein staining. Gel staining was performed with Coomassie blue. ADAMTS13 activity and antigen are indicated at the bottom of the panel. Lane C refers to rADAMTS13 (50  $\mu$ g/ml) used as a control. **B)** Detection of ADAMTS13 in the elution pool by Western blot. ADAMTS13 was detected in the elution pool using rabbit polyclonal anti-ADAMTS13 antibody followed by AP-conjugated goat anti-rabbit antibody. In panel A and B, molecular weights of marker proteins are indicated on the left.

Next, human IgGs were removed from the obtained elution pool by passage through a column of Protein G. pADAMTS13 in the flow-through fraction was significantly depleted of

IgGs as assessed by SDS-PAGE and total protein staining while maintaining a high specific activity of 0.88 U/ $\mu$ g (Figure 9A). Interestingly, only half of the loaded amount of purified pADAMTS13 antigen (~119  $\mu$ g/ml) recovered in the flow through fraction (~63  $\mu$ g/ml) (Figure 9A) whereas the remaining part was found in the elution pool as detected by antigen ELISA and the activity assay suggesting that these IgGs specifically bound to ADAMTS13. This result was also confirmed by Western blot analysis (Figure 9B). Since ADAMTS13 was still active in the elution pool, it is unlikely that these IgGs were ADAMTS13 functional inhibitors.

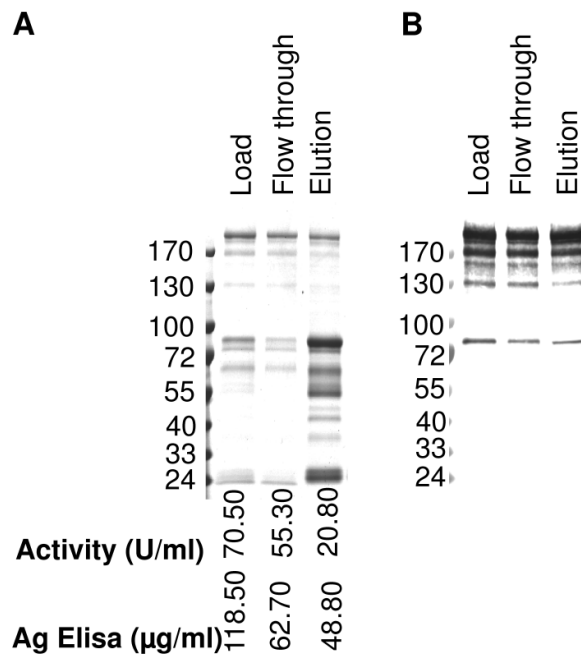


**Figure 9. Removal of IgG impurities from pADAMTS13.** Affinity purified pADAMTS13 variants were loaded on a Protein G column. Each sample representing the chromatographic procedure was subjected to SDS-PAGE (4-12%) under reducing conditions. Molecular weights of marker proteins are indicated on the left in panel A and B. **A)** Coomassie blue stained gel. ADAMTS13 activity and antigen concentrations are indicated on the bottom. The flow through containing pADAMTS13 was devoid of human IgGs and displayed high ADAMTS13 specific activity. **B)** Western blot analysis with rabbit polyclonal anti-ADAMTS13 antibody. A significant portion pADAMTS13 was co-eluted with human IgGs.

To obtain a pool enriched with full-length ADAMTS13 and devoid of potentially active C-terminally truncated ADAMTS13 variants, the IgG-free pADAMTS13 preparation was applied to a second immunoaffinity column coupled with mAb257A2 recognizing the C-terminal CUB domains of ADAMTS13. The 190 kDa pADAMTS13 was purified to almost apparent homogeneity with a specific activity of 0.6 U/ $\mu$ g (Figure 10A).

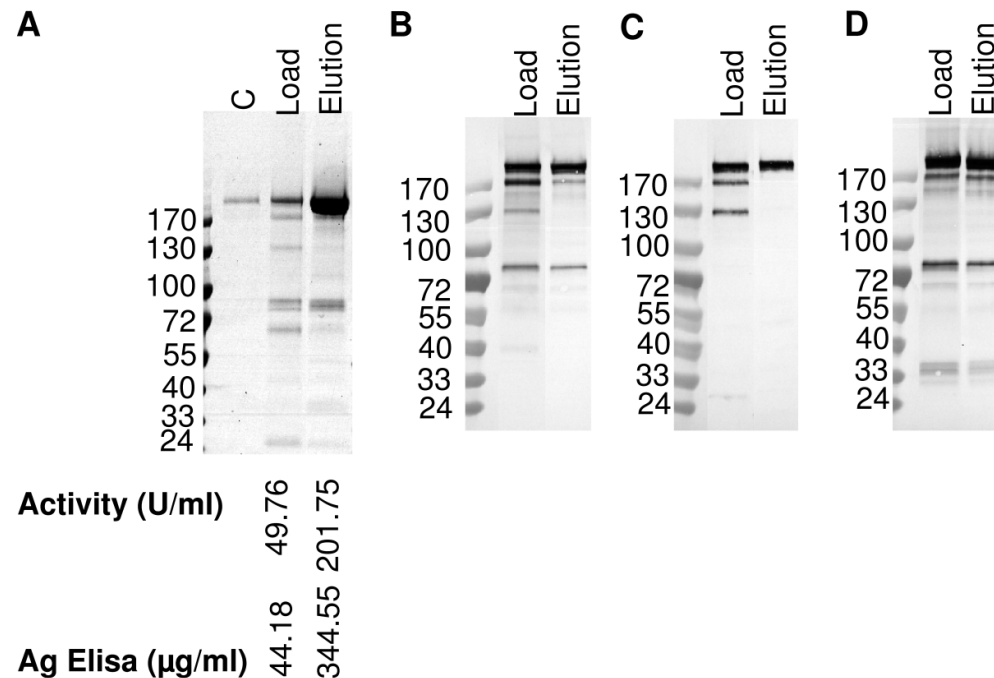


**Figure 10. Isolation of full-length pADAMTS13 with mAb257A2 recognizing the ADAMTS13 CUB domains.** IgG free pADAMTS13 was applied to a second immunoaffinity column coupled with monoclonal mAb257A2 recognizing the C-terminal CUB domains. The load and the elution pool were subjected to SDS-PAGE 4-12% under reducing conditions. Molecular weights of marker proteins are indicated on the left of each panel. **A)** Coomassie blue stained gel. Lane C: rADAMTS13 (50 µg/ml) used as a control. ADAMTS13 activity and antigen concentration are indicated on the bottom. Full-length ADAMTS13 was purified with a specific activity of 0.6 U/µg. **B-D)** Western blot analysis with goat polyclonal anti-ADAMTS13 (B) or mAb242H2 recognizing ADAMTS13 catalytic domain (C) or mAb257C2 detecting ADAMTS13 CUB domains. Equivalent amount of active units (25 U/ml) are loaded in each lane of panel B, C and D. The 190 kDa band present in the elution pool is the only active band since the two other ADAMTS13 variants (170 kDa and 80 kDa) (B) are free of the catalytic domain of ADAMTS13 (C).

An 80 kDa band was co-purified with full-length ADAMTS13. Western blot analysis with a rabbit polyclonal anti-ADAMTS13 antibody revealed this preparation to contain only a minor contamination with other ADAMTS13 variants (170 kDa and 130 kDa) (Figure 10B). Using mAb242H2 that recognizes its metalloprotease domain, the load contained full-length ADAMTS13 (190 kDa) as well as two C-terminally truncated variants of ADAMTS13 (170 and 130 kDa) (Figure 10C) whereas the elution pool contained only the 190 kDa ADAMTS13 variant. When mAb257C2 recognizing the ADAMTS13 CUB domains was employed for epitope mapping, two N-terminally truncated ADAMTS13 variants (~170 and 80 kDa) were

found together with the 190 kDa band in the load as well as in the final ADAMTS13 preparation (Figure 10D). In conclusion, these data indicate that the final preparation of pADAMTS13 contained full-length pADAMTS13 with minor impurities of truncated 170 kDa and 80 kDa variants both of which were free of the catalytic domain and therefore non-active. N-terminal sequencing of the 190 kDa band seen in the final preparation of pADAMTS13 revealed the expected sequence of AAGGI (single-letter amino acid codes). For the 80 kDa band, the N-terminal sequence EVQLV was identified, which is not present in ADAMTS13. Residual amounts of human immunoglobulin heavy chain that had not adequately been resolved from the 80 kDa ADAMTS13 variant on the gel might have been responsible for this result. The combined data suggest that the final pADAMTS13 preparation with the 190 kDa band contained mainly active variant and as a minor contamination, catalytic domain free- and therefore inactive ADAMTS13 variants.

#### **IV.1.3. Identification of multimer species of pADAMTS13 using agarose gel electrophoresis**

To gain information regarding the subunit composition of ADAMTS13, the elution pool containing the isolated full-length pADAMTS13 was separated on a reducing and a non-reducing high-resolution SDS-2.5% agarose gel. Surprisingly, visualization of ADAMTS13 using HRP-conjugated rabbit polyclonal anti-ADAMTS13 antibody revealed that pADAMTS13 as well as rADAMTS13 appeared to be multimeric under non-reducing conditions (Figure 11A). Under reducing conditions (Figure 11B) the multimeric pattern disappeared suggesting the possibility of disulfide-mediated oligomerization of the protease. As the multimeric pattern of ADAMTS13 was reminiscent of that of VWF, I checked whether VWF is complexed with the higher molecular weight forms of pADAMTS13. The final preparation of pADAMTS13 was subjected to non-reducing SDS-2.5% agarose gel electrophoresis followed by chemiluminescent visualization of VWF using a rabbit polyclonal anti-VWF antibody. Some VWF could indeed be detected in the purified pADAMTS13

sample. However, compared to the typical multimeric pattern of VWF, pADAMTS13 contained low molecular weight species of VWF (Figure 11C) indicating that ADAMTS13 multimers was not bound to typical VWF multimers.

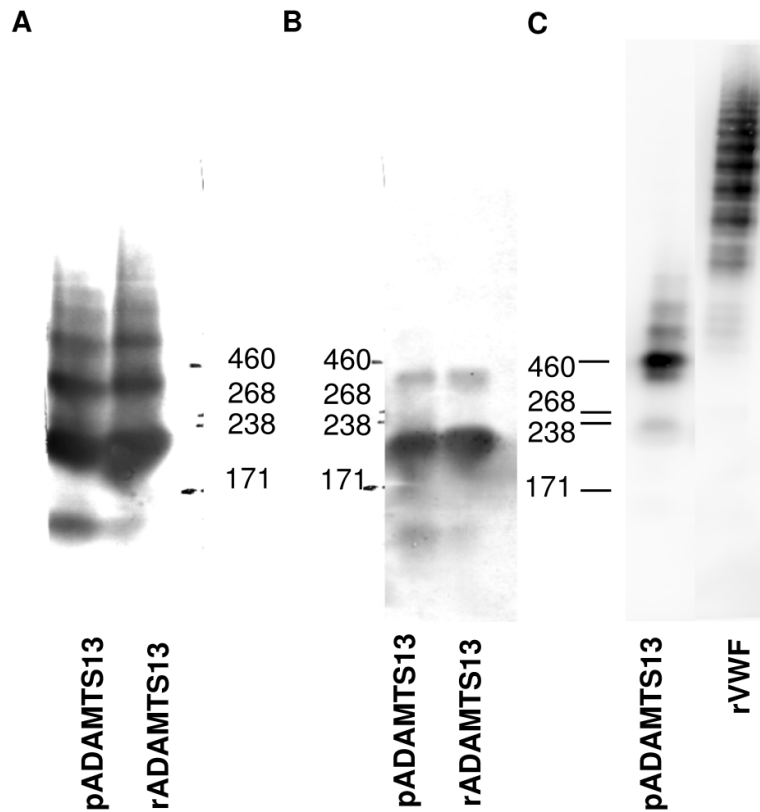


**Figure 11. Presence of ADAMTS13 oligomers in the final pADAMTS13 preparation. A-B)** Western blot analysis of ADAMTS13 in the final pADAMTS13 preparation. The final pADAMTS13 preparation (2.5 µg/Lane) as well as equivalent amounts of rADAMTS13 used as a control were subjected to 2.5% agarose gel electrophoresis under non-reducing (A) and reducing conditions (B) followed by Western blot analysis with rabbit polyclonal anti-ADAMTS13 antibody. Multimers were visualized by chemiluminescence using HRP-labeled rabbit anti-goat IgG secondary antibody. The final pADAMTS13 preparation contained ADAMTS13 oligomers. **C)** Co-purification of plasma VWF with pADAMTS13. pADAMTS13 (5 µg/lane) as well as rVWF (20 ng/Lane) used as a control were subjected to 2.5% agarose gel electrophoresis under non-reducing conditions followed by Western blot analysis with rabbit polyclonal anti-VWF antibody. Multimers were visualized by chemiluminescence using HRP-labeled goat anti-rabbit IgG secondary antibody. ADAMTS13 oligomers were co-purified with low molecular weight plasma derived VWF. Molecular weights of marker proteins (HiMark, Invitrogen) are indicated on each panel.

## IV.2. Functional characterization of anti-ADAMTS13 autoantibodies affinity-purified from plasma of acquired TTP patients and a healthy donor pool

### IV.2.1. Affinity purification of human anti-ADAMTS13 IgG antibodies

Anti-ADAMTS13 antibodies were purified by specific immuno-adsorption on an ADAMTS13 affinity matrix followed by protein G from three acquired TTP patients and somewhat surprisingly also from a HD plasma pool. The purity of the isolated IgGs was confirmed by SDS-PAGE under reducing conditions (Figure 12); no IgM or IgA was detected as measured by total human IgA and total human IgM ELISA (data not shown).

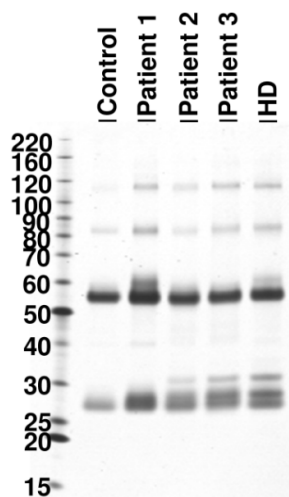


**Figure 12. Purity of the affinity-purified anti-ADAMTS13 IgG antibodies from acquired TTP patients and a HD pool.** Equal amounts of IgG (100 ng), isolated from pooled HD plasma and plasma from three acquired TTP patients by affinity chromatography, as well as purified human IgG (Control) were separated by SDS-PAGE (4-20%) under reducing conditions. The silver-stained gel revealed similar intensities for the heavy and the light chains of the affinity-purified IgGs and total IgG control.

IgG autoantibody yield and isotype distribution were quantitated by total human IgG ELISA (Table 4). The plasma bags of the three TTP patients contained 0.8-2.5  $\mu\text{g}$  and the HD plasma pool 0.8  $\mu\text{g}$  of ADAMTS13-specific IgGs per ml of plasma. All four IgG subclasses were present in the purified samples (Table 4); however, the isotype distribution differed from that usually seen in normal human plasma. Unexpectedly, and in contrast to earlier findings<sup>110</sup>, IgG2 was the major subclass in all preparations, followed by IgG1, then IgG3/IgG4. The low abundance particularly of IgG4 (Table 4) might have been caused by the preferential sequestration of this subclass in immune complexes in the starting material (Table 3).

**Table 4. Yield and subclass distribution of affinity-purified anti-ADAMTS13 IgG antibodies from Acquired TTP patients and a HD pool**

Starting material	Affinity purified anti-ADAMTS13 IgG ( $\mu\text{g}$ )*	Total human IgG Subclasses (%)**			
		IgG1	IgG2	IgG3	IgG4
Patient 1	0.81	25	69	3	3
Patient 2	0.95	16	73	1	10
Patient 3	2.50	34	57	8	1
HD	0.82	38	45	16	1

\* Normalized per 1 ml of plasma applied as a starting material to ADAMTS13 affinity matrix

\*\* Each IgG subclass is expressed as a percentage of the total concentration of IgG1-4 subclasses.

#### **IV.2.2. Specificity and affinity of purified anti-ADAMTS13 IgG antibodies**

The ability of affinity-purified antibodies to bind to ADAMTS13 as a solid phase antigen was assessed by ELISA. Autoantibodies from the TTP patients and the HD plasma pool bound in a dose-dependent manner to ADAMTS13 (Figure 13A), however, with significantly lower signals in the HD antibody preparations. Next, the antibodies' specificity was checked by competitive binding experiments. Soluble ADAMTS13, but not HSA, competed with the binding of autoantibodies to immobilized rADAMTS13 (Figure 13B). In all samples, albeit to a varying extent, such binding was suppressed in a dose-dependent manner by the added ADAMTS13 (Figure 13C).

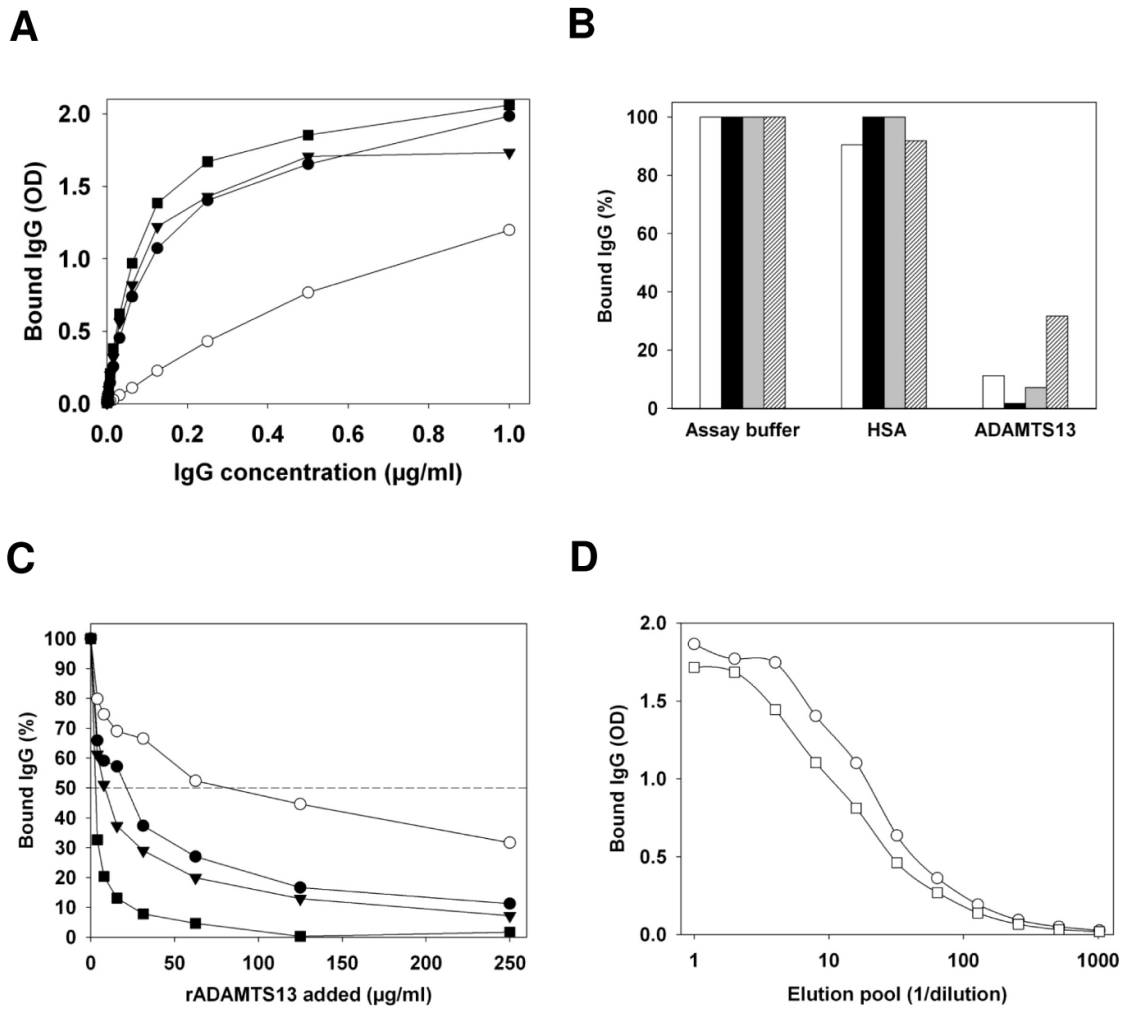


**Figure 13. Binding of affinity-purified anti-ADAMTS13 IgG antibodies from acquired TTP patients and a HD pool to ADAMTS13 using ELISA. A)** Binding to solid-phase ADAMTS13. Isolated anti-ADAMTS13 IgG antibodies from acquired TTP patients 1 (closed circle), 2 (closed square) and 3 (closed triangle), and the HD pool (open circle) were tested at various concentrations for their ability to bind to solid-phase ADAMTS13 by ELISA. All samples showed concentration-dependent binding with significantly lower signals for the HD antibody preparation. **B)** Specificity of binding to ADAMTS13 by competitive ELISA. rADAMTS13 (250 µg/ml) or 5% HSA were incubated with a fixed concentration (1 µg/ml) of IgGs from acquired TTP patients 1 (white bar), 2 (black bar) and 3 (gray bar) as well as the HD pool (dashed bar) for 2 h at 37°C. The mixture was then analyzed by anti-ADAMTS13 IgG ELISA. Binding of IgGs in the absence of soluble rADAMTS13 was set to 100%. All IgG preparations showed substantially reduced binding in the presence of soluble ADAMTS13 but not HSA. **C)** Dose-dependent competitive binding. Increasing amounts of rADAMTS13 ranging from 4 to 250 µg/ml were incubated with a fixed concentration (1 µg/ml) of IgGs from acquired TTP patients 1 (closed circle), 2 (closed square) and 3 (closed triangle) as well as the HD pool (open circle) as described in panel C. The dashed line indicates 50% of competitive suppression. Antibody binding decreased in an ADAMTS13 dose-dependent manner. **D)** Isolation of ADAMTS13-specific IgGs from a HD pool at different pH. HD autoantibodies to ADAMTS13 were purified by ADAMTS13 affinity chromatography using the HD plasma pool as a starting material. Elution was performed at pH 2.7 (open circle) or pH 3.7 (open square). Each elution pool was tested by the anti-ADAMTS13 IgG ELISA. The IgG binding values were plotted against increasing dilutions of the elution pool (log scale). The less stringent elution (pH 3.7) did not cause a lower ADAMTS13 binding response.

Elution of the anti-ADAMTS13 antibodies isolated from the HD pool with a buffer of lower stringency (pH 3.7) gave rise to an ADAMTS13 binding response that was similar to that using the standard preparation (Figure 13D), suggesting that these IgG autoantibodies exhibited no changed affinity due to elution conditions.

According to the ELISA dose-response curves shown in Figure 13A, the apparent  $K_D$  was 0.9 nM for patient 1 and 0.5 nM for patients 2 and 3 (Table 5). Binding parameters for the HD pool IgGs could not be determined as the dose-response curve did not achieve saturation. By using Biacore and a series of dilutions of rADAMTS13 (5-160 nM), the  $K_D$  ranged between 0.5 and 1.5 nM for the TTP antibodies. All patients shared comparable association and dissociation rate constants (Table 5).

**Table 5. Calculated dissociation constants for the interaction of TTP-associated IgG autoantibodies with rADAMTS13 and pADAMTS13 using ELISA and/or Biacore**

	ELISA	Biacore				
	Coated rADAMTS13	rADAMTS13 (5-160 nM)		rADAMTS13 (40 nM)	pADAMTS13 (40 nM)	
Source of IgG	Apparent $K_D$	$K_a$ ( $10^4 M^{-1} s^{-1}$ )	$K_d$ ( $10^{-4} s^{-1}$ )	$K_D$ (nM)	$K_D$ (nM)	$K_D$ (nM)
Patient 1	0.9	18.2	1.6	0.9	1.2	0.5
Patient 2	0.5	14.3	0.7	0.5	0.4	0.2
Patient 3	0.5	23.8	3.5	1.5	0.5	0.2

When pADAMTS13 was applied at a concentration of 40 nM on the Biacore chip, the calculated  $K_D$  ranged between 0.2 and 0.5 nM for the TTP antibodies. Binding of a comparable concentration of rADAMTS13 to the same IgG preparations revealed a slightly lower affinity ranging between 0.5 and 1.2 nM (Table 5). A rADAMTS13 binding was also discernible for IgGs from the HD pool, but the signals were too low for meaningful calculation

of kinetic parameters. Representative binding curves are shown in Figure 14A and 14B for patient 3 and the HD pool, respectively.

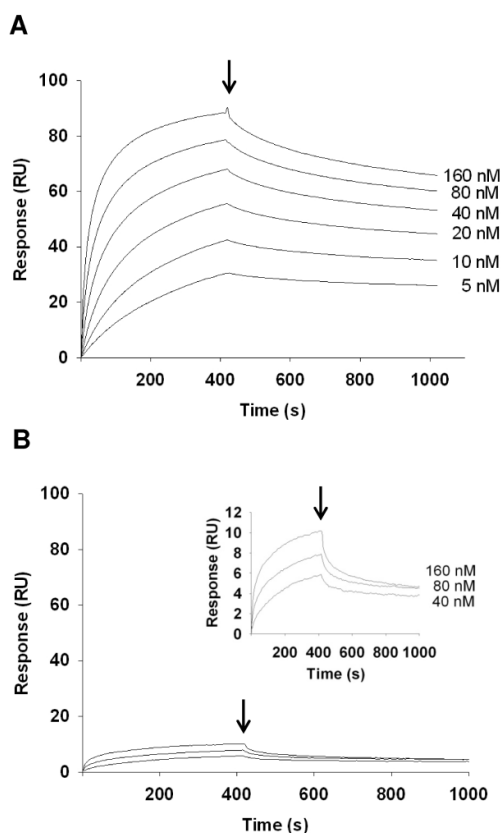


**Figure 14. Binding of affinity-purified anti-ADAMTS13 IgG antibodies to rADAMTS13 using Biacore.** Isolated IgG preparations from acquired TTP patient 3 (A) and a HD pool (B) were captured onto CM5 biosensor chips and real-time association and dissociation of ADAMTS13 was assessed at the indicated concentrations using Biacore equipment. The arrow indicates replacement of rADAMTS13 by running buffer. The ordinate represents the binding response as measured by resonance units (RU). The inset in (B) shows a zoom of the curves.

#### IV.2.3. Subclass-specific affinities of purified anti-ADAMTS13 IgG antibodies

To elucidate IgG subclass contributions to the observed affinities toward ADAMTS13, IgG preparations from TTP patients 2 and 3 and from the HD pool were assayed by ELISA for their capacity to bind ADAMTS13 using subclass-specific detection antibodies. Patient 1 derived IgG preparation was not available in sufficient amounts for this experiment. Figures 15A-D show the dose-response curves obtained for each subclass as well as the apparent calculated  $K_D$  for each positive subclass. ADAMTS13-specific responses were shown for IgG1, IgG2 and IgG4 but not IgG3, isolated from patient 2, and for IgG1, IgG2 and IgG3, but hardly for IgG4 from patient 3. For the HD pool, responses were weakly detectable for IgG1, IgG2 and IgG3 (Figure 15A-D).

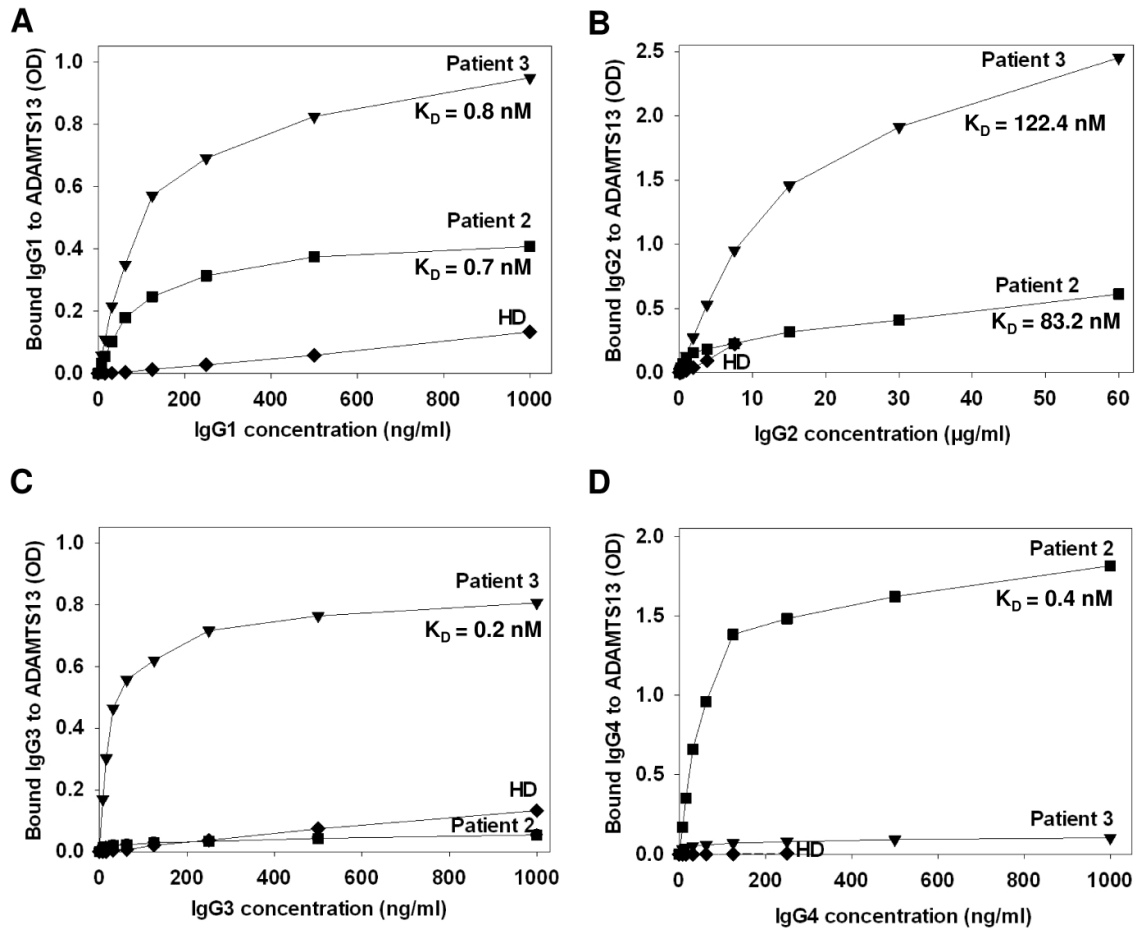


**Figure 15. Subclass-specific binding of affinity-purified anti-ADAMTS13 IgG antibodies to ADAMTS13 using ELISA.** Purified IgG preparations from patient 2 (square), patient 3 (triangle) and the HD plasma pool (diamond) were tested for their subclass-specific binding capacity to solid-phase ADAMTS13. The respective IgG subclass concentrations were adjusted according to the total human IgG subclass ELISA data (Table 4). Shown are the results for IgG1 (**A**), IgG2 (**B**), IgG3 (**C**) and IgG4 (**D**) as well as the calculated apparent dissociation constants ( $K_D$ ) for all positive subclasses. Substantially higher concentrations of IgG2 were required to achieve measurable binding to ADAMTS13.

All subclasses present in minute amounts (1%), i.e. IgG3 in patient 2 and IgG4 in patient 3, had very weak affinities toward ADAMTS13. The apparent  $K_D$  for each subclass in the TTP patients' preparations was 1 nM except for IgG2 which was ~100-fold higher for both patient plasmas. Thus, the apparent affinities were mainly caused by IgG1 and IgG4 for patient 2, and by IgG1 and IgG3 for patient 3, and were comparable to those determined for total IgG.

#### **IV.2.4. Neutralizing activity of purified anti-ADAMTS13 IgG autoantibodies**

Specific neutralizing activity of the TTP-antibodies was 0.1-0.5 BU per  $\mu\text{g}$  of affinity-purified IgG as determined by the FRETTS-VWF73 assay, and 0.1-0.4 BU/ $\mu\text{g}$  of IgG when full-length VWF was the substrate (Figure 16A). A goat IgG antiserum directed against human ADAMTS13 used as positive control exhibited low neutralizing activity (0.02 and 0.03 BU per  $\mu\text{g}$  of IgG according to FRETTS-VWF73 and CBA assay), as the goat anti-ADAMTS13 fraction was not affinity-purified against ADAMTS13 but total goat IgG. IgG autoantibodies from the HD plasma pool and purified human IgG used as negative control did not inhibit ADAMTS13 activity in either assay. When FRETTS-VWF73 activities were determined in the presence of serial dilutions of the IgG preparations from the three TTP patients, their distinct inhibitory potencies became particularly evident. An approximately 6-fold excess was required to decrease the ADAMTS13 activity by 50% for patient 3 compared to patient 2 (Figure 16B).

Residual proteolytic activity of ADAMTS13 determined by rVWF multimer analysis showed that in the presence of the TTP-antibodies and polyclonal goat antiserum VWF multimers were not degraded (Figure 16C). In contrast, ADAMTS13-specific IgGs from the HD pool showed a multimeric VWF pattern that was identical to that obtained for the purified human IgG control, indicating that these antibodies are non-neutralizing. Thus, all three assays showed strong neutralizing specific activity for the purified anti-ADAMTS13 antibodies from TTP patients and a non-inhibitory nature for the IgGs from the HD pool.

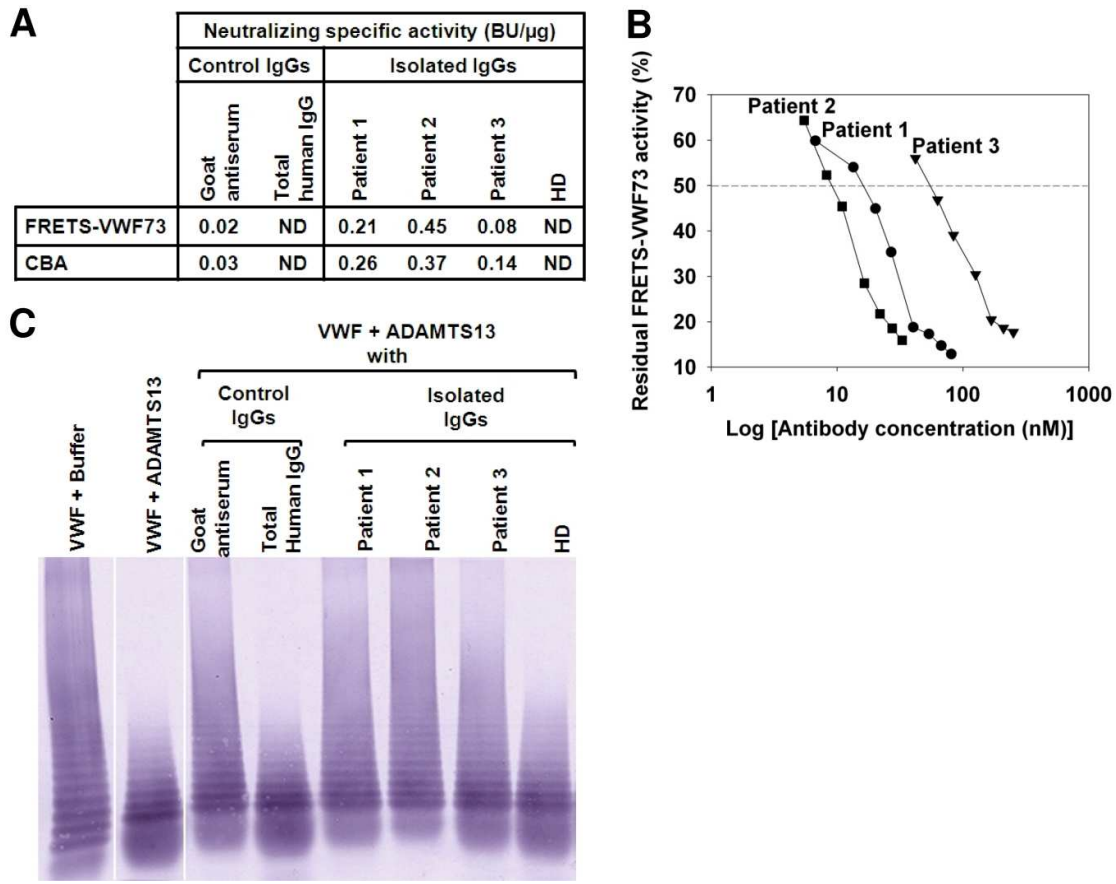


**Figure 16. Inhibitory activity of affinity-purified anti-ADAMTS13 IgG antibodies.** Purified IgG preparations from three acquired TTP patients and a HD plasma pool were tested for their capacity to inhibit ADAMTS13. Purified goat anti-ADAMTS13 IgG and total plasma IgG served as positive and negative control, respectively. **A)** Quantitative assessment of residual ADAMTS13 activity by FRETS-VWF73 and CBA assay. Neutralizing specific activities are expressed in BU/ $\mu$ g IgG. nd, non-detectable. **B)** Dose-response curves. The indicated concentrations of purified IgG from patients 1, 2 and 3 were incubated with NHP and FRETS-VWF73 activities measured. Residual ADAMTS13 activities are expressed relative to non-inhibited NHP (100%). Differences in specific inhibitory activity between patients were clearly discernible. **C)** Qualitative assessment of residual ADAMTS13 activity by multimer analysis. The extent of rVWF cleavage in the presence of the control IgGs (10  $\mu$ g/ml total human IgG and 95  $\mu$ g/ml goat antiserum IgG) or the isolated IgGs (10  $\mu$ g/ml) was visualized by agarose-gel electrophoresis. Samples without rADAMTS13 (VWF + buffer) and with buffer instead of antibody (VWF + ADAMTS13) served as additional controls.

#### IV.2.5. Influence of purified anti-ADAMTS13 IgG autoantibodies on the interaction between ADAMTS13 and VWF by ELISA

To investigate whether the isolated antibodies directly affect the interaction between ADAMTS13 and its substrate, an ADAMTS13-VWF binding ELISA was established. The interaction of the two proteins was dose related, with an apparent  $K_D$  of 0.4 nM (Figure 17A), suggesting that its affinity is significantly higher than previously reported (14 nM)<sup>66</sup>. The investigation of this issue is described in chapter IV.2.5.1. The interaction of rVWF and rADAMTS13 was inhibited in a dose-dependent manner by all TTP antibodies and the goat anti-ADAMTS13 antibody used as positive control, but not by antibodies purified from the HD pool (Figure 17B).

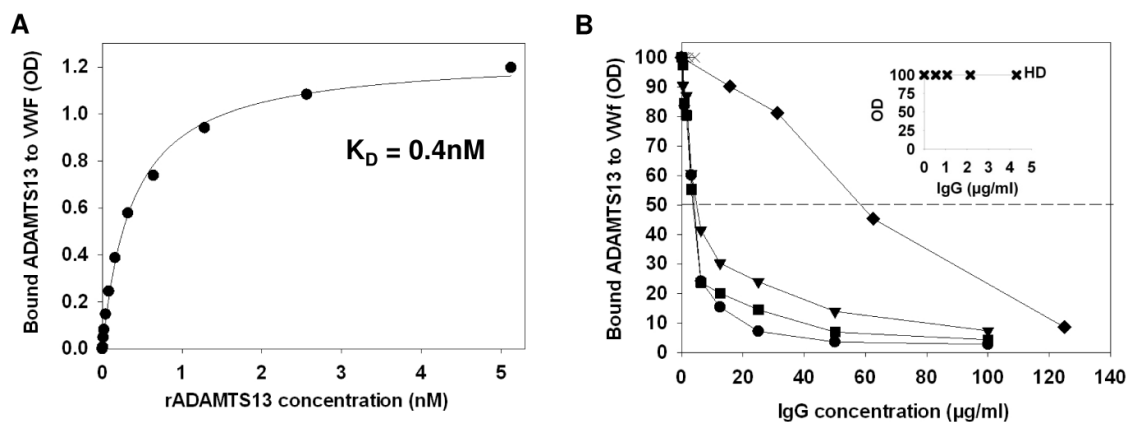


**Figure 17. Interference of affinity-purified anti-ADAMTS13 IgG antibodies with the rADAMTS13-rVWF interaction.** **A)** ELISA-based assay for the rADAMTS13-rVWF interaction. Purified rVWF (7.5  $\mu\text{g/ml}$ ) was coated onto a microtiter plate and incubated with increasing concentrations of rADAMTS13 (0 to 10 nM). Bound ADAMTS13 was detected using an affinity-purified polyclonal rabbit anti-ADAMTS13 antibody. The resulting binding curve was used to calculate the apparent  $K_D$  for the VWF-ADAMTS13 interaction. **B)** Inhibition of the VWF-ADAMTS13 interaction by isolated anti-ADAMTS13 IgG autoantibodies. ADAMTS13 (5 nM) was mixed with the indicated concentrations of IgGs from acquired TTP patient 1 (circle), patient 2 (square), patient 3 (triangle) and a HD pool (cross, in the inset) and tested for interaction with VWF. Goat anti-ADAMTS13 IgG (diamond) served as positive control. Results are expressed in terms of the binding of ADAMTS13 to VWF in the absence of antibody (100%). The dashed line indicates 50% inhibition. The inset shows a zoom of the data for the HD pool.

The antibody concentration required to achieve 50% inhibition was 4  $\mu\text{g/ml}$  for patients 1 and 2, and 5.2  $\mu\text{g/ml}$  for patient 3, corresponding to  $K_i$  values of 0.3 and 0.4 nM respectively.

#### **IV.2.5.1. Investigation of the root cause of the increased apparent affinity of ADAMTS13 to solid phase VWF by ELISA**

Compared to Majerus et al<sup>66</sup> who detected V5-tagged ADAMTS13 with an anti-V5 detection antibody, I employed for the ELISA a tag-free rADAMTS13 that was detected by an affinity-purified polyclonal rabbit IgG anti-human ADAMTS13 antibody. Therefore, in a first step, I checked whether distinct sources of ADAMTS13 bind rVWF with a different apparent affinity in an identical ELISA set-up. A comparison of His-tagged HEK derived rADAMTS13 with CHO derived non-tagged rADAMTS13 gave rise to apparent  $K_D$  values of 0.24 nM (Figure 18A) and 0.27 nM (Figure 18B), respectively, indicating that distinct sources of ADAMTS13 show comparable apparent affinities towards rVWF. In a second step, I used His-tagged HEK-derived ADAMTS13 and exchanged the ADAMTS13 detection antibody by a polyclonal rabbit IgG anti-His tag antibody. The calculated apparent affinity decreased from 0.24 nM to 8.98 nM (Figure 18C), a value that does not significantly differ from the one reported by Majerus et al<sup>66</sup>. Together, these data indicate that the antibody used for detection of ADAMTS13 in my set-up was the reason for the observed difference in affinity, probably because it recognizes several epitopes on ADAMTS13 compared to the single C-terminal His tag or V5 epitope.

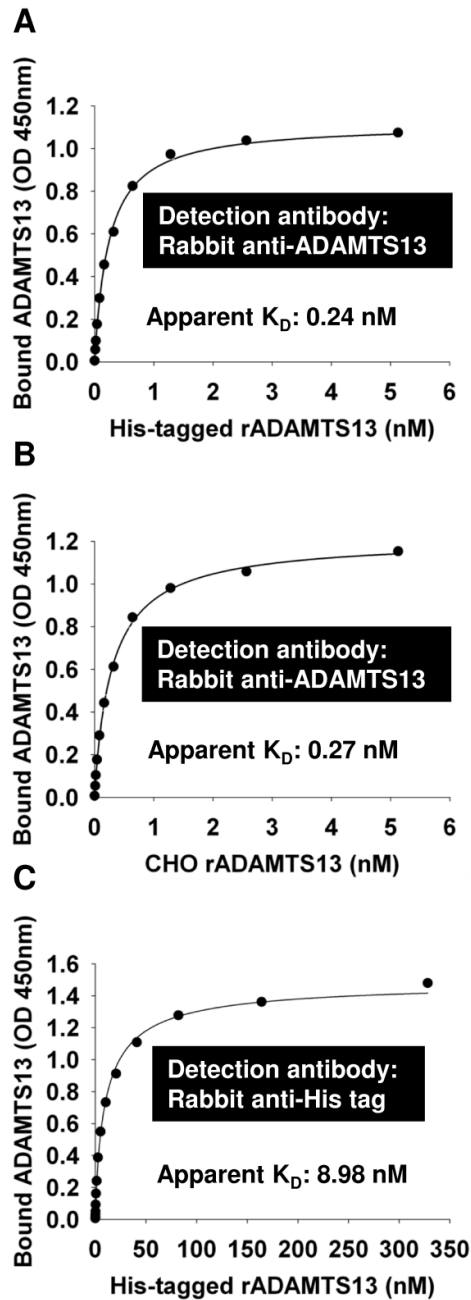


**Figure 18. Influence of the choice of the detection antibody in ADAMTS13-VWF binding ELISA on the apparent affinity of VWF to ADAMTS13. A-B)** ELISA-based assay for the rADAMTS13-rVWF interaction using His-tagged HEK derived rADAMTS13 (A) or CHO derived rADAMTS13 (B). Purified rVWF (7.5  $\mu\text{g/ml}$ ) was coated onto a microtiter plate and incubated with increasing concentrations of rADAMTS13 (0 to 5.1 nM). Bound ADAMTS13 was detected using an affinity-purified polyclonal rabbit IgG anti-ADAMTS13 antibody. Note that the calculated apparent  $K_D$  in panel A and B is comparable. **C)** ELISA-based assay for the rADAMTS13-rVWF interaction using His-tagged HEK derived rADAMTS13 and an anti-His tag antibody for detection. In this setup, the apparent  $K_D$  increased to  $\sim 9$  nM. In panel A, B and C, the resulting binding curves were used to calculate the apparent  $K_D$  for the VWF-ADAMTS13 interaction.

#### IV.2.6. Overriding of the inhibitory activity of the patients IgGs by rADAMTS13 and pADAMTS13 in vitro

The ability of rADAMTS13 and pADAMTS13 to override the neutralizing activity of the purified anti-ADAMTS13 IgGs inhibitors from patients 2 and 3 was investigated using the FRETs-VWF73 assay. ADAMTS13 was supplemented in at least four concentrations to

preadjusted inhibitor titers (1 BU/ml; 2 BU/ml and 4 BU/ml) and recovered activities were plotted against the added ADAMTS13 activities. The amounts of purified rADAMTS13 or pADAMTS13 necessary to saturate and overcome the neutralizing autoantibodies at each selected inhibitor titer were similar for both patients and increased proportionally to the inhibitor levels as illustrated in Figure 19A for patient 2 and in Figure 19B for patient 3.

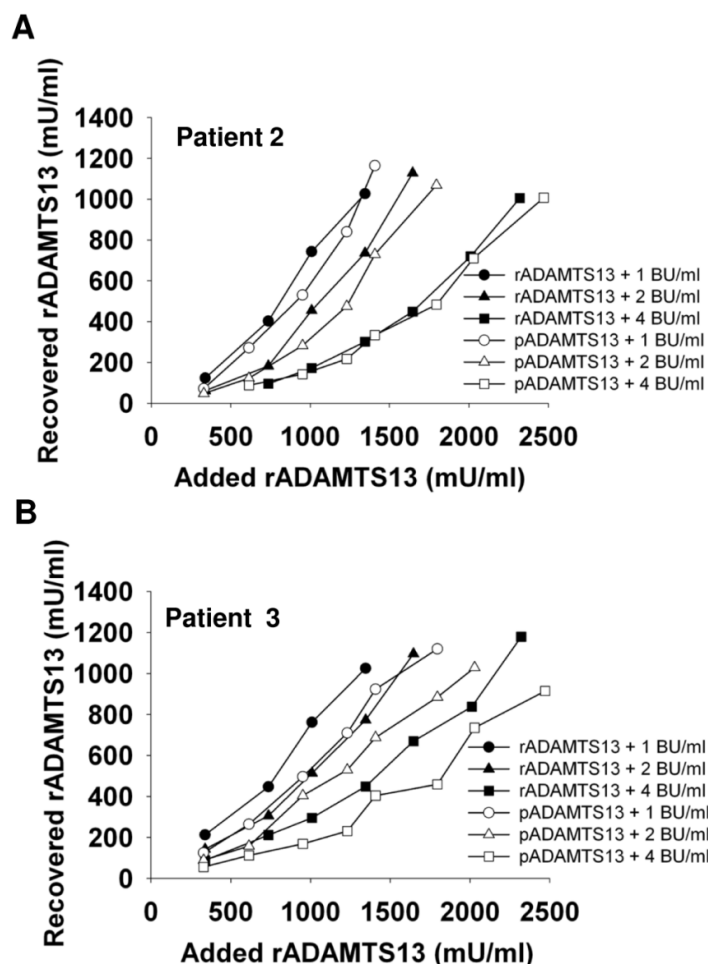


**Figure 19. ADAMTS13 recovery in the presence of IgG preparations from TTP patients with defined inhibitor titers.** IgG preparations derived from patient 2 (A) and patient 3 (B) were preadjusted to inhibitor titers of 1 BU/ml (circle); 2 BU/ml (triangle) and 4 BU/ml (diamond). Increasing amounts of rADAMTS13 (closed symbols) or pADAMTS13 (open symbols) were added and ADAMTS13 recovery was analyzed by the FRETs-VWF73 assay.

By extrapolating manually the required activity of ADAMTS13 to recover an effective concentration of 0.5 U/ml (EC50), the relation between inhibitor titers and EC50 of pADAMTS13 or rADAMTS13 in the patients' preparations was found to be linear (Figure 20)

yielding to the formulas:  $EC_{50} = 0.2 \times (\text{anti-ADAMTS13 inhibitor titer in BU/ml}) + 0.6$  for rADAMTS13 and  $EC_{50} = 0.3 \times (\text{anti-ADAMTS13 inhibitor titer in BU/ml}) + 0.6$  for pADAMTS13. These two formulas are comparable to that established by Plaimauer et al<sup>119</sup> ( $EC_{50} = 0.4077 \times \text{anti-ADAMTS13 inhibitor titer in BU/ml} + 0.733$ ) who used patients plasma instead of patients derived anti-ADAMTS13 IgGs preparations. In conclusion, I demonstrate that rADAMTS13 has an antibody neutralization capacity *in vitro* under static conditions comparable to that of pADAMTS13.

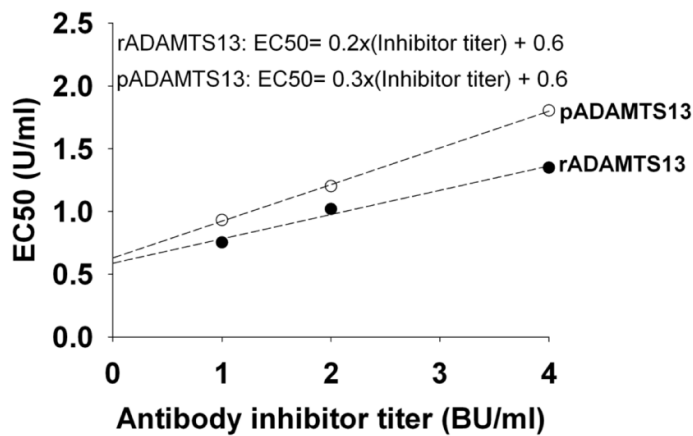


**Figure 20. Relation between anti-ADAMTS13 inhibitor titer and EC50.** A linear relation is found between the mean amounts of pADAMTS13 (open circles) or rADAMTS13 (close circles) needed to achieve an effective concentration of 0.5 U/ml ADAMTS13 activity (EC50) in the IgG preparations of two distinct patients at inhibitor titers of 1 BU/ml to 4 BU/ml.

### IV.3. Epitope mapping of affinity purified IgG autoantibodies from plasma of acquired TTP patients and healthy individuals

#### IV.3.1. Binding of the anti-ADAMTS13 IgG preparations to ADAMTS13 variants

The binding sites of the anti-ADAMTS13 IgG preparations were mapped by IP and Western blotting using full-length rADAMTS13 and a series of truncated variants (Figure 21A-B).

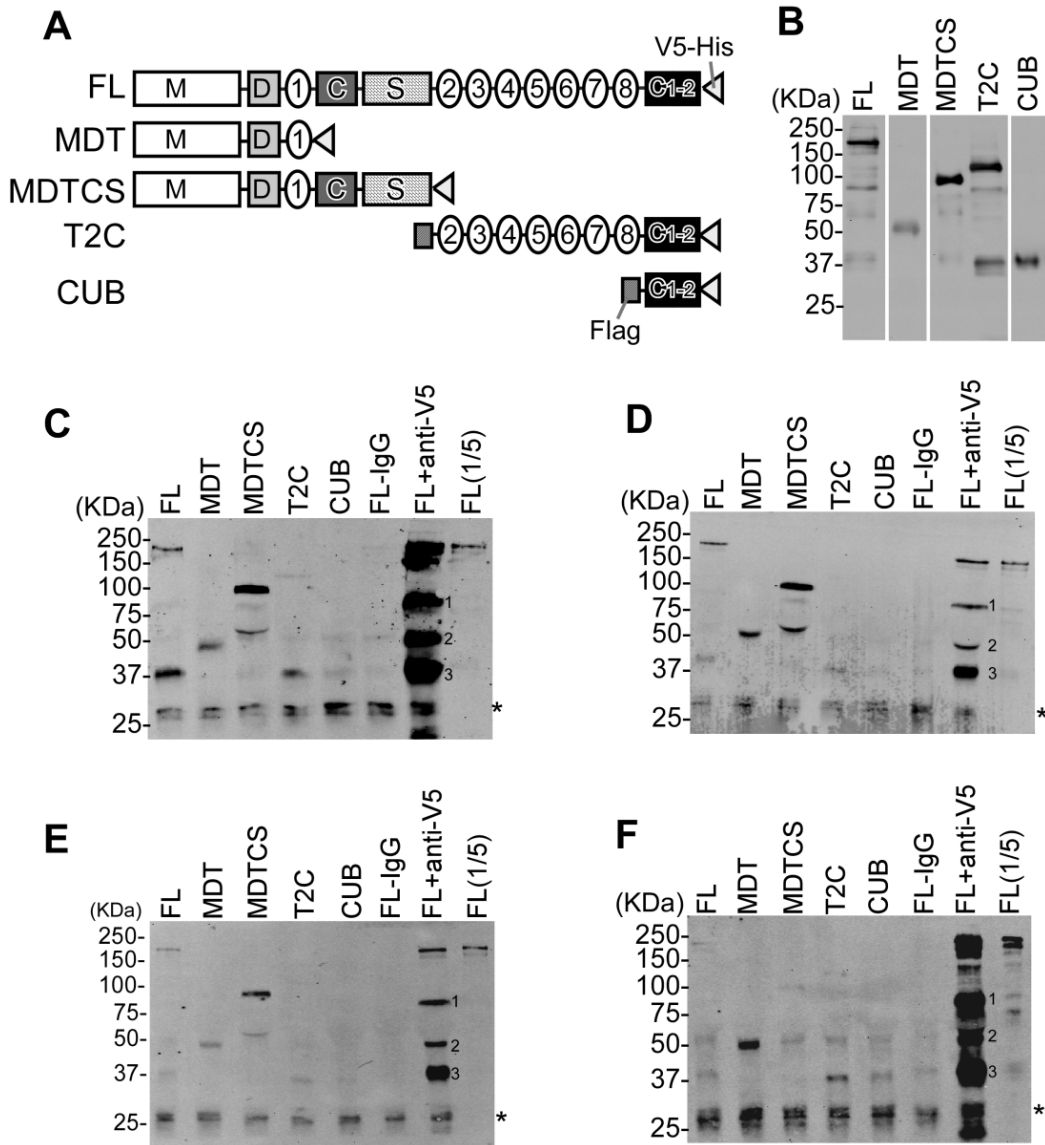


**Figure 21. Epitope mapping of affinity-purified anti-ADAMTS13 IgG antibodies by immunoprecipitation (IP) and Western blotting.** **A)** Schematic domain representation of rADAMTS13 and variants used. FL: Full-length; MDT: metalloprotease, disintegrin and 1st thrombospondin-type 1 repeat domains; MDTCS: metalloprotease, disintegrin, 1st thrombospondin type-1 repeat, Cys-rich and spacer domains; T2C: 2nd – 8th thrombospondin type-1 repeat and two CUB domains; CUB: two CUB domains. **B)** Detection of purified rADAMTS13 and variants (0.1  $\mu$ g/lane) by SDS-PAGE and Western blotting with mouse anti-V5 IgG and IRDye 800-labeled goat anti-mouse IgG. **C-F)** Binding pattern of the IgG preparations isolated from patient 1 (C), patient 2 (D), patient 3 (E) and a HD pool (F). FL-IgG (incubation of FL ADAMTS13 in the absence of IgG) and FL+anti-V5 (incubation of FL ADAMTS13 with mouse anti-V5 IgG) refer to the negative and positive control, respectively. FL(1/5) refers to FL ADAMTS13 (0.1  $\mu$ g) loaded directly on the gel. The loaded negative control “FL-IgG” in panels D&E refers to 1/5th of the amount loaded in panels C&F. The detected 75 kDa (1), 50 kDa (2) and 30 kDa (3) bands refer to degradation products of ADAMTS13 constructs that still have the V5 at their C-terminus. A non-specific 25 kDa double band discernible in all lanes is indicated by an asterisk.

The purified IgGs from all three TTP patients clearly interacted with full-length ADAMTS13 and the N-terminal fragments up to the spacer domain (MDT and MDTCS; Figure 21C-E). The stronger signal intensity for the MDTCS compared with the MDT fragment was in line with the presence of a major binding site within the spacer domain<sup>72;86;115</sup>. The more distal C-terminal domains of ADAMTS13 (T2C and CUB) were only weakly recognized by the antibodies (Figure 21D-E). The HD antibody preparation gave rise to a similar profile, except that it bound stronger to the MDT than to the MDTCS fragment (Figure 21F).

#### IV.3.2. Binding of the anti-ADAMTS13 IgG preparations to ADAMTS13 peptide arrays

To narrow down the binding sites identified by IP, epitopes were additionally determined using peptide arrays, a strategy previously used to identify antibodies linear binding epitopes<sup>85</sup>. Control incubation of these arrays resulted in a single hit (227GHSFGL232) located in the metalloprotease domain of ADAMTS13 (Figure 22, left panel). By contrast, and exemplified for the IgG preparation from patient 2 in the right panel of Figure 22, a clear polyclonal binding pattern was obtained for all the antibodies purified from acquired TTP patients and the HD pool.

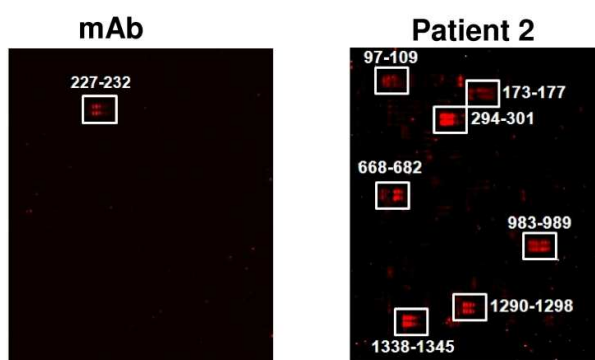


**Figure 22. Raw fluorescence images of representative peptide microarrays.** Shown are the blots for a monoclonal antibody directed against the metalloprotease (M) domain of ADAMTS13 (mAb) and for isolated IgGs from acquired TTP patient 2. Boxed spots denote positive epitopes and their position. Note the polyclonal nature of the patient-derived antibody.

All affinity-purified antibodies gave rise to multiple hits, indicative for their polyclonal nature (Figure 23). The antigenic regions were clustered in the metalloprotease (M), disintegrin (D), spacer (S), thrombospondin-type 1-8 (T1-8) and CUB domains. No positive spots were detected with any antibody for the cysteine-rich as well as the T1-1, T1-3, T1-5 and T1-7 domains.

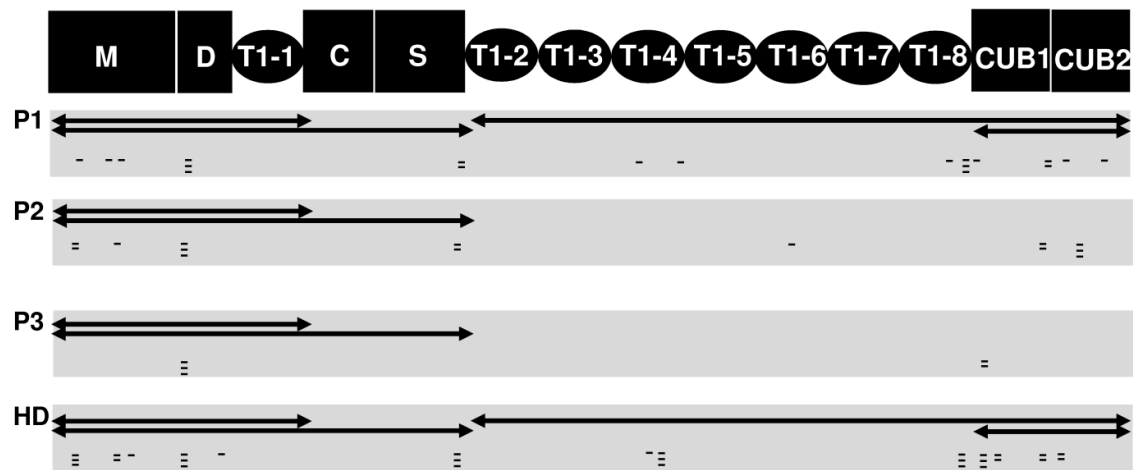


**Figure 23. Epitope mapping of affinity-purified anti-ADAMTS13 IgG antibodies by peptides array.** Schematic representation of the linear ADAMTS13 epitopes (dashes) that have interacted with the isolated antibodies from acquired TTP patient 1 (P1), patient 2 (P2), patient 3 (P3) and a HD pool (HD). The cartoon on top shows the structural domains of ADAMTS13 and illustrates the position of the identified epitopes. The intensities of the fluorescence spots were classified as weak (-), medium (=) or high (≡). Binding epitopes as determined by IP are indicated as double arrows. M: metalloprotease domain; D: disintegrin domain; T1/1 to T1/8: thrombospondin-type 1 repeats 1 to 8; C: cysteine-rich domain; S: spacer domain; CUB1 and CUB2: CUB1 and CUB2 domains.

Interestingly, the peptide recognition patterns of the antibody preparations from HD and the TTP patients were remarkably similar (Table 6). All four samples identified an epitope in the disintegrin domain (P296-P301) that also showed the strongest signals.

**Table 6. Linear ADAMTS13 peptide epitopes detected with isolated antibodies from acquired TTP patients and a HD pool.**

Binding domains		Patient 1*	Patient 2*	Patient 3*	HD*
<b>Shared Epitopes</b>	<b>M</b>	98-108	97-109	-	98-108
		173-178	173-177	-	173-177
	<b>D</b>	296-301	294-301	292-301	296-301
	<b>S</b>	673-682	668-682	-	676-682
	<b>T1-8</b>	1171-1175	-	-	1171-1175
	<b>CUB1</b>	-	-	1194-1204	1194-1204
<b>Non shared epitopes</b>	<b>M</b>	162-169	-	-	212-216
	<b>D</b>	-	-	-	355-360
	<b>T1-4</b>	834-844	-	-	855-866
		888-892	-	-	871-879
	<b>T1-6</b>	-	983-989	-	-
	<b>T1-8</b>	1141-1147	-	-	-
		1180-1191	-	-	-
	<b>CUB1</b>	1192-1194	-	-	1219-1227
	<b>CUB2</b>	1312-1321	-	-	-
		1382-1390	1338-1345	-	1309-1315

\* Identified peptide epitopes are given with delimiting amino acid residue numbers. The fluorescence intensities were classified as weak (light blue), medium (medium blue) or high (deep blue). A minus sign denotes absence of fluorescence spots.

Using the published crystal structure of an ADAMTS13 DTCS fragment and a modeled metalloprotease domain (based on the structures of human ADAMTS4/5), all but one (D173-Y177) epitopes were displayed on the surface of ADAMTS13 (Figure 24A-C), illustrating the accessibility of these binding sites to the isolated autoantibodies.

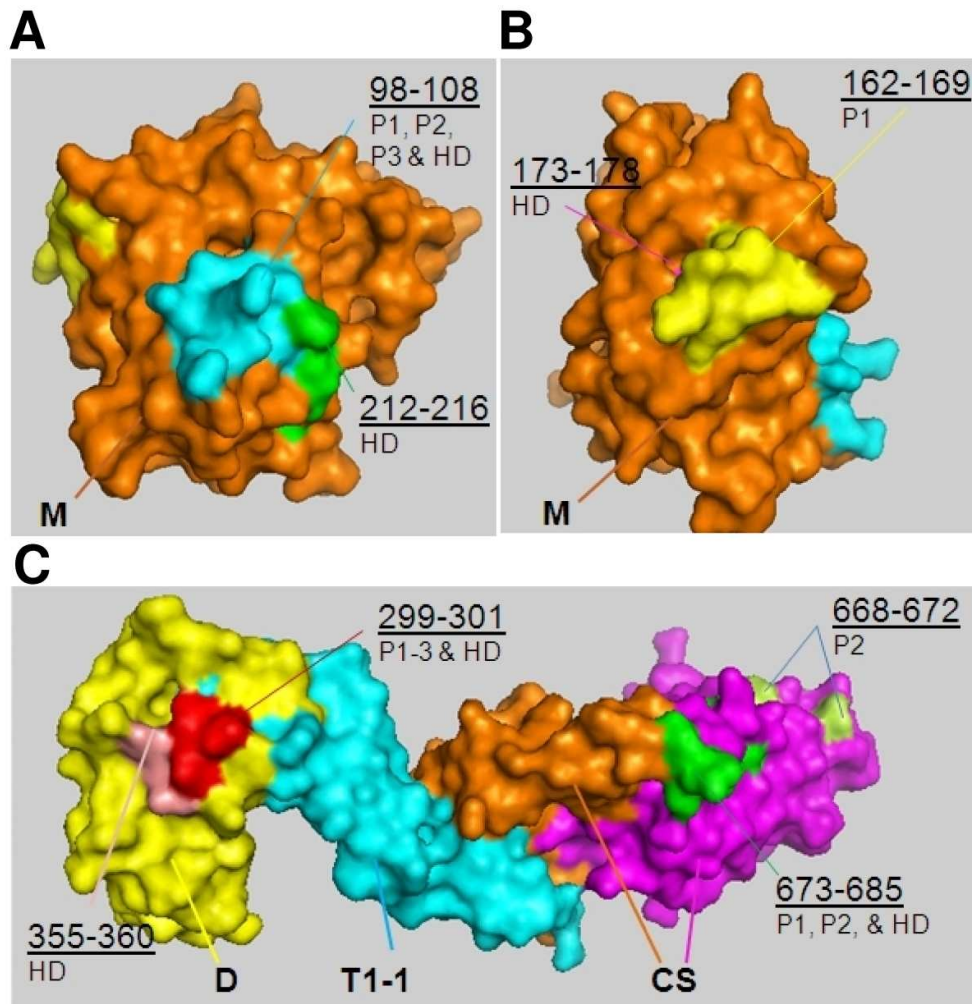


**Figure 24. Epitope mapping of affinity-purified anti-ADAMTS13 IgG antibodies using peptide arrays.** Antibody binding epitopes of patient 1 (P1), patient 2 (P2), patient 3 (P3) and healthy donors (HD) painted on the surface of the modeled ADAMTS13 metalloprotease domain (**A and B**) and the crystal structure of the ADAMTS13-DTCS fragment (**C**). Peptides 98-108 and 162-169 are painted blue (A) and yellow (B) respectively, on the surface of the metalloprotease domain (orange). Yellow, blue, orange, and magenta segments in C represent disintegrin domain, the first thrombospondin-type 1 repeat, cysteine-rich domain, and spacer domains, respectively. Peptides 299-301 and 355-360 are painted red and light pink, respectively, on the surface of the disintegrin domain; peptides 673-685 and 668-672 are shown on the surface of the spacer domain. The peptide 173-178 located in the metalloprotease domain is essentially buried (B).

## **IV.4. Assessment of the inhibitory activity of affinity purified ADAMTS13 autoantibodies from patients with TTP under flow conditions**

### **IV.4.1. Establishment of an ADAMTS13 activity assay under flow**

To study the inhibitory activity of anti-ADAMTS13 antibodies under shear stress, I developed an ADAMTS13-sensitive flow assay that simulates the events on the surface of a damaged vessel wall, where collagen of the exposed subendothelial matrix provides a binding scaffold for VWF, which in turn initiates platelet adhesion and aggregation.

For this purpose, microchannels of a biochip were sequentially coated with cellular fibronectin (cFN), collagen, and rVWF; the cFN as an adhesive binding substrate for collagen was required to achieve an even surface-coating of collagen fibers. The fluid phase was composed of physiological concentrations of fluorescently labeled platelets, erythrocytes which are known to push platelets close to the surface of a vessel, and VWF. Soluble VWF not only mediates inter-platelet cohesion but also covalently associates with immobilized VWF multimers, thereby forming extended string like structures<sup>47</sup> that provide a greater number of interacting sites for platelets.

Following perfusion at a physiological shear rate of  $1500 \text{ s}^{-1}$ , platelet clusters arrested at individual spots of the channel followed by the immediate formation of stable and non-rolling large aggregates (Figure 25A, lower panel). I hypothesized that this was due to inhomogeneous coating of the collagen-VWF layer. Visualization of the microchannels by phase contrast microscopy indeed revealed individual spots of thick layers of collagens fibers (Figure 25A, upper panel). This issue was resolved by sequentially coating microchannels with cFN, collagen and rVWF, whereat cFN as an adhesive binding substrate for collagen allowed the achievement of an even surface-coating of collagen fibers (Figure 25B, upper panel). As a consequence, perfusion of the same suspension over the coated channel surface led to reproducible platelet aggregate formation along collagen fibers (Figure 25, lower panel).

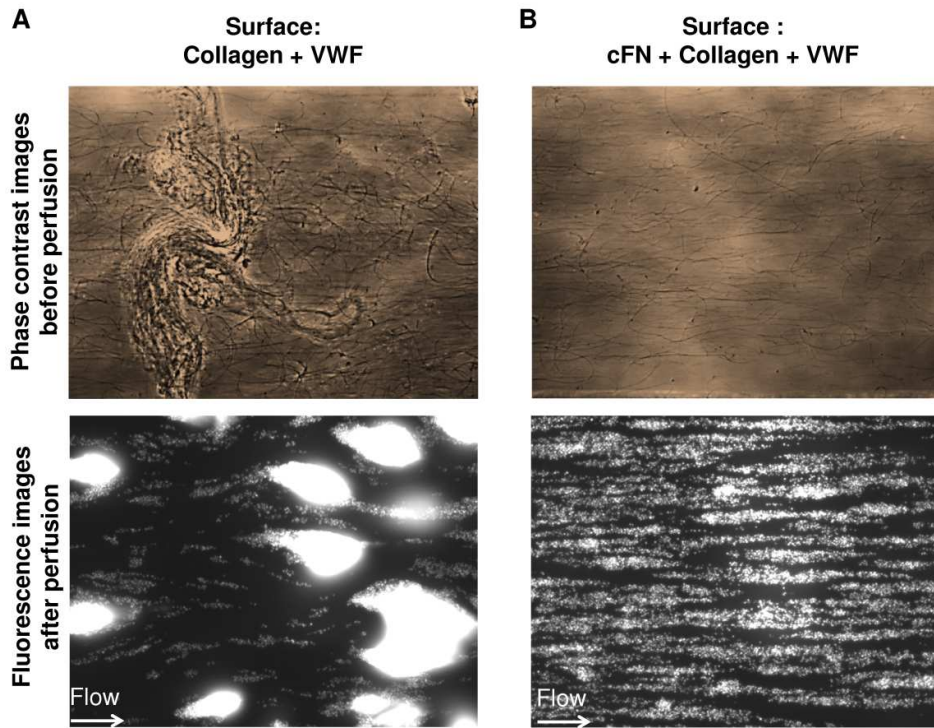


**Figure 25. Homogeneous chain like structures of platelet aggregates on a layer of cellular fibronectin (cFN), collagen and VWF.** Cell suspensions of fluorescently labeled platelets ( $2.5 \times 10^8$  platelets/ml), erythrocytes (40% Hct) and rVWF ( $10 \mu\text{g/ml}$ ) were perfused over a surface coated with collagen and rVWF (A) or cFN, collagen and rVWF (B). Before perfusion, phase contrast images were acquired to check the density and homogeneity of the collagen coated surface. After 5 min of perfusion at  $1500 \text{ s}^{-1}$  images were obtained in the middle of the channel. The flow direction is indicated by an arrow. Note that only by precoating the channel with cFN, aggregated platelets with string-like morphology covered homogeneously the whole channel surface, due to the presence of a homogeneous surface of collagen fibrils.

This coating procedure was therefore used for further experiments.

The extent of aggregation was strongly dependent on shear rate and increased as a function of time, with a maximum surface coverage at  $2600\text{ s}^{-1}$  after 5 min (Figure 26A-B).

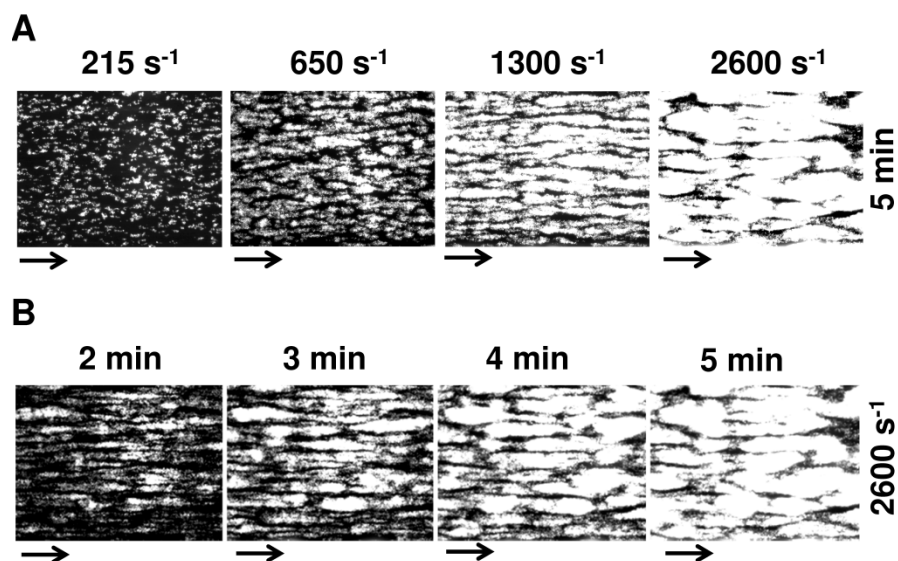


**Figure 26. Influence of shear and time on VWF-mediated platelet aggregate accumulation in a novel flow-based assay.** Cell suspensions of fluorescently labeled platelets ( $2.5 \times 10^8$  platelets/ml), erythrocytes (40% Hct) and rVWF (10  $\mu\text{g/ml}$ ) were perfused over a surface coated with cellular fibronectin, collagen and rVWF. Arrows indicate the direction of flow. **A)** Platelet aggregate formation at different shear rates. Images were obtained after 5 min of perfusion at the indicated shear rates and represent single frames from real time recordings. Small clusters of platelets that either adhered to or rolled on the channel surface were observed at a shear rate of  $215\text{ s}^{-1}$ . Aggregates increased in size at  $650\text{ s}^{-1}$ , became elongated and firmly attached to the surface at  $1300\text{ s}^{-1}$ , and finally reached their maximum size at  $2600\text{ s}^{-1}$ , covering almost the whole surface of the coated channel. **B)** Time course of platelet aggregate accumulation. Images were obtained at the indicated time points after perfusion at a shear rate of  $2600\text{ s}^{-1}$  and represent single frames from real time recordings. Note the progressive increase of surface coverage by platelet aggregates over time, peaking at 5 min.

The formation of aggregates strongly depended on the interaction of VWF with the platelet receptor  $\text{GP Ib}\alpha$ , as a blocking antibody against  $\text{GP Ib}\alpha$  eliminated aggregation (Figure 27). Based on these data, all subsequent experiments were performed at a shear rate of  $2500\text{ s}^{-1}$  and a perfusion time of 5 min.

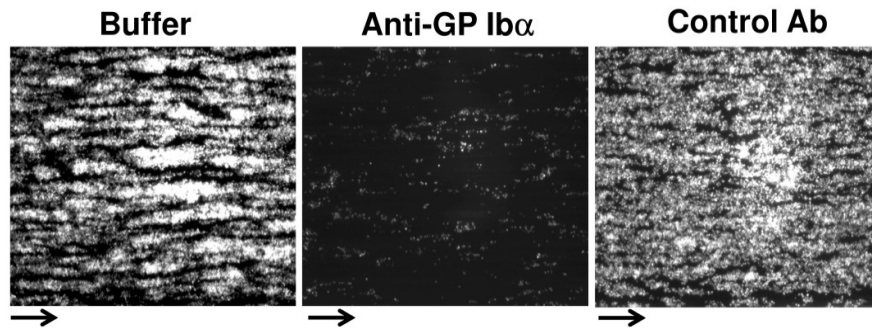


**Figure 27. VWF mediated platelet adhesion.** A cell suspension of  $2.5 \times 10^8$  platelets/ml and 40% Hct, containing  $2 \mu\text{M}$  DiOC<sub>6</sub> and  $10 \mu\text{g/ml}$  rVWF in the absence (Buffer) or presence of either a monoclonal antibody that blocks GP Ib $\alpha$  to immobilized VWF (anti-GP Ib $\alpha$ ) or a control monoclonal IgG1 antibody (Control Ab) was perfused at the wall shear rate of  $1500 \text{ s}^{-1}$  over a surface coated with cellular fibronectin, collagen and rVWF. The flow direction is indicated by an arrow on the bottom of each image. The antibodies were incubated in the cell suspension 15 min before initiating perfusion. Images selected in one field of view in the channel were obtained after 5 min of perfusion and represent single frames from real time recordings. Platelets adhesion and aggregation was hindered on the surface in the presence of specific anti-GP Ib $\alpha$  antibody that impaired platelet-surface interaction with the immobilized VWF at high shear rates as compared with the untreated or the control antibody containing cell suspension.

Adding increasing concentrations of rADAMTS13 (1-4 FRETs-VWF73 U/ml) to the cell suspension prior to perfusion dose-dependently reduced the surface coverage of platelet aggregates on the coated channels to 10% of the control lacking ADAMTS13 (Figure 28A). Plasma-derived ADAMTS13 reduced the accumulation of platelet aggregates similarly to rADAMTS13 (Figure 28B). The relative decrease in surface coverage was also comparable using platelets from different donors (not shown).

The effect of ADAMTS13 on the rate of platelet aggregate formation was then studied. The surface area covered with platelet aggregates after 5 min of flow in the absence of ADAMTS13 was set to 100%. After 30 sec of perfusion, a surface coverage of 16% was observed, and a half maximal surface coverage (50%) was achieved after approximately 2 min (Figure 28C). Adding 1 or 2 U/ml of rADAMTS13 did not prevent but significantly slowed down platelet aggregate accumulation. At a concentration of 4 U/ml, however, rADAMTS13 was clearly able to prevent the building up of platelet aggregates, as platelet aggregate coverage remained constant at 10% throughout perfusion (5 min). This residual coverage

likely reflects the portion of platelets bound to (partially cleaved) immobilized VWF or to exposed collagen fibrils through the platelets' collagen receptor GPVI<sup>30</sup>.

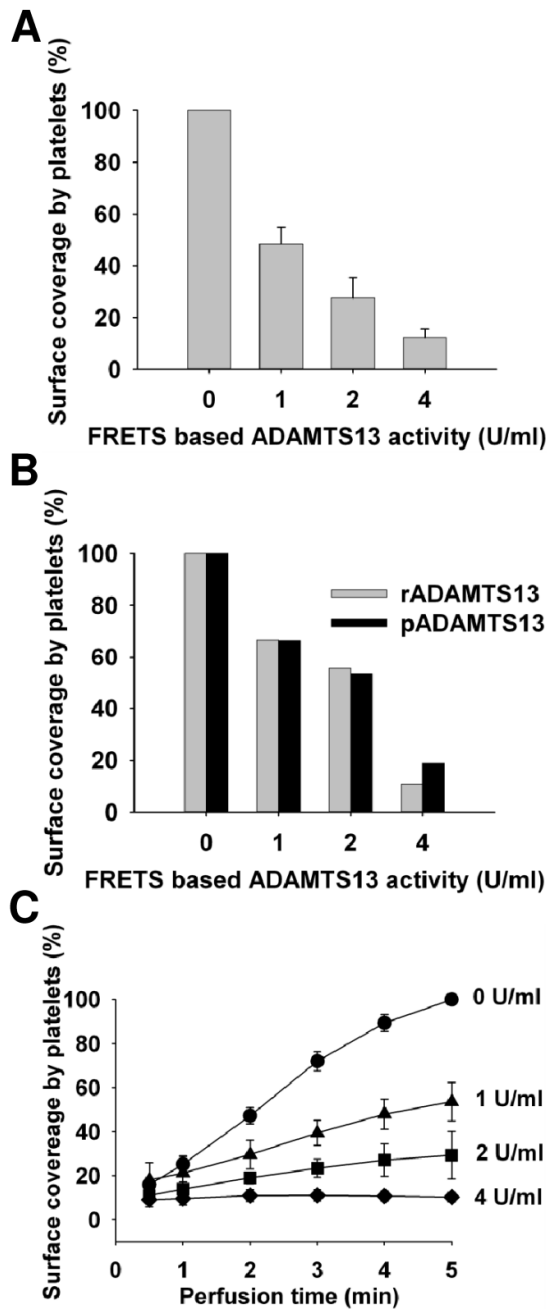


**Figure 28. Effect of ADAMTS13 on VWF-mediated platelet aggregate accumulation under flow conditions.** Cell suspensions of fluorescently labeled platelets ( $2.5 \times 10^8$  platelets/ml), erythrocytes (40% Hct) and rVWF (10  $\mu\text{g/ml}$ ) were mixed with the indicated concentrations of ADAMTS13 and perfused over a surface coated with cellular fibronectin, collagen and rVWF at a shear rate of  $2500 \text{ s}^{-1}$ . After continuous perfusion up to 5 min, the mean surface area covered with platelet-aggregates was calculated for each sample. In panel A, B and C, the surface coverage obtained in the absence of rADAMTS13 after 5 min of flow was set to 100%. **A)** Dose-dependent reduction of surface coverage by platelet aggregates in the presence of rADAMTS13. The bar graph shows the mean surface area ( $\pm$  SEM,  $n=4$ ) covered with platelet-aggregates after 5 min of continuous perfusion performed with platelets from different donors. Adding rADAMTS13 reduced the surface coverage of platelet aggregates on the coated channels in a dose-dependent manner. **B)** Comparison of the activity of recombinant and plasmatic ADAMTS13 under flow. The gray (rADAMTS13) and black (pADAMTS13) bar graphs show the surface area covered with platelet-aggregates after 5 min of continuous perfusion performed with platelets from the same donor. The results are representative of two sets of experiments, each of which was performed with a distinct platelet donor. **C)** Time course of the effect of rADAMTS13 on platelet aggregate accumulation. The bar graph shows the mean surface area ( $\pm$  SEM,  $n=4$ ) covered with platelet-aggregates at the indicated cumulative perfusion times performed with platelets from different donors. A concentration of 4 U/ml rADAMTS13 was required to prevent formation of initial platelets aggregates.

#### **IV.4.2. Assessment of ADAMTS13 inhibitors using the ADAMTS13 activity assay under flow**

A goat anti-human ADAMTS13 IgG preparation with a high (FRETS-VWF73-based) inhibitor titer was used to evaluate the flow assay for inhibitor assessment. A fixed amount of rADAMTS13 (4 U/ml) was mixed with increasing inhibitor titers of the goat antiserum (2-8 BU/ml) and added to the cell suspension. The extent of platelet aggregate accumulation was monitored after 5 min of perfusion at  $2500 \text{ s}^{-1}$ . A gradual increase in surface coverage from 10 to 100% was observed which correlated with the added inhibitor titer (Figure 29A), indicating that rADAMTS13 activity was fully blocked at the highest inhibitor concentration. Similar results were obtained for pADAMTS13; for both proteins, a surface coverage of 50% was reached with an inhibitor titer of 4.6 BU/ml (Figure 29A).

In a complementary setup, the ADAMTS13 concentrations required to recover 2 U/ml of ADAMTS13 activity was determined in the presence of inhibitor under flow conditions with reference to the FRETS-VWF73 assay. Increasing concentrations of FRETS-VWF73 ADAMTS13 activity were successively able to override the inhibitor under flow, with a clear correlation between increasing inhibitor titers and the amounts of ADAMTS13 activity required (Figure 29B). For instance, to recover 2 U/ml of ADAMTS13 in the presence of 1, 2, and 4 BU/ml of the anti-ADAMTS13 antibody, 5.8, 8.8, and 11.6 U/ml ADAMTS13, respectively, were required. These data indicated that the assay is suitable for assessing functional ADAMTS13 inhibitors under flow, and thus allows functional testing of inhibitors from acquired TTP patients under more physiological conditions.

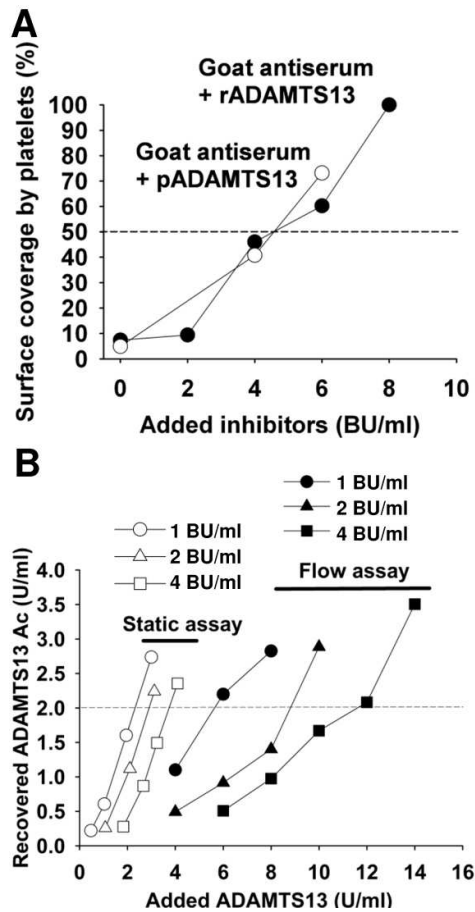


**Figure 29. Effect of goat ADAMTS13 antiserum on VWF-mediated platelet aggregate accumulation under flow conditions.** Cell suspensions of fluorescently labeled platelets ( $2.5 \times 10^8$  platelets/ml), erythrocytes (40% Hct) and rVWF (10  $\mu\text{g/ml}$ ) were mixed with the indicated antibody-antigen concentrations and perfused over a surface coated with cellular fibronectin, collagen and rVWF at a shear rate of  $2500 \text{ s}^{-1}$ . **A)** Inhibitor titer-dependent accumulation of platelet aggregates by goat ADAMTS13 antiserum. Mixtures of 4 U/ml of rADAMTS13 (closed circle) or pADAMTS13 (open circle) with anti-ADAMTS13 antibodies derived from goat antiserum (2-8 BU/ml; end titer, assessed by the FRETs-VWF73 assay) were added to the cell suspension prior to perfusion. The experiment was performed using the same platelet donor. The goat antiserum caused an inhibitor titer-dependent and comparable increase in the percentage of platelet aggregate surface coverage for rADAMTS13 and pADAMTS13. The dashed line represents 50% of surface coverage. **B)** Activity recovery by rADAMTS13 in the presence of goat anti-ADAMTS13 antiserum under flow conditions with reference to a conventional static assay. Increasing activity increments of rADAMTS13 were added to goat ADAMTS13 antiserum adjusted to inhibitor titers of 1 BU/ml (circle), 2 BU/ml (triangle) and 4 BU/ml (square). The mixtures were assessed for residual ADAMTS13 activity either under static conditions (open circles) by the FRETs-VWF73 assay or under flow conditions (closed circles). The experiments under flow were carried out using the same platelet donor. Reconstituted activities were plotted against the added rADAMTS13 activities and the required concentration of rADAMTS13 to recover 2 U/ml (dashed line) determined by manual extrapolation. With both assay conditions increasing inhibitor titers of the goat antiserum required supplementation of higher ADAMTS13 concentrations. Note that approximately three times higher ADAMTS13 concentrations were required under flow to recover 2 U/ml of ADAMTS13 activity.

Interestingly, when studying ADAMTS13 activity recovery in the presence of the same goat anti-ADAMTS13 antiserum used for the flow assay under static conditions, 2.4, 2.9, and 3.7 U/ml had to be supplemented to the 1, 2 and 4 BU/ml preparations, respectively to recover 2 U/ml of ADAMTS13 activity (Figure 29B). These data suggest that an approximately three fold molar excess of ADAMTS13 is required under flow to restore ADAMTS13 activity in the presence of inhibitors.

#### **IV.4.3. Inhibitory activity of purified anti-ADAMTS13 IgG autoantibodies under flow conditions**

To study the neutralizing profiles of the two purified antibody preparations under shear stress, the increase in surface coverage of platelet aggregates was again used to measure the extent of ADAMTS13 inhibition by the antibodies. Perfusion was performed in the presence of 4 U/ml rADAMTS13 and increasing inhibitor titers (0.3-12 BU/ml, determined by FRETs-VWF73 assay) of the anti-ADAMTS13 IgGs from TTP patients 2 and 3. Surprisingly, the same FRETs-VWF73-based inhibitor titers did not cause comparable inhibition of ADAMTS13 activity under flow, as reflected by vastly different surface coverage profiles (Figure 30A). For example, when an inhibitor titer of 3 BU/ml was added, IgGs from patient 3 led to more than 90% surface coverage, whereas those from patient 2 exhibited only 15%. Even adding 12 BU/ml did not achieve full surface coverage for the IgG preparation from patient 2 (Figure 30A), indicating that under flow the inhibitory activity of this antibody was much lower than for patient 3. This difference in surface coverage was also observed with pADAMTS13 instead of rADAMTS13 in the flow assay (Figure 30B) thereby excluding an influence of antigen source on the reactivity of the antibody.

The two IgG preparations were retested at various concentrations for their inhibitory activity in the static FRETs-VWF73-based Bethesda-like assay. When increasing inhibitor titers of the antibodies were mixed with NHP, ADAMTS13 activity was blocked in a similar, dose-dependent manner by both preparations (Figure 30C), confirming that under static conditions

the two preparations inhibit ADAMTS13 activity to a similar extent. The combined results thus indicate a discrepancy in inhibitor assessment when using static and flow-based assays.

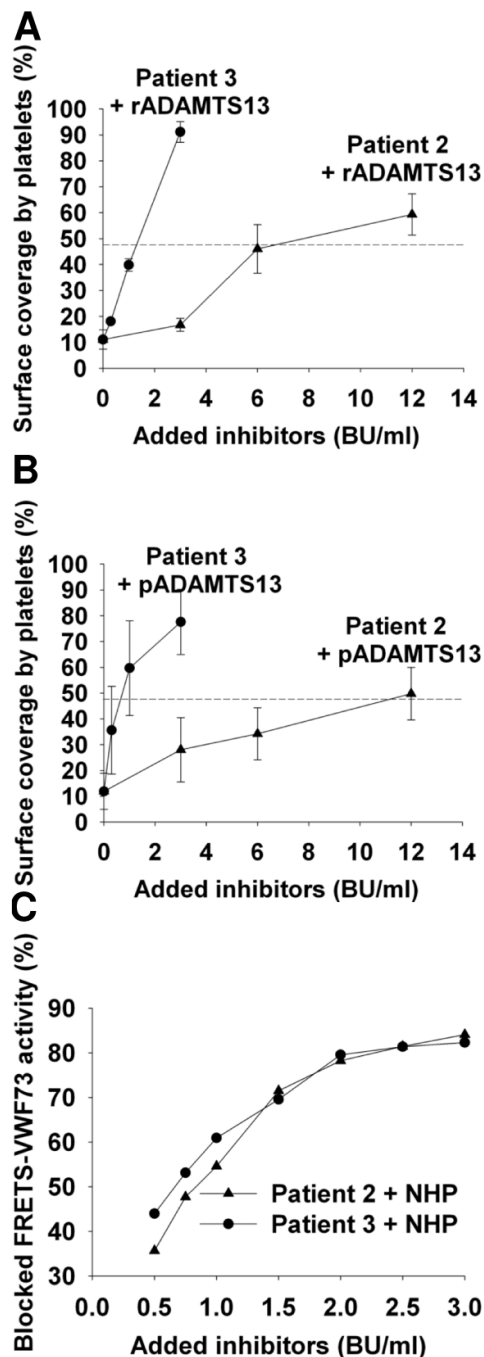


**Figure 30. Inhibitory activity of affinity-purified human anti-ADAMTS13 IgG antibodies under flow conditions.** The flow-based assay as described in Figure 26 and 29 was used to test purified IgG preparations from two acquired TTP patients for their ability to inhibit ADAMTS13. The results are expressed as means  $\pm$  SEM (n=2) using platelets from different donors. The surface coverage of platelet aggregates obtained without adding ADAMTS13 was set to 100%. **A)** Inhibitor assessment under flow in the presence of rADAMTS13. Mixtures of 4 U/ml of rADAMTS13 and increasing concentrations of anti-ADAMTS13 IgG antibodies isolated from patient 2 (3-12 BU/ml, end titer; assessed by the FRET-VWF73 assay; triangle) or patient 3 (0.3-3 BU/ml, end titer; assessed by the FRET-VWF73 assay; circle) were added to the cell suspension prior to perfusion. The percentage of platelet aggregate surface coverage was plotted against the added FRET-VWF73-based inhibitor titers. An increase in surface coverage to 50% (dashed line) was obtained with 8 BU/ml of IgG antibodies from patient 2 and 1.5 BU/ml of IgG antibodies from patient 3. **B)** Inhibitor assessment under flow in the presence of pADAMTS13. When the perfusion experiment used pADAMTS13 instead of rADAMTS13 under otherwise identical conditions, 50% surface coverage (dashed line) was obtained with 12 BU/ml of IgG antibodies from patient 2 and 0.7 BU/ml of IgG antibodies from patient 3. **C)** Control for inhibitory activity of the isolated IgG antibodies under static conditions. Increasing inhibitor titers (0.5-3 BU/ml, end titer; assessed by FRET-VWF73 assay) of the IgG antibodies from patient 2 (triangle) and patient 3 (circle) were assessed by a FRET-VWF73-based Bethesda-like assay. Both preparations showed a comparable profile over the entire concentration range.

## V. DISCUSSION

### V.1. Isolation of plasma derived ADAMTS13

A purification method for pADAMTS13 was established using hydrophobic interaction chromatography followed by a sequential affinity purification procedure involving ADAMTS13 capture by a goat polyclonal anti-ADAMTS13 antibody and a mouse monoclonal anti-ADAMTS13 antibody that binds to the C-terminal domain of ADAMTS13. Full-length pADAMTS13 was purified to apparent homogeneity with a specific activity of 0.6 U/ $\mu$ g and a single N-terminal amino acid sequence of AAGGI that confirmed the identity of the isolated protein.

Small amounts of truncated ADAMTS13 variants with a size of 170, 130 and 80 kDa were isolated together with full-length ADAMTS13. The presence of these variants is consistent with previously described purifications of ADAMTS13 from human plasma<sup>6</sup>, cryoprecipitates<sup>14</sup> or Cohn fraction I precipitates<sup>15</sup>. These truncations probably result from a proteolytic degradation of ADAMTS13 by thrombin, plasmin<sup>52:126</sup> and granulocyte elastase<sup>53</sup>. It is unlikely however that they contribute to the activity of the isolated pADAMTS13 material as Western blotting using a set of monoclonal antibodies directed either to the metalloprotease or to the CUB domains of ADAMTS13 revealed them to be free of the catalytic domain of ADAMTS13.

Following the polyclonal goat anti-ADAMTS13 affinity matrix step, contaminating IgGs were noted. Removal of IgG by protein G showed that only about 50% of the protease activity was recovered in the flow through whereas the rest co-eluted with the IgGs suggesting that a portion of pADAMTS13 was bound to these IgGs. According to the cold ethanol fractionation, the starting material used to purify pADAMTS13 is supposed free of IgGs since it represents the filter cake collected after separation of human IgGs by filtration. Apparently, IgGs specifically bound to ADAMTS13 remained in this fraction and became sufficiently

concentrated and therefore detectable upon purification of ADAMTS13. The presence of these IgGs may also explain the identification of elevated anti-ADAMTS13 IgG plasma levels in ~5% of healthy individuals<sup>109;127</sup>.

Using agarose gel electrophoresis and immunoblotting, the final pADAMTS13 preparation not only displayed ADAMTS13 monomers but also minor amounts of covalently bonded ADAMTS13 multimers, the latter disappearing under reducing conditions. Such results were obtained when rADAMTS13 was subjected to the same electrophoresis procedure. This finding is in line with an earlier study which reported on a high molecular weight (300 kDa) of the partially purified enzyme as determined by gel filtration and SDS-PAGE under non-reducing conditions<sup>6</sup>. At this early purification stage, the proteolytic activity described may have coincided with ADAMTS13 in its multimeric form. It is tempting to hypothesize that multimers of ADAMTS13 may be formed by at least one of the 6 free thiols shown to be exposed on the surface of ADAMTS13 by mass spectrometry<sup>128</sup>. It would be interesting to identify the free thiols in ADAMTS13 involved in disulfide bond formation of these multimers and determine whether such multimers are biologically relevant. On the other hand, the currently available data suggest that the oligomerization process might have been triggered by the conditions of the purification process.

The copurification of plasma VWF with pADAMTS13 is in agreement with previous finding demonstrating that 3% of ADAMTS13 in NHP circulate bound to globular VWF<sup>69</sup>. It is however unlikely that the multimeric structure of VWF is involved in the formation of pADAMTS13 as ADAMTS13 was copurified with low molecular weight plasma VWF only.

Taken together, the obtained preparation of plasma derived ADAMTS13 was considered as suitable reference material to rADAMTS13 to characterize anti-ADAMTS13 autoantibodies from patients with acquired TTP.

## **V.2. Functional characterization of anti-ADAMTS13 autoantibodies affinity-purified from plasma of acquired TTP patients and a healthy donor pool**

Anti-ADAMTS13 IgG antibodies from plasma of three acquired TTP patients were successfully isolated and characterized. Purification involving ADAMTS13-specific antibody capture on an ADAMTS13 matrix and IgG fraction isolation on a protein G matrix recovered 0.8 to 2.5 µg antibody per one ml of patient plasma. This yield is consistent with anti-ADAMTS13 IgGs reported in acquired TTP patients plasma (0.50 and 1.50 µg/ml)<sup>86</sup>, but likely underestimated as antibodies might be bound in immune-complexes<sup>120;129</sup>. Additionally, the ADAMTS13 given by transfusion presumably decreased the free antibody levels<sup>127</sup>.

All three TTP antibody preparations contained IgG subclasses 1 to 4 to a varying extent. Although undetectable in the starting material, IgG2 was the dominant subclass after affinity purification, followed by IgG1 and IgG3/IgG4. The obtained subclass distribution thus differs from that reported for plasma from acquired TTP patients in two studies, where IgG4 was most prominent followed by IgG1 then IgG2 and finally IgG3<sup>86;110</sup>. Also for patients 1 and 2, IgG4 was the most prominent subclass in the initial plasma samples, whereas in the respective eluates the amount of IgG4 was low. This discrepancy might be due to the presence of substantial amounts of IgG4-containing immune complexes in the starting material. Such complexes are likely to be inefficiently captured by the ADAMTS13 affinity, whereas free anti-ADAMTS13 antibodies are readily depleted.

The predominance of IgG2 in the purified IgG preparations but not in the initial plasma samples is less clear. One possible explanation is the preferential elution of the low affinity IgG2 antibodies from the ADAMTS13 affinity matrix. It is also conceivable that the IgG2 content in plasma samples is underestimated by the IgG2 subclass ELISA used because of a preferential loss of low affinity IgG2 antibodies during the washing steps. Here, an ADAMTS13-specific human IgG2 standard would be required for quantification, but such a preparation is currently not available.

These concerns notwithstanding, other investigators also found a significant proportion of ADAMTS13-specific IgG2 upon isolation of IgG autoantibodies from plasma of an acquired TTP patient who succumbed to the disease<sup>113</sup>. As this subclass is mainly induced by bacterial carbohydrate antigens, the authors proposed the presence of ADAMTS13-specific IgG2 in this patient to stem from bacterial infection. This finding is commensurate with a hypothetical model of molecular mimicry, where peptide(s) of a foreign pathogen from a preceding or concurrent infection resemble surface-exposed epitopes of ADAMTS13, ultimately generating cross-reactive IgG2-producing B cell clones<sup>79;130</sup>. A similar scenario is conceivable for the TTP patients tested here.

TTP antibodies for all three patients showed a high and comparable affinity for either rADAMTS13 or pADAMTS13 reflected by low  $K_D$  (0.5-1.2 nM for rADAMTS13 and 0.2-0.5 nM for pADAMTS13). Since this difference in affinity is <1 nM, I conclude that the purified autoantibodies bound pADAMTS13 and rADAMTS13 with comparable affinities and consequently that the native antigen does not exhibit a tighter binding to the TTP antibodies.

The specific neutralizing activities of the purified IgGs differed between patients (0.1-0.5 FRETS-VWF73-based BU/ $\mu$ g). Similar results were obtained by CBA assay using full-length VWF as substrate. Notably, inhibition of ADAMTS13 activity by 50% required a ~6-fold molar excess of the IgG preparation from patient 3 compared with that from patient 2. As plasma from all three patients had an inhibitor titer of ~1.5 BU/ml, acquired TTP patients with a similar titer may not necessarily have similar amounts of circulating inhibitors.

The contribution of each subclass to the observed affinities of total IgG toward ADAMTS13 for patients 2 and 3 was also addressed using an ELISA-based assay system. Data suggest that apparent affinities for total IgG are, depending on the patient's subclass distribution, driven by IgG1, and by IgG3/4, except when present in very low amounts (~1%). Nonetheless, results of these two patients suggest the antibody response to ADAMTS13 in acquired TTP to include a high prevalence of low affinity IgG2s. It thus appears that the

affinity maturation process for the IgG1, 3 and 4 subclasses proceeds at higher rates than for IgG2. Future experiments may help to understand whether the low affinity IgG2 subclass is at all involved in development of the autoimmune response in acquired TTP.

The inhibitory effect of purified TTP antibodies was partly due to their interference with the interaction between ADAMTS13 and its substrate VWF. For all patients, 50% inhibition was already achieved with a slight molar excess of anti-ADAMTS13 antibodies, which was also reflected by low  $K_i$  (~0.3 nM). Interestingly, due to the choice of detection antibody for ADAMTS13, the apparent affinity ( $K_D = 0.4$  nM) determined for this interaction was 35-fold of the one previously reported<sup>66</sup>. I used a tag-free rADAMTS13 detected by an affinity-purified polyclonal rabbit IgG anti-human ADAMTS13 antibody for my ELISA, whereas Majerus et al<sup>66</sup> used a V5-tagged rADAMTS13 combined with an anti-V5 detection antibody. Running the latter setup in the laboratory led to a similar apparent affinity indicating that detecting ADAMTS13 through a single C-terminal V5 epitope using a typical ELISA underestimates its apparent binding affinity to VWF.

A linear relation was determined between the inhibitor titer of the patient's derived IgG preparation and the amount of pADAMTS13 or rADAMTS13 necessary to overcome a specific inhibitory titer and reconstitute an ADAMTS13 activity of 0.5 U/ml. By linear regression, the formulas for the calculation of the EC50 for rADAMTS13 and pADAMTS13 were  $0.2 \times (\text{anti-ADAMTS13 inhibitor titer in BU/ml}) + 0.6$  and  $0.3 \times (\text{anti-ADAMTS13 inhibitor titer in BU/ml}) + 0.6$ , respectively. Both formulas are in line with the one established by Plaimauer et al<sup>119</sup> ( $\text{EC}_{50} = 0.4 \times (\text{inhibitor titer in BU/ml}) + 0.7$  where patient's plasma instead of affinity purified human anti-ADAMTS13 IgG preparations was used as an inhibitor source. Since the neutralization capacity of the antibodies was comparable between pADAMTS13 as the native antigen and rADAMTS13, the data support potential therapeutic application of rADAMTS13 in conjunction with plasma exchange therapy in acquired TTP.

Anti-ADAMTS13 IgG antibodies were also identified in a similarly processed HD plasma pool, although it initially tested negative. Two independent studies reported elevated anti-ADAMTS13 IgG plasma levels in 4/111 (3.6%)<sup>109</sup> and 2/40 (5%)<sup>127</sup> healthy individuals. The HD pool therefore may have contained plasma with anti-ADAMTS13 IgGs which were sufficiently concentrated upon affinity purification to become detectable. The isolated antibodies were specific for ADAMTS13 as they did not exhibit cross-reactivity with the human plasma protein albumin. The isotypic patterns of the isolated anti-ADAMTS13 IgGs of the HD pool and the TTP patients were similar, but HD-derived IgGs were non-neutralizing, had minimal affinity towards ADAMTS13 as measured by ELISA and Biacore, and did not affect the interaction between ADAMTS13 and VWF. Additionally, the presence of these non-neutralizing IgGs in the pooled plasma of healthy donors is in line with the copurification of anti-ADAMTS13 IgGs with pADAMTS13 from the Cohn fraction intermediate. Antibodies against several self-antigens such as FVIII (acquired hemophilia)<sup>131</sup>, DNA (lupus erythematosus)<sup>132</sup>, and others have already been measured in patients as well as in a fraction of the healthy population, whereby the natural antibodies have a significantly lower affinity<sup>133</sup>. Taken together, these data suggest that the isolated IgGs from the HD pool most likely represented bona fide autoantibodies against ADAMTS13.

### **V.3. Epitope mapping of affinity purified IgG autoantibodies from plasma of acquired TTP patients and healthy individuals**

Epitope mapping using a previously described immunoprecipitation (IP) and a novel method based on an ADAMTS13-specific peptide array revealed the patients derived IgGs to be polyclonal. All domains identified by IP were also hit by at least one immune-reactive peptide. A few positive peptides, however, were identified within the C-terminal domains of ADAMTS13 that did not test clearly positive by IP for IgG preparations from patients 2 and 3 likely due to a lower sensitivity of IP with folded native protein.

Interestingly, several epitopes were shared by purified IgGs from the TTP patients and the HD pool. The one epitope identified in all preparations was surface exposed and located in the disintegrin domain (P296-P301). This region has not yet been implicated in the literature as being immunogenic, but concurs with a reported antigenic site within the disintegrin / thrombospondin-type 1 repeat 1 region<sup>87</sup>. A monoclonal antibody targeting an adjacent region (Y305-E327) strongly inhibited ADAMTS13 activity<sup>134</sup>, which confirms the critical role of the disintegrin domain in binding to unfolded VWF<sup>67</sup>. Thus, antibodies against the epitope identified here probably also interfere with VWF interaction.

A sequence common to the HD pool and two patient samples was found in the spacer domain (T676-P682). This peptide is contained within the G662-V687 fragment that was isolated with autoantibodies from 5 of 13 TTP patients in a phage display screen where ADAMTS13 peptides with a length of 30 to 50 amino acids were expressed<sup>85</sup>. The same ADAMTS13 fragment was also identified as the major VWF-binding peptide using a similar phage display-based approach<sup>135</sup>. In the context of the larger MDTCS fragment, however, this epitope appears to be less important<sup>82</sup>. Rather, it is the adjacent site comprising residues R660, Y661 and Y665 that is considered the main target for autoantibodies in many acquired TTP patients<sup>72</sup>. No hit was observed for this peptide; given that R568 and F592 contribute to the formation of this epitope's antigenic surface<sup>86;115</sup>, it is plausible that the peptide array, designed to identify linear antigenic regions, failed to detect this epitope. This concern notwithstanding, the data shown here and those of Yamaguchi et al<sup>85</sup>, suggest that the potential role of the adjacent region (T676 - P682) as an ancillary target site for ADAMTS13 autoantibodies deserves further attention. Other shared linear epitopes between the HD pool and at least one TTP patient sample were found in the metalloprotease domain, the thrombospondin-type 1 repeat 8 domain and the CUB1 domain.

The identification of several common sites supports the idea that the antibodies isolated from a HD pool are indeed specific for ADAMTS13. Similar findings were reported for other autoimmune diseases such as anti-glomerular basement membrane (anti-GBM) disease,

where anti-GBM autoantibodies recognize the same major epitopes in patients and healthy individuals<sup>136</sup>, and systemic lupus erythematosus, where some common epitopes were likewise found for anti-caspase 8 antibodies<sup>137</sup>.

That the purified antibody preparations of the three TTP patients were inhibitory whereas those of the HD pool were not (despite recognizing common epitopes) is likely due to the vastly different affinities of the preparations towards ADAMTS13. The emergence of pathogenic autoantibodies may be caused by an enhanced frequency of somatic hypermutation of IgG memory B cells<sup>138</sup>. Another mechanism that likely contributes to the development of pathogenic antibodies is epitope spreading where additional epitopes are acquired as the disease progresses<sup>139</sup>. It will be interesting to determine whether healthy individuals with elevated anti-ADAMTS13 IgG plasma levels also test positive for the class 2 human leukocyte antigen haplotype HLA-DRB1\*11, which was identified as risk factor for acquired TTP<sup>77</sup>.

Based on these combined observations, I suggest that anti-ADAMTS13 IgG autoantibodies occurring in healthy individuals provide the template for emergence of high affinity and pathogenic IgG autoantibodies in acquired TTP. Future studies should address whether the presence of anti-ADAMTS13 antibodies precedes clinical disease onset in TTP, as shown for example in anti-glomerular basement membrane disease<sup>140</sup>. This may not only improve our understanding of the pathophysiology of acquired TTP, but also help to identify biomarkers for early diagnosis and possible therapeutic intervention.

#### **V.4. Assessment of the inhibitory activity of affinity purified ADAMTS13 autoantibodies from patients with TTP under flow conditions**

ADAMTS13 deficiency and neutralizing inhibitor titers as diagnosed in acquired TTP patients are usually explored using assays that measure the activity of ADAMTS13 under static conditions. However, these assays may not accurately mimic the situation *in vivo*, where

shear forces are required to expose the scissile bond within the A2 domain of VWF. Testing the neutralizing activity of purified anti-ADAMTS13 IgG autoantibodies from two TTP patients showed a remarkably different extent of inhibition when assayed under flow and under static conditions.

The flow-based assay developed for this study was based on ADAMTS13-dependent cleavage of platelet-adhering VWF multimers immobilized on an extra-cellular matrix-like surface (composed of fibronectin, collagen and VWF) and the extent of inhibition of the protease by anti-ADAMTS13 autoantibodies. Unlike previously described flow assays<sup>101;102;104</sup> performed in the presence of normal human plasma and thus possibly containing ill-defined cofactors affecting VWF proteolysis, cell suspensions with specified components including reconstituted erythrocytes, platelets, purified recombinant VWF, and recombinant or plasma-derived ADAMTS13 were used. Applying shear force as in arterial blood flow tethered platelets to the adhesive surface through interaction of the platelet receptor GP Iba with VWF and propagated them into stable aggregates through activation and interconnection with rVWF present in the fluid phase.

The decrease in platelet aggregate formation dose-dependently correlated with the activity of ADAMTS13 for both the recombinant and plasma-derived form of the enzyme. Compared with static assays which can readily measure ADAMTS13 activities down to a concentration of 0.1 U/ml, 1-4 U/ml were required to reliably determine the reduction in platelet aggregation. Furthermore, only at the highest concentration used (4 U/ml), platelet aggregates no longer built up over time. As the assay was intended to mimic the early events in vessel injury where ADAMTS13 is required to limit but not prevent thrombus formation, the concentration range identified appears to adequately resemble the *in vivo* situation. However, this correlation requires caution as the concentrations of surface-coated collagen and VWF as well as the actual shear forces occurring at a wounded vessel are likely to differ from those of the assay described here.

It is worth noting that flow assays based on cleavage of ULVWF strings attached to histamine-stimulated endothelial cells measure ADAMTS13 activity at a lower concentration range; for example, 0.5 U/ml ADAMTS13 (normal plasma diluted to 50%) was reported to cleave more than 95% of ULVWF-platelet strings formed in most healthy individuals<sup>101;141</sup>. Such a setup simulates the release of VWF into the circulation following secretion from intact endothelial cells. As this event can already occur under low shear stress<sup>50</sup>, it is plausible that the required ADAMTS13 concentrations are also lower than in primary hemostasis.

Most interestingly, adjusting the anti-ADAMTS13 IgG preparations from patients 2 and 3 to the same inhibitor titer as analyzed by FRET-S-VWF73 assay and applying in the flow assay showed a different degree of inhibition as manifested by a vastly different platelet aggregate surface coverage. For example, at an inhibitor titer of 3 BU/ml, the difference in surface coverage between the antibody preparations of the two patients was nearly 6-fold (90% versus 15%). This discrepancy did not stem from using rADAMTS13 in the flow assay (instead of NHP as used in the FRET-S-VWF73 assay), as similar results were obtained using pADAMTS13, indicating that the antibodies blocked the activity of pADAMTS13 and rADAMTS13 in a comparable manner. A surprising consequence of these data is that, under flow, the discrepancy between the two antibody preparations was smaller when assessing the inhibitory activities as a function of total IgG rather than the FRET-S-VWF73 based inhibitor titer. The anti-ADAMTS13 IgG preparation from patient 2 added at a concentration of 13 µg/ml (~6 BU/ml) and that from patient 3 added at 10 µg/ml (~1 BU/ml) led to a surface coverage of 40% and 46%, respectively, indicating that under flow, the two antibody preparations had almost identical specific inhibitory activities.

I presume the discrepancy to be caused by the distinct binding sites of the autoantibodies on the surface of ADAMTS13 that can selectively interfere with the docking of ADAMTS13 to VWF under flow conditions. Epitope mapping based on peptide scans showed that the IgG preparation from patient 3 not only recognized a common epitope in the disintegrin domain,

but also a unique epitope in the CUB1 domain (amino acids 1194-1204). It is thus tempting to speculate that blocking the latter binding site interferes with the regulation of enzymatic activity under flow. On the other hand, several epitopes spread over the entire protein were recognized by the antibody preparation from patient 2 only. It is therefore theoretically possible that antibody binding to one of these epitopes occurs only under static conditions or conversely, relieves ADAMTS13 from negative regulation under flow, thereby partially counteracting the overall inhibitory activity of the IgG preparation. The latter scenario would be in line with several reports indicating that the C-terminal domains of ADAMTS13 play a role in regulating its enzymatic activity, negatively or positively<sup>100;142-144</sup>. Future studies with monoclonal antibodies targeting specific epitopes may clarify whether sites critical for ADAMTS13 function selectively exist under flow.

The observed discrepancy in inhibitory activity of TTP patient plasma samples may have clinical implications when considering exogenous ADAMTS13 supplementation. If inhibitor titers measured by a flow assay were the primary determinant of the required dose of ADAMTS13<sup>119</sup>, patient 2 would need much less ADAMTS13 than patient 3 to saturate the inhibitors and restore ADAMTS13 activity. In this context, it is worth noting that the amounts of rADAMTS13 required to overcome the inhibitory activity of goat antiserum under flow are likely to overestimate the demand for patient 2 and underestimate that for patient 3, as the goat antiserum's inhibitor titer (Figure 29) was between that of patients 2 and 3 (Figure 30).

Interestingly, the doses of rADAMTS13 normalizing the enzyme activity in the presence of a goat antiserum under flow conditions were found to be approximately 3-fold higher than those under static conditions. These results, despite being generated *in vitro* and with a non-human anti-ADAMTS13 autoantibody, highlight for the first time that higher amounts of rADAMTS13 than those estimated by static assays may be necessary *in vivo* to saturate the inhibitors in acquired TTP. Until *in vivo* studies are performed, this information should be taken into account when developing rADAMTS13 dose regimens.

In summary, using purified IgG preparations from two TTP patients, I performed for the first time a side-by-side comparison of the inhibitory activity of such antibodies under static conditions and under flow. I demonstrated that two conceptually different static assays gave consistent yet discordant inhibitor titer estimates to the flow-based assay, suggesting that such assays may not always predict the true pathogenicity of anti-ADAMTS13 autoantibodies. Future work will require analysis of a larger cohort of TTP patients to determine whether this discrepancy is more common or just an idiosyncrasy of a single patient. In any case, caution is warranted when using inhibitor titers based on static assays as a guideline for treatment therapy and measuring treatment efficacy.

## VI. CONCLUSION

The thesis refers to the first comprehensive functional characterization of anti-ADAMTS13 IgG autoantibodies isolated from plasma of patients with acquired TTP and a HD pool. Using these polyclonal preparations of ADAMTS13-specific IgGs, the antibodies' subclass composition, specificity, affinity to ADAMTS13 and inhibitory activity under static and flow conditions are detailed. Affinity-purified anti-ADAMTS13 IgG antibody preparations from TTP patients displayed a high affinity to recombinant and plasma derived ADAMTS13 with a dissociation constant of ~1 nM. The antibodies comprised all four subclasses, with IgG2 being most abundant but most weakly affine IgG subclass. The subclass distribution was at variance with the measured IgG subclass titers in the starting material, possibly due to the presence of ADAMTS13 specific immune complexes which only inefficiently bind to the affinity matrix. IgGs purified from pooled normal human plasma shared some binding domains with those from acquired TTP patients suggesting that in a subset of healthy individuals, ADAMTS13-specific B cell clones pre-exist. Inhibitor testing of purified anti-ADAMTS13 IgG preparations from two TTP patients in a newly developed flow assay revealed a vastly different degree of inhibition compared to the measured FRETs-VWF73 based inhibitor titer. These results indicate a discrepancy in inhibitor assessment between static and flow conditions, suggesting that the true pathogenicity of anti-ADAMTS13 autoantibodies may not always be accurately predicted by routine assays in clinical practice. My data complement past and present studies describing functional properties of human anti-ADAMTS13 antibodies at the clonal level<sup>87;145</sup> and may shed new light on the development of inhibitory antibodies in acquired autoimmune TTP.

## REFERENCE LIST

1. Moschcowitz E. Hyaline thrombosis of the terminal arterioles and capillaries: a hitherto undescribed disease. *Proc.NY Pathol Soc* 1924;24:21-24.
2. Moake JL. Thrombotic microangiopathies. *N.Engl.J Med.* 2002;347:589-600.
3. Bukowski RM, Hewlett JS, Harris JW et al. Exchange transfusions in the treatment of thrombotic thrombocytopenic purpura. *Semin.Hematol.* 1976;13:219-232.
4. Bukowski RM, Hewlett JS, Reimer RR et al. Therapy of thrombotic thrombocytopenic purpura: an overview. *Semin.Thromb.Hemost.* 1981;7:1-8.
5. Moake JL, Rudy CK, Troll JH et al. Unusually large plasma factor VIII: von Willebrand factor multimers in chronic relapsing thrombotic thrombocytopenic purpura. *N.Engl.J.Med.* 1982;307:1432-1435.
6. Furlan M, Robles R, Lämmle B. Partial purification and characterization of a protease from human plasma cleaving von Willebrand factor to fragments produced by in vivo proteolysis. *Blood* 1996;87:4223-4234.
7. Tsai HM. Physiologic cleavage of von Willebrand factor by a plasma protease is dependent on its conformation and requires calcium ion. *Blood* 1996;87:4235-4244.
8. Dent JA, Galbusera M, Ruggeri ZM. Heterogeneity of plasma von Willebrand factor multimers resulting from proteolysis of the constituent subunit. *J.Clin.Invest* 1991;88:774-782.
9. Anderson PJ, Kokame K, Sadler JE. Zinc and calcium ions cooperatively modulate ADAMTS13 activity. *J Biol Chem.* 2006;281:850-857.

10. Furlan M, Robles R, Solenthaler M et al. Deficient activity of von Willebrand factor-cleaving protease in chronic relapsing thrombotic thrombocytopenic purpura. *Blood* 1997;89:3097-3103.
11. Furlan M, Robles R, Galbusera M et al. von Willebrand factor-cleaving protease in thrombotic thrombocytopenic purpura and the hemolytic-uremic syndrome. *N.Engl.J.Med.* 1998;339:1578-1584.
12. Tsai HM, Lian EC. Antibodies to von Willebrand factor-cleaving protease in acute thrombotic thrombocytopenic purpura. *N.Engl.J.Med.* 1998;339:1585-1594.
13. Fujikawa K, Suzuki H, McMullen B, Chung D. Purification of human von Willebrand factor-cleaving protease and its identification as a new member of the metalloproteinase family. *Blood* 2001;98:1662-1666.
14. Gerritsen HE, Robles R, Lammle B, Furlan M. Partial amino acid sequence of purified von Willebrand factor-cleaving protease. *Blood* 2001;98:1654-1661.
15. Soejima K, Mimura N, Hirashima M et al. A novel human metalloprotease synthesized in the liver and secreted into the blood: possibly, the von Willebrand factor-cleaving protease? *J.Biochem.(Tokyo)* 2001;130:475-480.
16. Levy GG, Nichols WC, Lian EC et al. Mutations in a member of the ADAMTS gene family cause thrombotic thrombocytopenic purpura. *Nature* 2001;413:488-494.
17. Zheng X, Chung D, Takayama TK et al. Structure of von Willebrand factor-cleaving protease (ADAMTS13), a metalloprotease involved in thrombotic thrombocytopenic purpura. *J.Biol.Chem.* 2001;276:41059-41063.

18. Wagner DD, Marder VJ. Biosynthesis of von Willebrand protein by human endothelial cells. Identification of a large precursor polypeptide chain. *J.Biol.Chem.* 1983;258:2065-2067.
19. Sporn LA, Chavin SI, Marder VJ, Wagner DD. Biosynthesis of von Willebrand protein by human megakaryocytes. *J Clin.Invest* 1985;76:1102-1106.
20. Sadler JE. Biochemistry and genetics of von Willebrand factor. *Annu.Rev.Biochem.* 1998;67:395-424.
21. Wagner DD. Cell biology of von Willebrand factor. *Annu.Rev.Cell Biol* 1990;6:217-246.
22. Padilla A, Moake JL, Bernardo A et al. P-selectin anchors newly released ultralarge von Willebrand factor multimers to the endothelial cell surface. *Blood* 2004;103:2150-2156.
23. Huang J, Roth R, Heuser JE, Sadler JE. Integrin alpha(v)beta(3) on human endothelial cells binds von Willebrand factor strings under fluid shear stress. *Blood* 2009;113:1589-1597.
24. Andrews RK, Lopez JA, Berndt MC. Molecular mechanisms of platelet adhesion and activation. *Int.J.Biochem.Cell Biol.* 1997;29:91-105.
25. Huizinga EG, Tsuji S, Romijn RA et al. Structures of glycoprotein Ibalpha and its complex with von Willebrand factor A1 domain. *Science* 2002;297:1176-1179.
26. Ruggeri ZM. Von Willebrand factor, platelets and endothelial cell interactions. *J.Thromb.Haemost.* 2003;1:1335-1342.

27. Fressinaud E, Baruch D, Girma JP et al. von Willebrand factor-mediated platelet adhesion to collagen involves platelet membrane glycoprotein IIb-IIIa as well as glycoprotein Ib. *J.Lab Clin.Med.* 1988;112:58-67.
28. Lankhof H, van Hoeij M, Schiphorst ME et al. A3 domain is essential for interaction of von Willebrand factor with collagen type III. *Thromb Haemost.* 1996;75:950-958.
29. Hoylaerts MF, Yamamoto H, Nuyts K et al. von Willebrand factor binds to native collagen VI primarily via its A1 domain. *Biochem.J.* 1997;324 ( Pt 1):185-191.
30. Nieswandt B, Watson SP. Platelet-collagen interaction: is GPVI the central receptor? *Blood* 2003;102:449-461.
31. Nuyttens BP, Thijs T, Deckmyn H, Broos K. Platelet adhesion to collagen. *Thromb.Res.* 2011;127 Suppl 2:S26-S29.
32. Ruggeri ZM. Platelet adhesion under flow. *Microcirculation.* 2009;16:58-83.
33. Leyte A, Verbeet MP, Brodniewicz-Proba T, van Mourik JA, Mertens K. The interaction between human blood-coagulation factor VIII and von Willebrand factor. Characterization of a high-affinity binding site on factor VIII. *Biochem.J* 1989;257:679-683.
34. Foster PA, Fulcher CA, Marti T, Titani K, Zimmerman TS. A major factor VIII binding domain resides within the amino-terminal 272 amino acid residues of von Willebrand factor. *J Biol Chem.* 1987;262:8443-8446.
35. Lenting PJ, Christophe OD, Gueguen P. The disappearing act of factor VIII. *Haemophilia.* 2010;16:6-15.

36. Weiss HJ, Sussman II, Hoyer LW. Stabilization of factor VIII in plasma by the von Willebrand factor. Studies on posttransfusion and dissociated factor VIII and in patients with von Willebrand's disease. *J Clin. Invest* 1977;60:390-404.
37. Koedam JA, Hamer RJ, Beeser-Visser NH, Bouma BN, Sixma JJ. The effect of von Willebrand factor on activation of factor VIII by factor Xa. *Eur J Biochem* 1990;189:229-234.
38. Nesheim M, Pittman DD, Giles AR et al. The effect of plasma von Willebrand factor on the binding of human factor VIII to thrombin-activated human platelets. *J Biol Chem.* 1991;266:17815-17820.
39. Lenting PJ, Donath MJ, van Mourik JA, Mertens K. Identification of a binding site for blood coagulation factor IXa on the light chain of human factor VIII. *J Biol Chem.* 1994;269:7150-7155.
40. Bendetowicz AV, Wise RJ, Gilbert GE. Collagen-bound von Willebrand factor has reduced affinity for factor VIII. *J.Biol.Chem.* 1999;274:12300-12307.
41. Sadler JE, Budde U, Eikenboom JC et al. Update on the pathophysiology and classification of von Willebrand disease: a report of the Subcommittee on von Willebrand Factor. *J Thromb Haemost.* 2006;4:2103-2114.
42. Kroll MH, Hellums JD, McIntire LV, Schafer AI, Moake JL. Platelets and shear stress. *Blood* 1996;88:1525-1541.
43. Siedlecki CA, Lestini BJ, Kottke-Marchant KK et al. Shear-dependent changes in the three-dimensional structure of human von Willebrand factor. *Blood* 1996;88:2939-2950.

44. Schneider SW, Nuschele S, Wixforth A et al. Shear-induced unfolding triggers adhesion of von Willebrand factor fibers. *Proc.Natl.Acad Sci U.S.A* 2007;104:7899-7903.
45. Zhang X, Halvorsen K, Zhang CZ, Wong WP, Springer TA. Mechanoenzymatic cleavage of the ultralarge vascular protein von Willebrand factor. *Science* 2009;324:1330-1334.
46. Fu X, Chen J, Gallagher R et al. Shear stress-induced unfolding of VWF accelerates oxidation of key methionine residues in the A1A2A3 region. *Blood* 2011;118:5283-5291.
47. Li Y, Choi H, Zhou Z et al. Covalent regulation of ULVWF string formation and elongation on endothelial cells under flow conditions. *J.Thromb.Haemost.* 2008;6:1135-1143.
48. Uemura M, Tatsumi K, Matsumoto M et al. Localization of ADAMTS13 to the stellate cells of human liver. *Blood* 2005;106:922-924.
49. Turner N, Nolasco L, Tao Z, Dong JF, Moake J. Human endothelial cells synthesize and release ADAMTS-13. *J Thromb Haemost.* 2006;4:1396-1404.
50. Turner NA, Nolasco L, Ruggeri ZM, Moake JL. Endothelial cell ADAMTS-13 and VWF: production, release, and VWF string cleavage. *Blood* 2009;114:5102-5111.
51. Liu L, Choi H, Bernardo A et al. Platelet-derived VWF-cleaving metalloprotease ADAMTS-13. *J Thromb Haemost.* 2005;3:2536-2544.
52. Crawley JT, Lam JK, Rance JB et al. Proteolytic inactivation of ADAMTS13 by thrombin and plasmin. *Blood* 2005;105:1085-1093.

53. Ono T, Mimuro J, Madoiwa S et al. Severe secondary deficiency of von Willebrand factor-cleaving protease (ADAMTS13) in patients with sepsis-induced disseminated intravascular coagulation: Its correlation to development of renal failure. *Blood* 2006;107:528-534.
54. Furlan M, Robles R, Morselli B, Sandoz P, Lammle B. Recovery and half-life of von Willebrand factor-cleaving protease after plasma therapy in patients with thrombotic thrombocytopenic purpura. *Thromb.Haemost.* 1999;81:8-13.
55. Majerus EM, Zheng X, Tuley EA, Sadler JE. Cleavage of the ADAMTS13 propeptide is not required for protease activity. *J.Biol.Chem.* 2003;278:46643-46648.
56. Gardner MD, Chion CK, de Groot R et al. A functional calcium-binding site in the metalloprotease domain of ADAMTS13. *Blood* 2009;113:1149-1157.
57. Soejima K, Matsumoto M, Kokame K et al. ADAMTS-13 cysteine-rich/spacer domains are functionally essential for von Willebrand factor cleavage. *Blood* 2003;102:3232-3237.
58. Akiyama M, Takeda S, Kokame K, Takagi J, Miyata T. Crystal structures of the noncatalytic domains of ADAMTS13 reveal multiple discontinuous exosites for von Willebrand factor. *Proc.Natl.Acad.Sci.U.S.A* 2009;106:19274-19279.
59. Zheng X, Nishio K, Majerus EM, Sadler JE. Cleavage of von Willebrand factor requires the spacer domain of the metalloprotease ADAMTS13. *J.Biol.Chem.* 2003;278:30136-30141.
60. Davis AK, Makar RS, Stowell CP, Kuter DJ, Dzik WH. ADAMTS13 binds to CD36: a potential mechanism for platelet and endothelial localization of ADAMTS13. *Transfusion* 2009;49:206-213.

61. Vomund AN, Majerus EM. ADAMTS13 bound to endothelial cells exhibits enhanced cleavage of von Willebrand factor. *J Biol Chem* 2009;284:30925-30932.
62. Shang D, Zheng XW, Niiya M, Zheng XL. Apical sorting of ADAMTS13 in vascular endothelial cells and Madin-Darby canine kidney cells depends on the CUB domains and their association with lipid rafts. *Blood* 2006;108:2207-2215.
63. Ricketts LM, Dlugosz M, Luther KB, Haltiwanger RS, Majerus EM. O-fucosylation is required for ADAMTS13 secretion. *J.Biol.Chem.* 2007;282:17014-17023.
64. Zhou W, Tsai HM. N-Glycans of ADAMTS13 modulate its secretion and von Willebrand factor cleaving activity. *Blood* 2009;113:929-935.
65. McKinnon TA, Chion AC, Millington AJ, Lane DA, Laffan MA. N-linked glycosylation of VWF modulates its interaction with ADAMTS13. *Blood* 2008;111:3042-3049.
66. Majerus EM, Anderson PJ, Sadler JE. Binding of ADAMTS13 to von Willebrand factor. *J.Biol.Chem.* 2005;280:21773-21778.
67. Crawley JT, de GR, Xiang Y, Luken BM, Lane DA. Unraveling the scissile bond: how ADAMTS13 recognizes and cleaves von Willebrand factor. *Blood* 2011;118:3212-3221.
68. Zanardelli S, Chion AC, Groot E et al. A novel binding site for ADAMTS13 constitutively exposed on the surface of globular VWF. *Blood* 2009;114:2819-2828.
69. Feys HB, Anderson PJ, Vanhoorelbeke K, Majerus EM, Sadler JE. Multi-step binding of ADAMTS13 to VWF. *J Thromb Haemost* 2009;7:2088-2095.
70. Kokame K, Matsumoto M, Fujimura Y, Miyata T. VWF73, a region from D1596 to R1668 of von Willebrand factor, provides a minimal substrate for ADAMTS-13. *Blood* 2004;103:607-612.

71. Gao W, Anderson PJ, Majerus EM, Tuley EA, Sadler JE. Exosite interactions contribute to tension-induced cleavage of von Willebrand factor by the antithrombotic ADAMTS13 metalloprotease. *Proc.Natl.Acad.Sci.U.S.A.* 2006;103:19099-19104.
72. Pos W, Crawley JT, Fijnheer R et al. An autoantibody epitope comprising residues R660, Y661, and Y665 in the ADAMTS13 spacer domain identifies a binding site for the A2 domain of VWF. *Blood* 2010;115:1640-1649.
73. de Groot R, Bardhan A, Ramroop N, Lane DA, Crawley JT. Essential role of the disintegrin-like domain in ADAMTS13 function. *Blood* 2009;113:5609-5616.
74. Xiang Y, de GR, Crawley JT, Lane DA. Mechanism of von Willebrand factor scissile bond cleavage by a disintegrin and metalloproteinase with a thrombospondin type 1 motif, member 13 (ADAMTS13). *Proc.Natl.Acad.Sci.U.S.A* 2011;108:11602-11607.
75. Lotta LA, Garagiola I, Palla R, Cairo A, Peyvandi F. ADAMTS13 mutations and polymorphisms in congenital thrombotic thrombocytopenic purpura. *Hum.Mutat.* 2010;31:11-19.
76. Terrell DR, Williams LA, Vesely SK et al. The incidence of thrombotic thrombocytopenic purpura-hemolytic uremic syndrome: all patients, idiopathic patients, and patients with severe ADAMTS-13 deficiency. *J.Thromb.Haemost.* 2005;3:1432-1436.
77. Coppo P, Busson M, Veyradier A et al. HLA-DRB1\*11: a strong risk factor for acquired severe ADAMTS13 deficiency-related idiopathic thrombotic thrombocytopenic purpura in Caucasians. *J.Thromb.Haemost.* 2010;8:856-859.
78. Ferrari S, Scheiflinger F, Rieger M et al. Prognostic value of anti-ADAMTS 13 antibody features (Ig isotype, titer, and inhibitory effect) in a cohort of 35 adult French

- patients undergoing a first episode of thrombotic microangiopathy with undetectable ADAMTS 13 activity. *Blood* 2007;109:2815-2822.
79. Pos W, Luken BM, Sorvillo N, Kremer Hovinga JA, Voorberg J. Humoral immune response to ADAMTS13 in acquired thrombotic thrombocytopenic purpura. *J.Thromb.Haemost.* 2011;9:1285-1291.
  80. Klaus C, Plaimauer B, Studt JD et al. Epitope mapping of ADAMTS13 autoantibodies in acquired thrombotic thrombocytopenic purpura. *Blood* 2004;103:4514-4519.
  81. Luken BM, Turenhout EA, Hulstein JJ et al. The spacer domain of ADAMTS13 contains a major binding site for antibodies in patients with thrombotic thrombocytopenic purpura. *Thromb.Haemost.* 2005;93:267-274.
  82. Luken BM, Turenhout EA, Kaijen PH et al. Amino acid regions 572-579 and 657-666 of the spacer domain of ADAMTS13 provide a common antigenic core required for binding of antibodies in patients with acquired TTP. *Thromb.Haemost.* 2006;96:295-301.
  83. Zhou W, Dong L, Ginsburg D, Bouhassira EE, Tsai HM. Enzymatically active ADAMTS13 variants are not inhibited by anti-ADAMTS13 autoantibodies: a novel therapeutic strategy? *J.Biol.Chem.* 2005;280:39934-39941.
  84. Zheng XL, Wu HM, Shang D et al. Multiple domains of ADAMTS13 are targeted by autoantibodies against ADAMTS13 in patients with acquired idiopathic thrombotic thrombocytopenic purpura. *Haematologica.* 2010;95:1555-1562.
  85. Yamaguchi Y, Moriki T, Igari A et al. Epitope analysis of autoantibodies to ADAMTS13 in patients with acquired thrombotic thrombocytopenic purpura. *Thromb.Res.* 2011;128:169-173.

86. Pos W, Sorvillo N, Fijnheer R et al. Residues Arg568 and Phe592 contribute to an antigenic surface for anti-ADAMTS13 antibodies in the spacer domain. *Haematologica* 2011;96:1670-1677.
87. Luken BM, Kaijen PH, Turenhout EA et al. Multiple B-cell clones producing antibodies directed to the spacer and disintegrin/thrombospondin type-1 repeat 1 (TSP1) of ADAMTS13 in a patient with acquired thrombotic thrombocytopenic purpura. *J.Thromb.Haemost.* 2006;4:2355-2364.
88. Veyradier A, Obert B, Houllier A, Meyer D, Girma JP. Specific von Willebrand factor-cleaving protease in thrombotic microangiopathies: a study of 111 cases. *Blood* 2001;98:1765-1772.
89. Gerritsen HE, Turecek PL, Schwarz HP, Lammle B, Furlan M. Assay of von Willebrand factor (vWF)-cleaving protease based on decreased collagen binding affinity of degraded vWF: a tool for the diagnosis of thrombotic thrombocytopenic purpura (TTP). *Thromb.Haemost.* 1999;82:1386-1389.
90. Bohm M, Vigh T, Scharrer I. Evaluation and clinical application of a new method for measuring activity of von Willebrand factor-cleaving metalloprotease (ADAMTS13). *Ann.Hematol.* 2002;81:430-435.
91. Obert B, Tout H, Veyradier A et al. Estimation of the von Willebrand factor-cleaving protease in plasma using monoclonal antibodies to vWF. *Thromb.Haemost.* 1999;82:1382-1385.
92. Whitelock JL, Nolasco L, Bernardo A et al. ADAMTS-13 activity in plasma is rapidly measured by a new ELISA method that uses recombinant VWF-A2 domain as substrate. *J.Thromb.Haemost.* 2004;2:485-491.

93. Zhou W, Tsai HM. An enzyme immunoassay of ADAMTS13 distinguishes patients with thrombotic thrombocytopenic purpura from normal individuals and carriers of ADAMTS13 mutations. *Thromb.Haemost.* 2004;91:806-811.
94. Kato S, Matsumoto M, Matsuyama T et al. Novel monoclonal antibody-based enzyme immunoassay for determining plasma levels of ADAMTS13 activity. *Transfusion* 2006;46:1444-1452.
95. Wu JJ, Fujikawa K, Lian EC et al. A rapid enzyme-linked assay for ADAMTS-13. *J Thromb Haemost.* 2006;4:129-136.
96. Cruz MA, Whitelock J, Dong JF. Evaluation of ADAMTS-13 activity in plasma using recombinant von Willebrand Factor A2 domain polypeptide as substrate. *Thromb.Haemost.* 2003;90:1204-1209.
97. Kokame K, Nobe Y, Kokubo Y, Okayama A, Miyata T. FRETTS-VWF73, a first fluorogenic substrate for ADAMTS13 assay. *Br.J Haematol.* 2005;129:93-100.
98. Jin M, Casper TC, Cataland SR et al. Relationship between ADAMTS13 activity in clinical remission and the risk of TTP relapse. *Br.J Haematol.* 2008;141:651-658.
99. Tripodi A, Peyvandi F, Chantarangkul V et al. Second international collaborative study evaluating performance characteristics of methods measuring the von Willebrand factor cleaving protease (ADAMTS-13). *J Thromb Haemost* 2008;6:1534-1541.
100. Muia J, Gao W, Haberichter SL et al. An optimized fluorogenic ADAMTS13 assay with increased sensitivity for the investigation of patients with thrombotic thrombocytopenic purpura. *J.Thromb.Haemost.* 2013;11:1511-1518.

101. Dong JF, Moake JL, Nolasco L et al. ADAMTS-13 rapidly cleaves newly secreted ultralarge von Willebrand factor multimers on the endothelial surface under flowing conditions. *Blood* 2002;100:4033-4039.
102. Shenkman B, Inbal A, Tamarin I et al. Diagnosis of thrombotic thrombocytopenic purpura based on modulation by patient plasma of normal platelet adhesion under flow condition. *Br.J.Haematol.* 2003;120:597-604.
103. Shim K, Anderson PJ, Tuley EA, Wiswall E, Sadler JE. Platelet-VWF complexes are preferred substrates of ADAMTS13 under fluid shear stress. *Blood* 2008;111:651-657.
104. Han Y, Xiao J, Falls E, Zheng XL. A shear-based assay for assessing plasma ADAMTS13 activity and inhibitors in patients with thrombotic thrombocytopenic purpura. *Transfusion* 2011;51:1580-1591.
105. Feys HB, Liu F, Dong N et al. ADAMTS-13 plasma level determination uncovers antigen absence in acquired thrombotic thrombocytopenic purpura and ethnic differences. *J.Thromb.Haemost.* 2006;4:955-962.
106. Rieger M, Ferrari S, Kremer Hovinga JA et al. Relation between ADAMTS13 activity and ADAMTS13 antigen levels in healthy donors and patients with thrombotic microangiopathies (TMA). *Thromb Haemost.* 2006;95:212-220.
107. Yang S, Jin M, Lin S, Cataland S, Wu H. ADAMTS13 activity and antigen during therapy and follow-up of patients with idiopathic thrombotic thrombocytopenic purpura: correlation with clinical outcome. *Haematologica* 2011;96:1521-1527.
108. Froehlich-Zahnd R, George JN, Vesely SK et al. Evidence for a role of anti-ADAMTS13 autoantibodies despite normal ADAMTS13 activity in recurrent thrombotic thrombocytopenic purpura. *Haematologica* 2012;97:297-303.

109. Rieger M, Mannucci PM, Kremer Hovinga JA et al. ADAMTS13 autoantibodies in patients with thrombotic microangiopathies and other immunomediated diseases. *Blood* 2005;106:1262-1267.
110. Ferrari S, Mudde GC, Rieger M et al. IgG subclass distribution of anti-ADAMTS13 antibodies in patients with acquired thrombotic thrombocytopenic purpura. *J Thromb Haemost* 2009;7:1703-1710.
111. Barbot J, Costa E, Guerra M et al. Ten years of prophylactic treatment with fresh-frozen plasma in a child with chronic relapsing thrombotic thrombocytopenic purpura as a result of a congenital deficiency of von Willebrand factor-cleaving protease. *Br.J Haematol.* 2001;113:649-651.
112. George JN. How I treat patients with thrombotic thrombocytopenic purpura - 2010. *Blood* 2010;116:4060-4069.
113. Dong L, Chandrasekaran V, Zhou W, Tsai HM. Evolution of ADAMTS13 antibodies in a fatal case of thrombotic thrombocytopenic purpura. *Am.J.Hematol.* 2008;83:815-817.
114. Hiura H, Matsui T, Matsumoto M et al. Proteolytic fragmentation and sugar chains of plasma ADAMTS13 purified by a conformation-dependent monoclonal antibody. *J.Biochem.* 2010;148:403-411.
115. Jian C, Xiao J, Gong L et al. Gain-of-function ADAMTS13 variants that are resistant to autoantibodies against ADAMTS13 in patients with acquired thrombotic thrombocytopenic purpura. *Blood* 2012;119:3836-3843.
116. Plaimauer B, Zimmermann K, Volkel D et al. Cloning, expression, and functional characterization of the von Willebrand factor-cleaving protease (ADAMTS13). *Blood* 2002;100:3626-3632.

117. Turecek PL, Schrenk G, Rottensteiner H et al. Structure and function of a recombinant von Willebrand factor drug candidate. *Semin.Thromb.Hemost.* 2010;36:510-521.
118. Ruggeri ZM, Zimmerman TS. The complex multimeric composition of factor VIII/von Willebrand factor. *Blood* 1981;57:1140-1143.
119. Plaimauer B, Kremer Hovinga JA, Juno C et al. Recombinant ADAMTS13 normalizes von Willebrand factor-cleaving activity in plasma of acquired TTP patients by overriding inhibitory antibodies. *J Thromb Haemost* 2011;9:936-944.
120. Ferrari S, Palavra K, Gruber B et al. Persistence of circulating ADAMTS13-specific immune complexes in patients with acquired thrombotic thrombocytopenic purpura. *Haematologica* 2013; Nov 15. [Epub ahead of print]
121. Naser WL. Single incubation multilayer immune technique. *J.Immunol.Methods* 1990;129:151-157.
122. Dati F, Schumann G, Thomas L et al. Consensus of a group of professional societies and diagnostic companies on guidelines for interim reference ranges for 14 proteins in serum based on the standardization against the IFCC/BCR/CAP Reference Material (CRM 470). International Federation of Clinical Chemistry. Community Bureau of Reference of the Commission of the European Communities. College of American Pathologists. *Eur.J.Clin.Chem.Clin.Biochem.* 1996;34:517-520.
123. Schauer U, Stemberg F, Rieger CH et al. IgG subclass concentrations in certified reference material 470 and reference values for children and adults determined with the binding site reagents. *Clin.Chem.* 2003;49:1924-1929.

124. Aihara M, Sawada Y, Ueno K et al. Visualization of von Willebrand factor multimers by immunoenzymatic stain using avidin-biotin peroxidase complex. *Thromb.Haemost.* 1986;55:263-267.
125. Mosyak L, Georgiadis K, Shane T et al. Crystal structures of the two major aggrecan degrading enzymes, ADAMTS4 and ADAMTS5. *Protein Sci.* 2008;17:16-21.
126. Lam JK, Chion CK, Zanardelli S, Lane DA, Crawley JT. Further characterization of ADAMTS-13 inactivation by thrombin. *J Thromb Haemost* 2007;5:1010-1018.
127. Tsai HM, Raoufi M, Zhou W et al. ADAMTS13-binding IgG are present in patients with thrombotic thrombocytopenic purpura. *Thromb Haemost.* 2006;95:886-892.
128. Yeh HC, Zhou Z, Choi H et al. Disulfide bond reduction of von Willebrand factor by ADAMTS-13. *J.Thromb.Haemost.* 2010;8:2778-2788.
129. Lotta LA, Valsecchi C, Pontiggia S et al. Measurement and prevalence of circulating ADAMTS13-specific immune complexes in autoimmune thrombotic thrombocytopenic purpura. *J.Thromb.Haemost.* 2014;12:329-336.
130. Fuchs TA, Kremer Hovinga JA, Schatzberg D, Wagner DD, Lammle B. Circulating DNA and myeloperoxidase indicate disease activity in patients with thrombotic microangiopathies. *Blood* 2012;120:1157-1164.
131. Whelan SF, Hofbauer CJ, Horling FM et al. Distinct characteristics of antibody responses against factor VIII in healthy individuals and in different cohorts of hemophilia A patients. *Blood* 2013;121:1039-1048.
132. Williams WM, Isenberg DA. A cross-sectional study of anti-DNA antibodies in the serum and IgG and IgM fraction of healthy individuals, patients with systemic lupus erythematosus and their relatives. *Lupus* 1996;5:576-586.

133. Coutinho A, Kazatchkine MD, Avrameas S. Natural autoantibodies. *Curr.Opin.Immunol.* 1995;7:812-818.
134. Igari A, Nakagawa T, Moriki T et al. Identification of epitopes on ADAMTS13 recognized by a panel of monoclonal antibodies with functional or non-functional effects on catalytic activity. *Thromb.Res.* 2012;130:e79-e83.
135. Moriki T, Maruyama IN, Igari A, Ikeda Y, Murata M. Identification of ADAMTS13 peptide sequences binding to von Willebrand factor. *Biochem.Biophys.Res.Commun.* 2010;391:783-788.
136. Yang R, Cui Z, Hellmark T et al. Natural anti-GBM antibodies from normal human sera recognize alpha3(IV)NC1 restrictively and recognize the same epitopes as anti-GBM antibodies from patients with anti-GBM disease. *Clin.Immunol.* 2007;124:207-212.
137. Ueki A, Isozaki Y, Tomokuni A et al. Intramolecular epitope spreading among anti-caspase-8 autoantibodies in patients with silicosis, systemic sclerosis and systemic lupus erythematosus, as well as in healthy individuals. *Clin.Exp.Immunol.* 2002;129:556-561.
138. Mietzner B, Tsuiji M, Scheid J et al. Autoreactive IgG memory antibodies in patients with systemic lupus erythematosus arise from nonreactive and polyreactive precursors. *Proc.Natl.Acad.Sci.U.S.A* 2008;105:9727-9732.
139. Roth AJ, Ooi JD, Hess JJ et al. Epitope specificity determines pathogenicity and detectability in ANCA-associated vasculitis. *J.Clin.Invest* 2013;123:1773-1783.
140. Olson SW, Arbogast CB, Baker TP et al. Asymptomatic autoantibodies associate with future anti-glomerular basement membrane disease. *J.Am.Soc.Nephrol.* 2011;22:1946-1952.

141. Dong JF, Whitelock J, Bernardo A, Ball C, Cruz MA. Variations among normal individuals in the cleavage of endothelial-derived ultra-large von Willebrand factor under flow. *J.Thromb.Haemost.* 2004;2:1460-1466.
142. Tao Z, Wang Y, Choi H et al. Cleavage of ultralarge multimers of von Willebrand factor by C-terminal-truncated mutants of ADAMTS-13 under flow. *Blood* 2005;106:141-143.
143. Tao Z, Peng Y, Nolasco L et al. Recombinant CUB-1 domain polypeptide inhibits the cleavage of ULVWF strings by ADAMTS13 under flow conditions. *Blood* 2005;106:4139-4145.
144. De MB, De Meyer SF, Feys HB et al. The distal carboxyterminal domains of murine ADAMTS13 influence proteolysis of platelet-decorated VWF strings in vivo. *J.Thromb.Haemost.* 2010;8:2305-2312.
145. Pos W, Luken BM, Kremer Hovinga JA et al. VH1-69 germline encoded antibodies directed towards ADAMTS13 in patients with acquired thrombotic thrombocytopenic purpura. *J.Thromb.Haemost.* 2009;7:421-428.

## APPENDED PUBLICATIONS

- 1- **Anti-ADAMTS13 IgG autoantibodies present in healthy individuals share linear epitopes with those in patients with thrombotic thrombocytopenic purpura.**

Grillberger R, Casina VC, Turecek PL, Zheng XL, Rottensteiner H, Scheiflinger F. Haematologica 2014; Feb 14. [Epub ahead of print]

- 2- **Development of a flow-based assay to test ADAMTS13 activity reveals discrepancies in inhibitor assessment compared to conventional clinical static assays.** Rana Grillberger, Bernadette Gruber, Susanna Skalicky, Gerald Schrenk, Paul Knöbl, Barbara Plaimauer, Peter L. Turecek, Friedrich Scheiflinger and Hanspeter Rottensteiner (Submitted for publication)





EUROPEAN  
HEMATOLOGY  
ASSOCIATION

 **haematologica**  
Journal of the European Hematology Association

## Anti-ADAMTS13 IgG autoantibodies present in healthy individuals share linear epitopes with those in patients with thrombotic thrombocytopenic purpura

by Rana Grillberger, Veronica C. Casina, Peter L. Turecek, X. Long Zheng, Hanspeter Rottensteiner, and Friedrich Scheifflinger

Haematologica 2013 [Epub ahead of print]

Citation: Grillberger R, Casina VC, Turecek PL, Zheng XL, Rottensteiner H, and Scheifflinger F. Anti-ADAMTS13 IgG autoantibodies present in healthy individuals share linear epitopes with those in patients with thrombotic thrombocytopenic purpura. *Haematologica*. 2014; 99:xxx  
doi:10.3324/haematol.2013.100685

### *Publisher's Disclaimer.*

*E-publishing ahead of print is increasingly important for the rapid dissemination of science. Haematologica is, therefore, E-publishing PDF files of an early version of manuscripts that have completed a regular peer review and have been accepted for publication. E-publishing of this PDF file has been approved by the authors. After having E-published Ahead of Print, manuscripts will then undergo technical and English editing, typesetting, proof correction and be presented for the authors' final approval; the final version of the manuscript will then appear in print on a regular issue of the journal. All legal disclaimers that apply to the journal also pertain to this production process.*

**Anti-ADAMTS13 IgG autoantibodies present in healthy individuals share linear epitopes with those in patients with thrombotic thrombocytopenic purpura**

Rana Grillberger<sup>1</sup>, Veronica C. Casina<sup>2</sup>, Peter L. Turecek<sup>1</sup>, X. Long Zheng<sup>2</sup>, Hanspeter Rottensteiner<sup>1\*</sup> and Friedrich Scheiflinger<sup>1</sup>

1) Baxter Innovations GmbH, Vienna, Austria

2) Department of Pathology and Laboratory Medicine, the Children's Hospital of Philadelphia and the University of Pennsylvania Perelman School of Medicine, Philadelphia, PA

\* Correspondence to:

Hanspeter Rottensteiner

Baxter Innovations GmbH

Industriestrasse 67

1221 Vienna, Austria

Phone: +43 1 20100 2472941

Fax: +43 1 20100 5046

E-Mail: [Hanspeter.Rottensteiner@baxter.com](mailto:Hanspeter.Rottensteiner@baxter.com)

Anti-ADAMTS13 autoantibodies, predominantly of the IgG class, are found in plasma of patients with acquired thrombotic thrombocytopenic purpura (TTP)<sup>1</sup> but also in about 5% of healthy individuals<sup>1</sup>. Antibodies from TTP patients have previously been studied using various epitope mapping techniques<sup>2,3,4,5</sup>. Applying patient-derived monoclonal antibodies and point mutated variants of ADAMTS13, these studies revealed that IgG autoantibodies target a major binding site on the surface of the spacer domain of ADAMTS13<sup>6,7,8</sup>, and identified additional epitopes located in other domains of the protease<sup>2,4,5,9</sup>. By contrast, ADAMTS13-specific autoantibodies from healthy individuals remain ill-defined and their binding specificities are unknown.

To determine which epitopes are recognized by anti-ADAMTS13 antibodies from healthy individuals, a plasma pool (~ 1 l) of 45 randomly selected healthy donors (HD), donated by the Baxter plasma center Vienna (Austria) was used as starting material. As a sufficient amount of plasma with a positive anti-ADAMTS13 IgG titer from one single healthy donor was not available, we assumed, based on the reported prevalence (5%)<sup>1</sup> of elevated anti-ADAMTS13 IgG titers in healthy individuals, that a pool of 45 must contain at least 2 to 3 positive donors. IgG anti-ADAMTS13 autoantibodies were isolated in a two-step chromatographic purification procedure using an ADAMTS13 affinity matrix and protein G. Plasma samples of three acquired TTP patients with positive IgG titers and known inhibitors served as a reference (Table 1). ADAMTS13-specific IgGs, recovered from the HD plasma pool and detected by ELISA, showed low affinity towards ADAMTS13 using Biacore, and were non-neutralizing in the FRETs-VWF73 activity assay. As expected, autoantibodies derived from the three TTP patients were of high affinity and inhibited ADAMTS13 activity (Table 1).

A rough mapping of binding epitopes was achieved by testing the antibody preparations for interaction with full-length rADAMTS13 and a series of truncated variants thereof (Figure 1A-B). The antigen-antibody complexes that eventually formed were isolated by protein G, and co-

immunoprecipitated ADAMTS13 fragments visualized by Western blot according to a published protocol<sup>4,8</sup>. The purified IgGs from all three TTP patients clearly interacted with full-length ADAMTS13 and the N-terminal fragments up to the spacer domain (MDT and MDTCS; Figure 1C-E). The stronger signal intensity for the MDTCS compared with the MDT fragment was in line with the presence of a major binding site within the spacer domain<sup>6,7,8</sup>. The more distal C-terminal domains of ADAMTS13 (T2C and CUB) were only weakly recognized by the antibodies (Figure 1C-E). The HD antibody preparation gave rise to a similar profile, except that it bound stronger to the MDT than to the MDTCS fragment (Figure 1F).

To narrow down the binding sites identified by immunoprecipitation, epitopes were additionally determined using peptide arrays (PEPperMAP<sup>®</sup>; PEPperPRINT GmbH, Heidelberg, Germany), a strategy previously used to identify antibodies' linear binding epitopes<sup>10</sup>. Incubation of these arrays, which had spotted the entire sequence of ADAMTS13 in the form of 13mer peptides with a 12 amino acid overlap, with a control monoclonal anti-ADAMTS13 antibody resulted in a single hit located in the metalloprotease domain of ADAMTS13 (not shown). By contrast, all affinity-purified antibodies gave rise to multiple hits, indicative of their polyclonal nature (Table 2). The antigenic regions were clustered in the metalloprotease (M), disintegrin (D), spacer (S), thrombospondin 1-8 (T1-8) and CUB domains. No positive spots were detected with any antibody for the cysteine-rich as well as the T1-1, T1-3, T1-5 and T1-7 domains. Using the published crystal structure of an ADAMTS13 DTCS fragment and a modeled metalloprotease domain (based on the structures of human ADAMTS4/5), all but one (D173-Y177) epitopes were displayed on the surface of ADAMTS13 (Supplementary Figure 1), illustrating the accessibility of these binding sites to the isolated autoantibodies.

Interestingly, the peptide recognition patterns of the antibody preparations from HD and the TTP patients were remarkably similar (Table 2). All four samples identified an epitope in the disintegrin

domain (P296-P301) that also showed the strongest signals. Such an epitope has not yet been implicated in the literature as being immunogenic, but concurs with a reported antigenic site within the D/T1-1 region<sup>9</sup>. A monoclonal antibody targeting an adjacent region (Y305-E327) strongly inhibited ADAMTS13 activity<sup>11</sup>, which confirms the critical role of the D domain in binding to unfolded VWF<sup>12</sup>. Thus, antibodies against the epitope identified here probably also interfere with VWF interaction.

A sequence common to the HD pool and two patient samples was found in the spacer domain (T676-P682). This peptide is contained within the G662-V687 fragment that was isolated with autoantibodies from 5 of 13 TTP patients in a phage display screen where ADAMTS13 peptides with a length of 30 to 50 amino acids were expressed<sup>5</sup>. The same ADAMTS13 fragment was also identified as the major VWF-binding peptide using a similar phage display-based approach<sup>13</sup>. In the context of the larger MDTCS fragment, however, this epitope appears to be less important<sup>3</sup>. Rather, it is the adjacent site comprising residues R660, Y661 and Y665 that is considered the main target for autoantibodies from many acquired TTP patients<sup>6</sup>. No hit was observed for this peptide; given that R568 and F592 contribute to the formation of this epitope's antigenic surface<sup>7,8</sup>, it is plausible that the peptide array, designed to identify linear antigenic regions, failed to detect this epitope. This concern notwithstanding, our data and those of Yamaguchi et al<sup>5</sup>, suggest that the potential role of the adjacent region (T676 - P682) as an ancillary target site for ADAMTS13 autoantibodies deserves further attention.

Other shared linear epitopes between the HD pool and at least one TTP patient sample were found in the M domain, the T1-8 domain and the CUB1 domain (Table 2). The identification of several common sites supports the idea that the antibodies isolated from a HD pool are indeed specific for ADAMTS13. Similar findings were reported for other autoimmune diseases such as anti-glomerular basement membrane (anti-GBM) disease, where anti-GBM autoantibodies recognize the same

major epitopes in patients and healthy individuals<sup>14</sup>, and systemic lupus erythematosus, where some common epitopes were likewise found for anti-caspase 8 antibodies<sup>15</sup>.

That the purified antibody preparations of the three TTP patients were inhibitory whereas those of the HD pool were not (despite recognizing common epitopes) is likely due to the vastly different affinities of the preparations towards ADAMTS13. The emergence of pathogenic autoantibodies may be caused by an enhanced frequency of somatic hypermutation of IgG memory B cells<sup>16</sup>.

Another mechanism that likely contributes to the development of pathogenic antibodies is epitope spreading where additional epitopes are acquired as the disease progresses<sup>17</sup>. It will be interesting to see if healthy individuals with elevated anti-ADAMTS13 IgG plasma levels also test positive for the class 2 human leukocyte antigen haplotype HLA-DRB1\*11, which was identified as risk factor for acquired TTP<sup>18</sup>.

Based on our combined data, it is tempting to suggest that anti-ADAMTS13 IgG autoantibodies occurring in healthy individuals provide the template for emergence of high affinity and pathogenic IgG autoantibodies in acquired TTP. Future studies should address whether the presence of anti-ADAMTS13 antibodies precedes clinical disease onset in TTP, as shown for instance in anti-GBM disease<sup>19</sup>. This may not only improve our understanding of the pathophysiology of acquired TTP, but also help to identify biomarkers for early diagnosis and possible therapeutic intervention.

## Reference List

1. Rieger M, Mannucci PM, Kremer Hovinga JA, Herzog A, Gerstenbauer G, Konetschny C et al. ADAMTS13 autoantibodies in patients with thrombotic microangiopathies and other immunomediated diseases. *Blood*. 2005;106(4):1262-7.
2. Klaus C, Plaimauer B, Studt JD, Dorner F, Lammler B, Mannucci PM et al. Epitope mapping of ADAMTS13 autoantibodies in acquired thrombotic thrombocytopenic purpura. *Blood*. 2004;103(12):4514-9.
3. Luken BM, Turenhout EA, Kaijen PH, Greuter MJ, Pos W, Van Mourik JA et al. Amino acid regions 572-579 and 657-666 of the spacer domain of ADAMTS13 provide a common antigenic core required for binding of antibodies in patients with acquired TTP. *Thromb Haemost*. 2006;96(3):295-301.
4. Zheng XL, Wu HM, Shang D, Falls E, Skipwith CG, Cataland SR et al. Multiple domains of ADAMTS13 are targeted by autoantibodies against ADAMTS13 in patients with acquired idiopathic thrombotic thrombocytopenic purpura. *Haematologica*. 2010;95(9):1555-62.
5. Yamaguchi Y, Moriki T, Igari A, Nakagawa T, Wada H, Matsumoto M et al. Epitope analysis of autoantibodies to ADAMTS13 in patients with acquired thrombotic thrombocytopenic purpura. *Thromb Res*. 2011;128(2):169-73.
6. Pos W, Crawley JT, Fijnheer R, Voorberg J, Lane DA, and Luken BM. An autoantibody epitope comprising residues R660, Y661, and Y665 in the ADAMTS13 spacer domain identifies a binding site for the A2 domain of VWF. *Blood*. 2010;115(8):1640-9.
7. Pos W, Sorvillo N, Fijnheer R, Feys HB, Kaijen PH, Vidarsson G et al. Residues Arg568 and Phe592 contribute to an antigenic surface for anti-ADAMTS13 antibodies in the spacer domain. *Haematologica*. 2011;96(11):1670-7.
8. Jian C, Xiao J, Gong L, Skipwith CG, Jin SY, Kwaan HC et al. Gain-of-function ADAMTS13 variants that are resistant to autoantibodies against ADAMTS13 in patients with acquired thrombotic thrombocytopenic purpura. *Blood*. 2012;119(16):3836-43.
9. Luken BM, Kaijen PH, Turenhout EA, Kremer Hovinga JA, Van Mourik JA, Fijnheer R et al. Multiple B-cell clones producing antibodies directed to the spacer and disintegrin/thrombospondin type-1 repeat 1 (TSP1) of ADAMTS13 in a patient with acquired thrombotic thrombocytopenic purpura. *J Thromb Haemost*. 2006;4(11):2355-64.
10. Shukla NM, Salunke DB, Balakrishna R, Mutz CA, Malladi SS, and David SA. Potent adjuvanticity of a pure TLR7-agonistic imidazoquinoline dendrimer. *PLoS One*. 2012;7(8):e43612.
11. Igari A, Nakagawa T, Moriki T, Yamaguchi Y, Matsumoto M, Fujimura Y et al. Identification of epitopes on ADAMTS13 recognized by a panel of monoclonal antibodies with functional or non-functional effects on catalytic activity. *Thromb Res*. 2012;130(3):e79-e83.

12. Crawley JT, de GR, Xiang Y, Luken BM, and Lane DA. Unraveling the scissile bond: how ADAMTS13 recognizes and cleaves von Willebrand factor. *Blood*. 2011;118(12):3212-21.
13. Moriki T, Maruyama IN, Igari A, Ikeda Y, and Murata M. Identification of ADAMTS13 peptide sequences binding to von Willebrand factor. *Biochem Biophys Res Commun*. 2010;391(1):783-8.
14. Yang R, Cui Z, Hellmark T, Segelmark M, Zhao MH, and Wang HY. Natural anti-GBM antibodies from normal human sera recognize alpha3(IV)NC1 restrictively and recognize the same epitopes as anti-GBM antibodies from patients with anti-GBM disease. *Clin Immunol*. 2007;124(2):207-12.
15. Ueki A, Isozaki Y, Tomokuni A, Hatayama T, Ueki H, Kusaka M et al. Intramolecular epitope spreading among anti-caspase-8 autoantibodies in patients with silicosis, systemic sclerosis and systemic lupus erythematosus, as well as in healthy individuals. *Clin Exp Immunol*. 2002;129(3):556-61.
16. Mietzner B, Tsuiji M, Scheid J, Velinzon K, Tiller T, Abraham K et al. Autoreactive IgG memory antibodies in patients with systemic lupus erythematosus arise from nonreactive and polyreactive precursors. *Proc Natl Acad Sci U S A*. 2008;105(28):9727-32.
17. Roth AJ, Ooi JD, Hess JJ, van Timmeren MM, Berg EA, Poulton CE et al. Epitope specificity determines pathogenicity and detectability in ANCA-associated vasculitis. *J Clin Invest*. 2013;123(4):1773-83.
18. Coppo P, Busson M, Veyradier A, Wynckel A, Poullin P, Azoulay E et al. HLA-DRB1\*11: a strong risk factor for acquired severe ADAMTS13 deficiency-related idiopathic thrombotic thrombocytopenic purpura in Caucasians. *J Thromb Haemost*. 2010;8(4):856-9.
19. Olson SW, Arbogast CB, Baker TP, Owshalimpur D, Oliver DK, Abbott KC et al. Asymptomatic autoantibodies associate with future anti-glomerular basement membrane disease. *J Am Soc Nephrol*. 2011;22(10):1946-52.

**Table 1. ADAMTS13-related variables measured in plasma of 3 acquired TTP patients and a HD pool, and characteristics of the affinity-purified anti-ADAMTS13 IgGs derived thereof**

		<b>Patient 1</b>	<b>Patient 2</b>	<b>Patient 3</b>	<b>HD pool</b>
<b>Plasma</b>	<b>ADAMTS13 antigen</b> ( $\mu\text{g/ml}$ )	0.21	0.04	0.03	0.61
	<b>ADAMTS13 activity</b> (U/ml)	<0.05	<0.05	<0.05	0.95
	<b>Inhibitors (BU/ml)</b>	1.60	1.75	1.33	-
	<b>Anti-ADAMTS13 IgG titer</b>	1:50	1:50	1:200	Negative
<b>Purified IgGs</b>	<b>Yield (<math>\mu\text{g}^*</math>)</b>	0.81	0.95	2.50	0.82
	<b><math>K_D</math> (nM)**</b>	0.9	0.5	1.5	Weak binding
	<b>Neutralizing specific activity (BU/<math>\mu\text{g}</math>)</b>	0.21	0.45	0.08	-

\* Normalized per 1 ml of plasma applied as a starting material to ADAMTS13 affinity matrix

\*\*  $K_D$  refers to the dissociation constant calculated for the interaction of the isolated IgGs with rADAMTS13 using Biacore

A minus sign denotes absence of inhibition

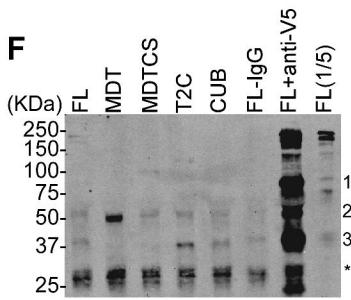
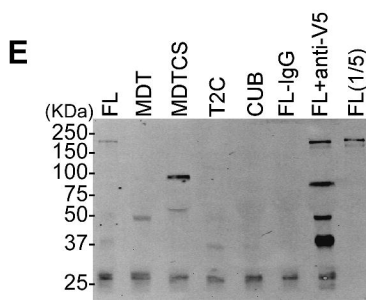
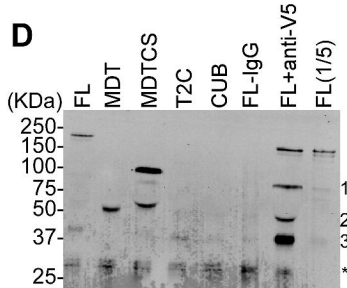
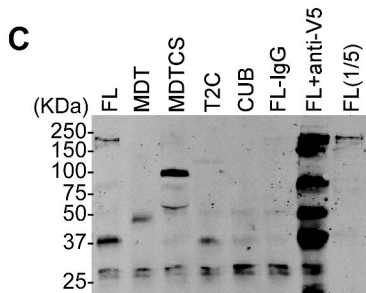
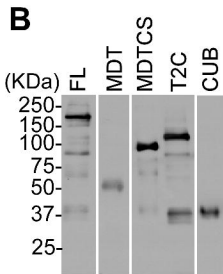
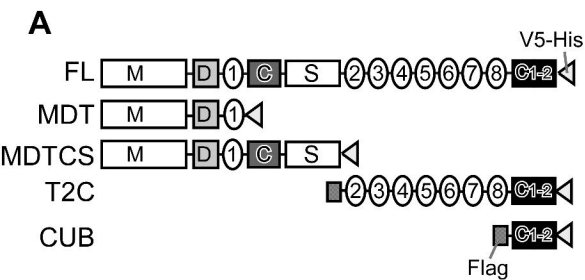
**Table 2. Linear ADAMTS13 peptide epitopes detected with isolated antibodies from acquired TTP patients and a HD pool.**

Binding domains		Patient 1*	Patient 2*	Patient 3*	HD*
<b>Shared Epitopes</b>	<b>M</b>	98-108	97-109	-	98-108
		173-178	173-177	-	173-177
	<b>D</b>	296-301	294-301	292-301	296-301
	<b>S</b>	673-682	668-682	-	676-682
	<b>T1-8</b>	1171-1175	-	-	1171-1175
	<b>CUB1</b>	-	-	1194-1204	1194-1204
1291-1298		1290-1298	-	1292-1296	
<b>Non shared epitopes</b>	<b>M</b>	162-169	-	-	212-216
	<b>D</b>	-	-	-	355-360
	<b>T1-4</b>	834-844	-	-	855-866
		888-892	-	-	871-879
	<b>T1-6</b>	-	983-989	-	-
	<b>T1-8</b>	1141-1147	-	-	-
		1180-1191	-	-	-
	<b>CUB1</b>	1192-1194	-	-	1219-1227
	<b>CUB2</b>	1312-1321	1338-1345	-	1309-1315
		1382-1390	-	-	-

\* Identified peptide epitopes are given with delimiting amino acid residue numbers. The fluorescence intensities were classified as weak (light gray), medium (medium gray) or high (deep gray). A minus sign denotes absence of fluorescence spots.

## Figure legend

**Figure 1. Epitope mapping of affinity-purified anti-ADAMTS13 IgG antibodies by immunoprecipitation and Western blotting.** **(A)** Schematic domain representation of rADAMTS13 and variants used. FL: Full length; MDT: metalloprotease, disintegrin and 1<sup>st</sup> thrombospondin type 1 repeat domains; MDTCS: metalloprotease, disintegrin, 1<sup>st</sup> thrombospondin type 1 repeat, Cys-rich and spacer domains; T2C: 2<sup>nd</sup> – 8<sup>th</sup> thrombospondin type 1 repeat and two CUB domains; CUB: two CUB domains. **(B)** Detection of purified rADAMTS13 and variants (0.1 µg/lane) by SDS-PAGE and Western blotting with mouse anti-V5 IgG (1:5,000) (Invitrogen, Carlsbad, CA) and IRDye 800-labeled goat anti-mouse IgG (1:10,000) (LI-COR Bioscience, Lincoln, Nebraska) **(C-F)** Binding pattern of the IgG preparations isolated from patient 1 (C), patient 2 (D), patient 3 (E) and a HD pool (F). 0.5 µg of the distinct IgG preparations and near equivalent amounts (0.5 µg) of either full length rADAMTS13 or variants were incubated with 30 µl protein G-conjugated Sepharose beads (GE Healthcare, Uppsala, Sweden) in 200 µl binding buffer (50 mM Tris-HCl, pH 7.6, 150 mM NaCl, 0.1% Triton X100 and 0.1% Tween20 containing 0.1% casein, 5 mM EDTA, and 0.2% protease inhibitor cocktail from Sigma) overnight at 4°C with rocking. After being washed, the antibody-antigen complex was eluted from the protein G beads with 30 µl 5X SDS buffer and heated for 10 min at 100°C. The bound ADAMTS13 and variants were determined by Western blotting as described in panel B. FL-IgG (incubation of FL ADAMTS13 in the absence of IgG) and FL+anti-V5 (incubation of FL ADAMTS13 with mouse anti-V5 IgG) refer to the negative and positive control, respectively. FL(1/5) refers to FL ADAMTS13 (0.1 µg) loaded directly on the gel. The loaded negative control “FL-IgG” in panels D&E refers to 1/5<sup>th</sup> of the amount loaded in panels C&F. The discernible 75 kDa (1), 50 kDa (2) and 37 kDa (3) bands refer to degradation products of ADAMTS13 constructs that still have the V5 at their C-terminus. A non-specific 25 kDa double band discernible in all lanes is indicated by an asterisk.





**Development of a flow-based assay to test ADAMTS13 activity reveals discrepancies in inhibitor assessment compared to conventional clinical static assays**

Rana Grillberger<sup>1</sup>, Bernadette Gruber<sup>1</sup>, Susanna Skalicky<sup>1</sup>, Gerald Schrenk<sup>1</sup>, Paul Knöbl<sup>2</sup>, Barbara Plaimauer<sup>1</sup>, Peter L. Turecek<sup>1</sup>, Friedrich Scheiflinger<sup>1\*</sup>, and Hanspeter Rottensteiner<sup>1</sup>

1) Baxter Innovations GmbH, Vienna, Austria

2) Medical University of Vienna, Department of Medicine, Vienna, Austria

\* Correspondence to:

Friedrich Scheiflinger

Baxter Innovations GmbH

Vienna DC Tower

Donau-City Straße 7

1220 Vienna, Austria

Phone: +43 1 20100 2473410

Fax: +43 1 20100 5038

E-Mail: fritz\_scheiflinger@baxter.com

Word count Abstract: 223

Word count Text: 4563

Figures: 6

Table: 1

Supplementary figure: 1

## ABSTRACT

Acquired TTP is caused by development of neutralizing autoantibodies against ADAMTS13. Several static Bethesda-type assays are currently used in clinical practice to determine ADAMTS13 inhibitors. The inhibitory activity of these antibodies, however, has yet not been thoroughly evaluated under the more physiological condition of flow. We therefore developed a flow-based assay based on platelet aggregate formation upon perfusion of a suspension containing platelets, erythrocytes, and VWF over a surface coated with extra-cellular matrix components. Spiking ADAMTS13 to the mobile phase resulted in a consistent and concentration-dependent decrease in surface coverage of platelet aggregates (range 1-4 U/ml) which was reversible by adding goat ADAMTS13 antiserum. This new method thus proved suitable for determining the neutralizing activity of anti-ADAMTS13 antibodies as well as measuring ADAMTS13 activity, and allowed us to analyze autoantibodies from TTP patients under static conditions and under flow. ADAMTS13-specific IgG antibodies were affinity purified from two acquired TTP patients and their neutralizing specific activities measured with 0.1 and 0.5 BU/ $\mu$ g in the static FRETTS-VFW73 assay. Testing these antibody preparations in the flow assay according to their FRETTS-VWF73-based inhibitor titers demonstrated vastly different inhibitory effects, suggesting that titers determined by static assays may not accurately predict the actual inhibiting activity of ADAMTS13 autoantibodies *in vivo*. Consequently, the course of disease and treatment efficacy may vary among TTP patients despite common inhibitor titers.

### **What is known on this topic?**

- Acquired TTP is mainly caused by development of inhibitory autoantibodies against ADAMTS13
- The inhibitory activity of ADAMTS13 autoantibodies in patients' plasma is currently tested using a Bethesda-type setup and static activity assays
- The most commonly used activity assay in clinical practice is the FRETTS-VWF73 assay

### **What does this paper add?**

- Introduction of a novel assay that mimics the early events on the surface of a damaged vessel wall, thus enabling determination of the neutralizing activity of anti-ADAMTS13 antibodies under flow
- Inhibitor titers determined by the FRETTS-VWF73 assay-based setup are not necessarily predictive of the inhibiting activity of ADAMTS13 autoantibodies under flow
- The true pathogenicity of anti-ADAMTS13 autoantibodies in TTP patients may not always be adequately recognized by the assays commonly used in clinical practice

**Keywords:** ADAMTS13, Thrombotic thrombocytopenic purpura, Autoantibodies, Shear stress, von Willebrand factor

## INTRODUCTION

Von Willebrand factor (VWF) is a large multimeric plasma glycoprotein that is essential in tethering platelets at sites of vascular injury. Its hemostatic activity is regulated by ADAMTS13 (a disintegrin and metalloproteinase with a thrombospondin type 1 motif, member 13)<sup>1-3</sup>, which specifically cleaves VWF at a single site in its A2 domain (Tyr<sub>1605</sub>-Met<sub>1606</sub>), thereby generating smaller and less active forms of the protein. VWF cleavage requires shear stress-dependent unraveling of the cryptic peptide bond which occurs upon VWF secretion when the protein is still anchored to the endothelial surface<sup>4</sup> or upon exposure to elevated shear stress in the microcirculation when bound to platelets<sup>5</sup>. In the absence of ADAMTS13, the highest molecular weight multimers (ultra-large-VWF or ULVWF) persist and their accumulation can lead to disseminated microvascular thrombosis characteristic for thrombotic thrombocytopenic purpura (TTP), a life threatening disorder associated with microangiopathic hemolytic anemia, thrombocytopenia, and renal impairment or neurological abnormalities<sup>6</sup>.

TTP can be congenital or acquired. The exceedingly rare congenital form is caused by mutations in the ADAMTS13 gene<sup>2</sup>, while the acquired form is mediated by anti-ADAMTS13 autoantibodies<sup>7-9</sup> mainly of the IgG isotype, predominantly IgG4 and IgG1<sup>9;10</sup>. IgM and IgA autoantibodies in combination with IgG have also occasionally been observed<sup>7-9</sup>. In most cases of acquired TTP, these autoantibodies neutralize the proteolytic activity of ADAMTS13; however, non-inhibitory anti-ADAMTS13 antibodies have been reported in 10-15% of TTP patients<sup>11;12</sup>. Anti-ADAMTS13 autoantibodies usually target a major binding site located in the spacer domain of ADAMTS13<sup>13-16</sup>, but additional epitopes throughout the protein have also been identified<sup>13;14;17-19</sup>.

The two most commonly used assays to test plasma samples for ADAMTS13 inhibitors in clinical practice are of the Bethesda-type and employ the FRETs-VWF73<sup>20</sup> and collagen binding (CB)<sup>21</sup> assay. Both assays are performed under static conditions without the vascular

shear stress known to make the peptide bond in the VWF A2 domain accessible for cleavage by ADAMTS13 under physiological conditions. In the FRETTS-VWF73 assay, cleavage is enabled using a short peptide substrate, whereas in the CB assay, a denaturing agent is used to expose the cleavage site in full-length VWF. To circumvent the potential pitfalls of such assays, various shear-based systems for determining ADAMTS13 activity have been developed<sup>4,22-24</sup>, including one that measures the cleavage of multimeric VWF upon simulation of fluid shear conditions by a vortexer<sup>24</sup>, and one that evaluates in a parallel flow chamber the extent of cleavage of ULVWF when attached to endothelial cells<sup>4</sup>.

Although such assays are unlikely to be implemented for routine inhibitor testing, comparative measurements of patient plasma samples under static and shear conditions have been described. In one study, the vortex-based shear assay yielded inhibitor titers that were consistent with those obtained by FRETTS-VWF73 assay<sup>24</sup>. Another research group described for longitudinal samples from one acquired TTP patient experiencing multiple acute episodes of the disease discrepancies in ADAMTS13 activity levels when measured with static activity assays and the endothelial cell-based flow assay<sup>25</sup>.

Our study investigated whether flow-based assays that more closely mimic the *in vivo* situation might more accurately predict the pathogenicity of autoantibodies in acquired TTP patients than conventional static assays. For this purpose, we developed a flow assay based on perfusion of a platelet-, erythrocyte-, VWF- and ADAMTS13-containing suspension over a surface coated with extracellular matrix (ECM) components. The ability of this assay to quantify inhibitors was demonstrated with a goat ADAMTS13 antiserum and further investigated using affinity-purified IgG antibodies from TTP patients. The results of this study are discussed in terms of discrepancies in inhibitor assessment when determined by a static and a flow-based assay. We also consider possible molecular mechanisms underlying these observations and their potential clinical implications.

## **MATERIALS AND METHODS**

### **Sources of human plasma**

To purify anti-ADAMTS13 IgG autoantibodies, about 2 L of plasma obtained during plasma exchange therapy from two patients with idiopathic acquired TTP (designated patient A and patient B) were used as starting material. Both participants provided informed consent according to the Declaration of Helsinki. The two plasma samples were tested for ADAMTS13 antigen (ADAMTS13: Ag)<sup>26</sup>, ADAMTS13 activity (ADAMTS13: Ac)<sup>20</sup>, and functional ADAMTS13 inhibitors using the FRETs-VWF73 assay<sup>20</sup>, and for total IgG, IgM, and IgA anti-ADAMTS13 antibodies using ELISA<sup>27;28</sup> (Table 1).

### **Isolation of human anti-ADAMTS13 IgG antibodies**

Plasma samples were loaded onto an affinity matrix generated by coupling 2 mg of recombinant ADAMTS13 (rADAMTS13; Baxter Bioscience, Vienna, Austria) to 1 ml of NHS-activated Sepharose 4FF (GE Healthcare, Uppsala, Sweden) according to the manufacturer's instructions. Bound antibodies were eluted with 0.1 M glycine-HCl at pH 2.7. After neutralization, the elution pool was applied to a 1 ml protein G Sepharose 4 Fast Flow column (GE Healthcare). The IgG fraction was eluted with 0.1 M glycine-HCl at pH 2.7, then immediately neutralized and dialyzed against Tris-buffered saline at pH 7.4. The purity of the isolated IgG was assessed by SDS-PAGE under reducing conditions on Novex 4-20% Tris-glycine gels (Invitrogen, Carlsbad, CA) and silver staining using the SilverQuest Silver Staining Kit (Invitrogen). Elution pools were analyzed for total human IgG levels using a commercial ELISA kit (Bethyl Laboratories, Montgomery, TX) and for ADAMTS13-specific IgG antibodies by ELISA<sup>27</sup>. The same antibody preparations were previously used in epitope mapping studies<sup>19</sup>.

### **Calculation of binding parameters of anti-ADAMTS13 IgG antibodies to ADAMTS13**

Affinities of the purified antibodies to rADAMTS13 were determined by surface plasmon resonance technology using Biacore T200 (GE Healthcare). Purified autoantibodies were captured on a CM5 sensor chip via monoclonal mouse anti-human IgG (Fc) antibodies (Human antibody capture kit, GE Healthcare). A series of dilutions of rADAMTS13 (5-160 nM) diluted in HEPES buffered saline containing 3 mM EDTA and 0.05% v/v surfactant P20 at pH 7.4 as running buffer was applied to the chip. The  $K_D$  was calculated assuming a homogeneous 1:1 interaction between the antibodies and rADAMTS13.

### **Purification of ADAMTS13 from plasma (pADAMTS13)**

ADAMTS13 was purified from a cold ethanol-fractionated human plasma intermediate of the Cohn fractionation process (Baxter Bioscience). Briefly, the filter cake obtained from filtration of resuspended Fraction II+III (Baxter plasma center, Vienna, Austria) was resuspended in Tris buffer saline (TBS) containing 0.5 M  $(\text{NH}_4)_2\text{SO}_4$ , 1 mM PMSF, 10 mM Benzamidine, pH 7.4 and filtered through a 0.22  $\mu\text{m}$  membrane. The filtrate was subjected to hydrophobic interaction chromatography followed by ammonium sulfate precipitation. Precipitates were resuspended in TBS and subjected to sequential affinity chromatography using a goat antiserum to ADAMTS13 (Z797; Baxter Bioscience) and monoclonal antibodies directed against the C-terminal CUB domains of ADAMTS13 (mAb 257A2-2; Baxter Bioscience). The final elution pool contained full-length ADAMTS13 purified to homogeneity with a specific activity of 1.9 U/ $\mu\text{g}$ .

### **ADAMTS13 activity assay under flow**

The ADAMTS13 activity assay is based on preventing VWF-dependent platelet aggregate formation by ADAMTS13 under flow and uses a microflow system called Cellix VenaFlux, where microchannels (Vena8 Biochip) are mounted on the stage of a Zeiss Axiovert 40 CFL inverted Epi-Fluorescence microscope (Cellix, Dublin, Ireland). Microchannels were

precoated with 100 µg/ml cellular fibronectin (cFN) from human fibroblasts (Sigma, St. Louis, MO). After blocking with 4% bovine serum albumin (BSA; Sigma), the channels were washed and additionally coated with 160 µg/ml Horm equine tendon collagen (Type I) (Nycomed, Linz, Austria) followed by 100 µg/ml recombinant human VWF (rVWF; Baxter Bioscience).

Platelets and erythrocytes were obtained as concentrates from the Red Cross Vienna (Austria). Platelet concentrates were washed (1:1) with calcium-free Krebs Ringer buffer (107 mM NaCl, 20 mM NaHCO<sub>3</sub>, 4 mM KCl, 2 mM Na<sub>2</sub>SO<sub>4</sub>, 19 mM Tri Na Citrate x 2 H<sub>2</sub>O, 0.5% D+ Glucose, pH 7.35) containing 10 mM acetylsalicylic acid (Sigma) to inhibit platelet activation. Following centrifugation at 1300x g for 10 min at 10°C, pellets were resuspended in Krebs Ringer buffer containing 2.5 mM CaCl<sub>2</sub> in a volume equivalent to the supernatant and centrifuged as described above to prepare a final platelet stock suspension of 10<sup>9</sup> platelets/ml. Erythrocyte concentrates were washed (1:1) with a buffer containing 10 mM HEPES and 150 mM NaCl, pH 7.35 and centrifuged at 1300x g for 10 min at 10°C. The supernatant was discarded and the erythrocytes resuspended in calcium-containing Krebs Ringer buffer to generate an erythrocyte stock suspension of 80% hematocrit (Hct). A cell suspension was then prepared from the two stock solutions, where platelet and erythrocyte concentrations were adjusted to physiological blood levels (2.5x10<sup>8</sup> platelets/ml and 40% Hct) with Krebs Ringer buffer containing 2.5 mM calcium. Finally, the cell suspension was treated with 2 µM DiOC<sub>6</sub> (Invitrogen) to render platelets fluorescent, then mixed with rVWF (10 µg/ml) and perfused over the coated microchannels by aspiration with a PC-controlled syringe pump at a shear rate of 2500 s<sup>-1</sup>. Five minutes after the onset of flow, images of seven fields along each channel were acquired via a cooled high-resolution Hamamatsu ORCA-03 digital camera connected to the microscope. The mean area covered with platelet-aggregates was estimated as the percentage of platelet coverage using Image-Pro Plus Analysis Software.

Dependency of the observed platelet aggregation on interaction of VWF with GP Ib $\alpha$  was analyzed by adding 50  $\mu$ g/ml of a mouse monoclonal anti-human GP Ib $\alpha$  antibody (CD42b; eBioscience, San Diego, CA) or an isotype control (mouse IgG1 kappa; DakoCytomation, Carpinteria, CA, USA) to the cell suspension prior to perfusion.

In this setup, ADAMTS13 activity was tested by adding increasing amounts (1-4 FRET-S-VWF73 U/ml) of recombinant or plasma-derived ADAMTS13 to the cell suspension. ADAMTS13 activity was defined as the ability to reduce the percentage of platelet coverage, setting coverage in the absence of ADAMTS13 to 100%. By plotting platelet surface coverage (%) against ADAMTS13 activity, a standard curve was generated using SigmaPlot software 12.0 (Systat Software, San Jose, CA, USA). Data were fitted by a 4-parameter logistic function.

#### **Inhibitor assessment of anti-ADAMTS13 IgG antibodies under static conditions**

ADAMTS13 neutralizing activity was tested under static conditions using two conventional, quantitative Bethesda-like methods: the FRET-S-VWF73<sup>20</sup> and collagen binding assay<sup>21</sup>. In the FRET-S-VWF73 assay, equal volumes of normal human plasma (NHP) and various dilutions of the respective antibody solutions in 25 mM HEPES, 175 mM NaCl pH 7.4 containing 0.5% BSA were mixed and incubated for 2 h at 37°C, then measured for ADAMTS13 residual activity as described<sup>20</sup>. Collagen-binding activity (CBA) (Technoclone, Vienna, Austria) was measured as described<sup>21</sup> with minor modifications. Equal volumes of rADAMTS13 (2 U/ml) and various dilutions of the respective antibody solutions in 0.9% (w/v) NaCl containing 0.1% BSA were mixed and incubated for 2 h at 37°C. Samples were then diluted (1:10) in 1.5 M urea, 5 mM Tris, pH 8.0 and mixed with 9.3 mM BaCl<sub>2</sub> and 2 U/ml of rVWF. After incubation for 2.5 h at 37°C, samples were assessed for ADAMTS13 residual activity. The purified antibodies' inhibitory activity was calculated using one BU as the inhibitory activity that lowers the ADAMTS13 activity of plasma by 50%. The inhibitor titer of the IgG preparations was calculated using an appropriate dilution to obtain a 30-70%

residual ADAMTS13 activity of that of the control mixture of NHP and inhibitor dilution buffer. ADAMTS13-neutralizing specific activity (BU/ $\mu$ g purified IgG) was calculated by dividing the inhibitor titer (BU/ml) of the IgG preparation by its concentration ( $\mu$ g/ml).

### **ADAMTS13 inhibitor assessment under flow**

The ability of the established ADAMTS13 activity flow assay to measure ADAMTS13 inhibitors was assessed with a goat antiserum to ADAMTS13 (Z797). In one set of experiments, the serum was adjusted to various FRETTS-VWF73-based inhibitor titers (2-8 BU/ml), mixed with a fixed amount of rADAMTS13 or pADAMTS13 (4 U/ml end concentration), and incubated for 2 h at 37°C. The ADAMTS13-IgG antibody-containing solutions were then added to the cell suspension containing rVWF (10  $\mu$ g/ml) and immediately perfused over the rVWF-coated microchannels at a shear rate of 2500 s<sup>-1</sup>. The increase as a percentage of surface coverage by platelet aggregates after 5 min of continuous flow was plotted against the added FRETTS-VWF73-based inhibitor titer of the antibody.

Alternatively, predefined inhibitor titers (1, 2, and 4 BU/ml) of the goat antiserum Z797 were mixed with increasing concentrations of ADAMTS13 activity (1-16 U/ml). Recovery of ADAMTS13 activity was evaluated at 0.5-4 U/ml, which is equivalent to 80-30% of surface coverage according to a standard curve generated in the absence of inhibitors and using 0.5-4 U/ml rADAMTS13. Reconstituted activity was plotted against the rADAMTS13 activity added and the required concentration of rADAMTS13 to recover 2 U/ml ADAMTS13 activity was estimated by manual extrapolation for each inhibitor titer.

The TTP-associated IgG antibody preparations were adjusted to predefined FRETTS-VWF73-based inhibitor titers (0.3-12 BU/ml end titer) and analyzed as described above.

## RESULTS

### Establishment of an ADAMTS13 activity assay under flow

To study the inhibitory activity of anti-ADAMTS13 antibodies under shear stress, we developed an ADAMTS13-sensitive flow assay that simulates the events on the surface of a damaged vessel wall, where collagen of the exposed subendothelial matrix provides a binding scaffold for VWF, which in turn initiates platelet adhesion and aggregation.

For this purpose, microchannels of a biochip were sequentially coated with cellular fibronectin (cFN), collagen, and rVWF; the cFN as an adhesive binding substrate for collagen was required to achieve an even surface-coating of collagen fibers. The fluid phase was composed of physiological concentrations of fluorescently labeled platelets, erythrocytes which are known to push platelets close to the surface of a vessel, and VWF. Soluble VWF not only mediates inter-platelet cohesion but also covalently associates with immobilized VWF multimers, thereby forming extended string like structures<sup>29</sup> that provide a greater number of interacting sites for platelets.

Perfusion of this suspension over the coated channel surface caused reproducible platelet aggregate formation along collagen fibers. The extent of aggregation was strongly dependent on shear rate and increased as a function of time, with a maximum surface coverage at  $2600\text{ s}^{-1}$  after 5 min (Figure 1A-B). The formation of aggregates strongly depended on the interaction of VWF with the platelet receptor GP Ib $\alpha$ , as a blocking antibody against GP Ib $\alpha$  eliminated aggregation (Supplementary Figure 1). Based on these data, all subsequent experiments were performed at a shear rate of  $2500\text{ s}^{-1}$  and a perfusion time of 5 min.

Adding increasing concentrations of rADAMTS13 (1-4 FRETs-VWF73 U/ml) to the cell suspension prior to perfusion dose-dependently reduced the surface coverage of platelet aggregates on the coated channels to 10% of the control lacking ADAMTS13 (Figure 2A). Plasma-derived ADAMTS13 reduced the accumulation of platelet aggregates similarly to

rADAMTS13 (Figure 2B). The relative decrease in surface coverage was also comparable using platelets from different donors (not shown).

We then studied the effect of ADAMTS13 on the rate of platelet aggregate formation. The surface area covered with platelet aggregates after 5 min of flow in the absence of ADAMTS13 was set to 100%. After 30 sec of perfusion, a surface coverage of 16% was observed, and a half maximal surface coverage (50%) was achieved after approximately 2 min (Figure 2C). Adding 1 or 2 U/ml of rADAMTS13 did not prevent but significantly slowed down platelet aggregate accumulation. At a concentration of 4 U/ml, however, rADAMTS13 was clearly able to prevent the building up of platelet aggregates, as platelet aggregate coverage remained constant at 10% throughout perfusion (5 min). This residual coverage likely reflects the portion of platelets bound to (partially cleaved) immobilized VWF or to exposed collagen fibrils through the platelets' collagen receptor GPVI<sup>30</sup>.

Taken together, our flow assay was capable of simulating VWF-mediated platelet aggregate formation and allowed measurement of ADAMTS13 activity under flow in a defined concentration window (1-4 FRETs-VWF73 U/ml).

#### **Assessment of ADAMTS13 inhibitors using the ADAMTS13 activity assay under flow**

A goat anti-human ADAMTS13 IgG preparation with a high (FRETs-VWF73-based) inhibitor titer was used to validate the flow assay for inhibitor assessment. A fixed amount of rADAMTS13 (4 U/ml) was mixed with increasing inhibitor titers of the goat antiserum (2-8 BU/ml) and added to the cell suspension. The extent of platelet aggregate accumulation was monitored after 5 min of perfusion at  $2500 \text{ s}^{-1}$ . A gradual increase in surface coverage from 10 to 100% was observed which correlated with the added inhibitor titer (Figure 3A), indicating that rADAMTS13 activity was fully blocked at the highest inhibitor concentration. Similar results were obtained for pADAMTS13; for both proteins, a surface coverage of 50% was reached with an inhibitor titer of 4.6 BU/ml (Figure 3A).

In a complementary setup, we determined the ADAMTS13 concentrations required to recover 2 U/ml of ADAMTS13 activity in the presence of inhibitor. Increasing concentrations of ADAMTS13 activity (FRETs-VWF73 assay) were successively able to override the inhibitor under flow, with a clear correlation between increasing inhibitor titers and the amounts of ADAMTS13 activity required (Figure 3B). For instance, to recover 2 U/ml of ADAMTS13 in the presence of 1, 2, and 4 BU/ml of the anti-ADAMTS13 antibody, 5.8, 8.8, and 11.6 U/ml ADAMTS13, respectively, were required. These data indicated that the assay is suitable for assessing functional ADAMTS13 inhibitors under flow, and thus allows functional testing of inhibitors from acquired TTP patients under more physiological conditions.

#### **Assessment of inhibitory activity of purified ADAMTS13 inhibitors from two acquired TTP patients under static conditions**

To determine whether functional inhibitors from acquired TTP patients show similar characteristics in the flow assay to the anti-ADAMTS13 antibody generated via immunization of a goat, anti-ADAMTS13 antibodies from two patients with idiopathic TTP were purified in a two-step chromatographic procedure involving an ADAMTS13 affinity matrix and protein G. The purity of the isolated IgGs was confirmed by SDS-PAGE under reducing conditions (Figure 4A) and the IgG antibody yield quantitated by ELISA (0.95 and 2.50  $\mu\text{g}$  of ADAMTS13-specific IgGs per ml of plasma; Table 1). The IgG autoantibodies dose-dependently bound to ADAMTS13 as a solid phase antigen (Figure 4B) and their binding could be competed by soluble ADAMTS13, but not by human serum albumin (Figure 4C). The affinities ( $K_D$ ) of the purified IgG antibodies were 0.5 nM and 1.5 nM, respectively, with similar association and dissociation rate constants (Table 1).

The specific neutralizing activity of the two affinity-purified IgG antibodies was 0.45 and 0.08 BU/ $\mu\text{g}$  as determined by FRETs-VWF73 assay, and 0.37 and 0.14 BU/ $\mu\text{g}$  using full-length VWF as substrate (Table 1). Determining FRETs-VWF73 activities in the presence of serial

dilutions of the autoantibodies from the two TTP patients revealed the distinct inhibitory potencies of the two IgG preparations. An approximately 6-fold excess to decrease the ADAMTS13 activity by 50% was required for patient B compared with patient A (Figure 5).

### **Inhibitory activity of purified anti-ADAMTS13 IgG autoantibodies under flow conditions**

To study the neutralizing profiles of the two purified antibody preparations under shear stress, the increase in surface coverage of platelet aggregates was again used to measure the extent of ADAMTS13 inhibition by the antibodies. Perfusion was performed in the presence of 4 U/ml rADAMTS13 and increasing inhibitor titers (0.3-12 BU/ml, determined by FRETs-VWF73 assay) of the anti-ADAMTS13 IgGs from the two TTP patients. Surprisingly, the same FRETs-VWF73-based inhibitor titers did not cause comparable inhibition of ADAMTS13 activity under flow, as reflected by vastly different surface coverage profiles (Figure 6A). For example, when an inhibitor titer of 3 BU/ml was added, IgGs from patient B led to more than 90% surface coverage, whereas those from patient A exhibited only 15%. Even adding 12 BU/ml did not achieve full surface coverage for the IgG preparation from patient A (Figure 6A), indicating that under flow the inhibitory activity of this antibody was much lower than for patient B. This difference in surface coverage was also observed with pADAMTS13 instead of rADAMTS13 in the flow assay (Figure 6B), thereby excluding an influence of antigen source on the reactivity of the antibody.

The two IgG preparations were retested at various concentrations for their inhibitory activity in the static FRETs-VWF73-based Bethesda-like assay. When increasing inhibitor titers of the antibodies were mixed with NHP, ADAMTS13 activity was blocked in a similar, dose-dependent manner by both preparations (Figure 6C), confirming that under static conditions the two preparations inhibit ADAMTS13 activity to a similar extent. The combined results thus indicate a discrepancy in inhibitor assessment when using static and flow-based assays.

## DISCUSSION

ADAMTS13 deficiency and neutralizing inhibitor titers as diagnosed in acquired TTP patients are usually explored using assays that measure the activity of ADAMTS13 under static conditions. However, these assays may not accurately mimic the situation *in vivo*, where shear forces are required to expose the scissile bond within the A2 domain of VWF. Testing the neutralizing activity of purified anti-ADAMTS13 IgG autoantibodies from two TTP patients showed a remarkably different extent of inhibition when assayed under flow and under static conditions.

The flow-based assay developed for this study was based on ADAMTS13-dependent cleavage of platelet-adhering VWF multimers immobilized on an extra-cellular matrix-like surface (composed of fibronectin, collagen and VWF) and the extent of inhibition of the protease by anti-ADAMTS13 autoantibodies. Unlike previously described flow assays<sup>4;22;24</sup> performed in the presence of normal human plasma and thus possibly containing ill-defined cofactors affecting VWF proteolysis, we used cell suspensions with specified components including reconstituted erythrocytes, platelets, purified recombinant VWF, and recombinant or plasma-derived ADAMTS13. Applying shear force as in arterial blood flow tethered platelets to the adhesive surface through interaction of the platelet receptor GP I $\beta$  $\alpha$  with VWF and propagated them into stable aggregates through activation and interconnection with rVWF present in the fluid phase.

The decrease in platelet aggregate formation dose-dependently correlated with the activity of ADAMTS13 for both the recombinant and plasma-derived form of the enzyme. Compared with static assays which can readily measure ADAMTS13 activities down to a concentration of 0.1 U/ml, 1-4 U/ml were required to reliably determine the reduction in platelet aggregation. Furthermore, only at the highest concentration used (4 U/ml), platelet aggregates no longer built up over time. As we intended our assay to mimic the early events in vessel injury where ADAMTS13 is required to limit but not prevent thrombus formation, the

concentration range identified appears to adequately resemble the *in vivo* situation. However, this correlation requires caution as the concentrations of surface-coated collagen and VWF as well as the actual shear forces occurring at a wounded vessel are likely to differ from those of our assay.

It is worth noting that flow assays based on cleavage of ULVWF strings attached to histamine-stimulated endothelial cells measure ADAMTS13 activity at a lower concentration range; for example, 0.5 U/ml ADAMTS13 (normal plasma diluted to 50%) was reported to cleave more than 95% of ULVWF-platelet strings formed in most healthy individuals<sup>4;31</sup>. Such a setup simulates the release of VWF into the circulation following secretion from intact endothelial cells. As this event can already occur under low shear stress<sup>32</sup>, it is plausible that the required ADAMTS13 concentrations are also lower than in primary hemostasis.

To test the inhibitors of TTP patients, ADAMTS13-specific antibodies were purified from patient plasma in a capture step on an ADAMTS13 affinity matrix and subsequent isolation of the IgG fraction on a protein G matrix. This purification strategy recovered 1-2.5  $\mu\text{g}$  of ADAMTS13-specific IgGs per ml of patient plasma, which is consistent with a previous report (0.50 and 1.50  $\mu\text{g}/\text{ml}$ )<sup>9</sup>. Based on recent publications showing that a portion of the anti-ADAMTS13 antibodies are present as immune complexes<sup>28;33</sup>, the actual IgG concentrations were probably underestimated as immune complexes are expected to inefficiently bind to the affinity column. Anti-ADAMTS13 antibodies of both TTP patients showed a high affinity for ADAMTS13, which was reflected by low  $K_D$  values: 0.5 nM for patient A and 1.5 nM for patient B. When the specific neutralizing activities of the two IgG preparations were measured using the static FRETs-VWF73 assay, 0.5 BU/ $\mu\text{g}$  were obtained for patient A and 0.1 BU/ $\mu\text{g}$  for patient B. This difference was also reflected by the ~6-fold molar excess of the IgG preparation required from patient B to inhibit FRETs-VWF73 activity by 50% compared with patient A. Comparable results were obtained using the CB assay with full-length VWF as substrate.

Most interestingly, adjusting the anti-ADAMTS13 IgG preparations from patients A and B to the same inhibitor titer as analyzed by FRETTS-VWF73 assay and applying in the flow assay showed a different degree of inhibition as manifested by a vastly different platelet aggregate surface coverage. For example, at an inhibitor titer of 3 BU/ml, the difference in surface coverage between the antibody preparations of the two patients was nearly 6-fold (90% versus 15%). This discrepancy did not stem from using rADAMTS13 in the flow assay (instead of NHP as used in the FRETTS-VWF73 assay), as similar results were obtained using pADAMTS13, indicating that the antibodies blocked the activity of pADAMTS13 and rADAMTS13 in a comparable manner. A surprising consequence of these data is that, under flow, the discrepancy between the two antibody preparations was smaller when assessing the inhibitory activities as a function of total IgG rather than the FRETTS-VWF73 based inhibitor titer. The anti-ADAMTS13 IgG preparation from patient A added at a concentration of 13 µg/ml (~6 BU/ml) and that from patient B added at 10 µg/ml (~1 BU/ml) led to a surface coverage of 40% and 46%, respectively, indicating that under flow, the two antibody preparations had almost identical specific inhibitory activities.

We presume the discrepancy to be caused by the distinct binding sites of the autoantibodies on the surface of ADAMTS13 that can selectively interfere with the docking of ADAMTS13 to VWF under flow conditions. Epitope mapping based on peptide scans showed that the IgG preparation from patient B not only recognized a common epitope in the disintegrin domain, but also a unique epitope in the CUB1 domain (amino acids 1194-1204)<sup>19</sup>. It is thus tempting to speculate that blocking the latter binding site interferes with the regulation of enzymatic activity under flow. On the other hand, several epitopes spread over the entire protein were recognized by the antibody preparation from patient A only<sup>19</sup>. It is therefore theoretically possible that antibody binding to one of these epitopes occurs only under static conditions or conversely, relieves ADAMTS13 from negative regulation under flow, thereby partially counteracting the overall inhibitory activity of the IgG preparation. The latter scenario would be in line with several reports indicating that the C-terminal domains of ADAMTS13 play a

role in regulating its enzymatic activity, negatively or positively<sup>34-37</sup>. Future studies with monoclonal antibodies targeting specific epitopes may clarify whether sites critical for ADAMTS13 function selectively exist under flow.

The observed discrepancy in inhibitory activity of TTP patient plasma samples may have clinical implications when considering exogenous ADAMTS13 supplementation. If inhibitor titers measured by a flow assay were the primary determinant of the required dose of ADAMTS13<sup>27</sup>, patient A would need much less ADAMTS13 than patient B to saturate the inhibitors and restore ADAMTS13 activity. In this context, it is worth noting that the amounts of rADAMTS13 found to overcome the goat antiserum (Figure 3B) whose inhibitory activity under flow (Figure 3A) was between that of patients A and B (Figure 6A-B) are likely to overestimate the demand for patient A and underestimate that for patient B. While waiting for studies in vivo, such information should be taken into account when developing rADAMTS13 dose regimens.

In summary, using purified IgG preparations from two TTP patients, we performed for the first time a side-by-side comparison of the inhibitory activity of such antibodies under static conditions and under flow. We demonstrated that two conceptually different static assays gave consistent yet discordant inhibitor titer estimates to the flow-based assay, suggesting that such assays may not always predict the true pathogenicity of anti-ADAMTS13 autoantibodies. Future work will require analysis of a larger cohort of TTP patients to determine whether this discrepancy is more common or just an idiosyncrasy of a single patient. In any case, caution is warranted when using inhibitor titers based on static assays as a guideline for treatment therapy and measuring treatment efficacy.

## **ACKNOWLEDGEMENTS**

The authors thank Karima Benamara for expert editorial assistance.

**Table 1. ADAMTS13-related variables measured in plasma from two acquired TTP patients and characteristics of the affinity-purified anti-ADAMTS13 IgGs derived thereof**

			<b>Patient A</b>	<b>Patient B</b>
<b>Plasma</b>	<b>ADAMTS13 antigen</b>	<b>(<math>\mu\text{g/ml}</math>)</b>	0.04	0.03
	<b>ADAMTS13 activity</b>	<b>(U/ml)</b>	<0.05	<0.05
	<b>Functional inhibitors</b>	<b>(BU/ml)</b>	1.75	1.33
		<b>IgG titer</b>	1:50	1:200
	<b>Anti-ADAMTS13 immunoglobulins</b>	<b>IgA titer</b>	Negative	Negative
		<b>IgM titer</b>	Negative	Negative
<b>Purified IgGs</b>	<b>Yield</b>	<b>(<math>\mu\text{g}^*</math>)</b>	0.95	2.50
	<b>Binding constants</b>	<b><math>K_a</math> (<math>10^4\text{M}^{-1}\text{s}^{-1}</math>)</b>	14.3	23.8
		<b><math>K_d</math> (<math>10^{-4}\text{s}^{-1}</math>)</b>	0.7	3.5
		<b><math>K_D</math> (nM)</b>	0.5	1.5
	<b>Neutralizing specific activity</b>	<b>FRETS-VWF73 (BU/<math>\mu\text{g}</math>)</b>	0.45	0.08
		<b>CBA (BU/<math>\mu\text{g}</math>)</b>	0.37	0.14

\* Normalized per 1 ml of plasma applied as starting material to the ADAMTS13 affinity matrix

## Figure legends

**Figure 1. Influence of shear and time on VWF-mediated platelet aggregate accumulation in a novel flow-based assay.** Cell suspensions of fluorescently labeled platelets ( $2.5 \times 10^8$  platelets/ml), erythrocytes (40% Hct), and rVWF (10  $\mu\text{g/ml}$ ) were perfused over a surface coated with cellular fibronectin, collagen, and rVWF. Arrows indicate the direction of flow. **A)** Platelet aggregate formation at different shear rates. Images were obtained after 5 min of perfusion at the indicated shear rates and represent single frames from real time recordings. Small clusters of platelets that either adhered to or rolled on the channel surface were observed at a shear rate of  $215 \text{ s}^{-1}$ . Aggregates increased in size at  $650 \text{ s}^{-1}$ , became elongated and firmly attached to the surface at  $1300 \text{ s}^{-1}$ , and finally reached their maximum size at  $2600 \text{ s}^{-1}$ , covering almost the whole surface of the coated channel. **B)** Time course of platelet aggregate accumulation. Images were obtained at the indicated time points after perfusion at a shear rate of  $2600 \text{ s}^{-1}$  and represent single frames from real time recordings. Note the progressive increase in surface coverage by platelet aggregates over time, peaking at 5 min.

**Figure 2: Effect of ADAMTS13 on VWF-mediated platelet aggregate accumulation under flow conditions.** Cell suspensions of fluorescently labeled platelets ( $2.5 \times 10^8$  platelets/ml), erythrocytes (40% Hct), and rVWF (10  $\mu\text{g/ml}$ ) were mixed with the indicated concentrations of ADAMTS13 and perfused over a surface coated with cellular fibronectin, collagen, and rVWF at a shear rate of  $2500 \text{ s}^{-1}$ . After continuous perfusion up to 5 min, the mean surface area covered with platelet-aggregates was calculated for each sample. In panels A, B, and C, the surface coverage obtained in the absence of rADAMTS13 after 5 min of flow was set to 100%. **A)** Dose-dependent reduction of surface coverage by platelet aggregates in the presence of rADAMTS13. The bar graph shows the mean surface area ( $\pm$  SEM,  $n=4$ ) covered with platelet-aggregates after 5 min of continuous perfusion performed with platelets from different donors. Adding rADAMTS13 reduced the surface coverage of

platelet aggregates on the coated channels in a dose-dependent manner. **B)** Comparison of the activity of recombinant and plasmatic ADAMTS13 under flow. The gray (rADAMTS13) and black (pADAMTS13) bar graphs show the surface area covered with platelet aggregates after 5 min of continuous perfusion performed with platelets from the same donor. The results are representative of two sets of experiments, each of which was performed with a distinct platelet donor. **C)** Time course of the effect of rADAMTS13 on platelet aggregate accumulation. The bar graph shows the mean surface area ( $\pm$  SEM, n=4) covered with platelet aggregates at the indicated cumulative perfusion times performed with platelets from different donors. A concentration of 4 U/ml rADAMTS13 was required to prevent formation of initial platelet aggregates.

**Figure 3. Effect of goat ADAMTS13 antiserum on VWF-mediated platelet aggregate accumulation under flow conditions.** Cell suspensions of fluorescently labeled platelets ( $2.5 \times 10^8$  platelets/ml), erythrocytes (40% Hct), and rVWF (10  $\mu$ g/ml) were mixed with the indicated antibody-antigen concentrations and perfused over a surface coated with cellular fibronectin, collagen, and rVWF at a shear rate of  $2500 \text{ s}^{-1}$ . **A)** Inhibitor titer-dependent accumulation of platelet aggregates by goat ADAMTS13 antiserum. Mixtures of 4 U/ml of rADAMTS13 (closed circle) or pADAMTS13 (open circle) with anti-ADAMTS13 antibodies derived from goat antiserum (2-8 BU/ml; end titer, assessed by the FRETs-VWF73 assay) were added to the cell suspension prior to perfusion. The experiment was performed using the same platelet donor. The goat antiserum caused an inhibitor titer-dependent and comparable increase in the percentage of platelet aggregate surface coverage for rADAMTS13 and pADAMTS13. The dashed line represents 50% of surface coverage. **B)** Activity recovery by rADAMTS13 in the presence of goat ADAMTS13 antiserum. Increasing amounts of rADAMTS13 were added to three preparations of goat ADAMTS13 antiserum adjusted to FRETs-VWF73-based inhibitor titers of 1 (circle), 2 (triangle), and 4 (square) BU/ml. A standard curve was generated to calculate the residual activities under flow. The experiments were carried out using the same platelet donor. Reconstituted activities were

plotted against the added rADAMTS13 activities and the required concentration of rADAMTS13 to recover 2 U/ml (dashed line) determined by manual extrapolation. Note that increasing inhibitor titers of the goat antiserum required supplementation of higher ADAMTS13 concentrations.

**Figure 4. Characterization of affinity-purified anti-ADAMTS13 IgG antibodies from acquired TTP patients. A)** Purity of affinity-purified anti-ADAMTS13 IgG from acquired TTP patients. Equal amounts of IgG (100 ng), isolated from plasma from two acquired TTP patients by affinity chromatography, as well as purified human IgG (Control), were separated by SDS-PAGE under reducing conditions. Silver-stained gel revealed similar intensities for the heavy and the light chains of the affinity-purified IgGs and total IgG control. **B)** Binding to solid-phase ADAMTS13. Isolated anti-ADAMTS13 IgG antibodies from acquired TTP patients A (circle) and B (triangle) were tested at various concentrations for their ability to bind to solid-phase ADAMTS13 by ELISA. Both samples showed concentration-dependent binding. **C)** ADAMTS13 binding specificity testing by ELISA. Purified IgG preparations (1 µg/ml) from acquired TTP patients A (black bars) and B (gray bars) were incubated with rADAMTS13 (250 µg/ml), 5% human serum albumin (HSA; Sigma), or assay buffer for 2 h at 37°C. Thereafter, samples were analyzed using an anti-ADAMTS13 IgG ELISA. The signal intensities obtained in the presence of assay buffer were set to 100%. Both IgG preparations showed substantially reduced binding in the presence of soluble ADAMTS13 but not HSA.

**Figure 5. Dose-response inhibitory activity of affinity-purified human anti-ADAMTS13 IgG antibodies using a conventional static assay.** The indicated concentrations of purified IgG from acquired TTP patients A (circle) and B (triangle) were incubated with NHP and FRETs-VWF73 activities measured. Residual ADAMTS13 activities are expressed relative to non-inhibited NHP (100%). Differences in specific inhibitory activity between patients were clearly discernible.

**Figure 6. Inhibitory activity of affinity-purified human anti-ADAMTS13 IgG antibodies under flow conditions.**

The flow-based assay as described in Figure 1 was used to test purified IgG preparations from two acquired TTP patients for their ability to inhibit ADAMTS13. The results are expressed as means  $\pm$  SEM (n=2) using platelets from different donors. The surface coverage of platelet aggregates obtained without adding ADAMTS13 was set to 100%. **A)** Inhibitor assessment under flow in the presence of rADAMTS13. Mixtures of 4 U/ml of rADAMTS13 and increasing concentrations of anti-ADAMTS13 IgG antibodies isolated from patient A (3-12 BU/ml, end titer; assessed by the FRETs-VWF73 assay; triangle) or patient B (0.3-3 BU/ml, end titer; assessed by the FRETs-VWF73 assay; circle) were added to the cell suspension prior to perfusion. The percentage of platelet aggregate surface coverage was plotted against the added FRETs-VWF73-based inhibitor titers. An increase in surface coverage to 50% (dashed line) was obtained with 8 BU/ml of IgG antibodies from patient A and 1.5 BU/ml of IgG antibodies from patient B. **B)** Inhibitor assessment under flow in the presence of pADAMTS13. When the perfusion experiment used pADAMTS13 instead of rADAMTS13 under otherwise identical conditions, 50% surface coverage (dashed line) was obtained with 12 BU/ml of IgG antibodies from patient A and 0.7 BU/ml of IgG antibodies from patient B. **C)** Control for inhibitory activity of the isolated IgG antibodies under static conditions. Increasing inhibitor titers (0.5-3 BU/ml, end titer; assessed by FRETs-VWF73 assay) of the IgG antibodies from patient A (triangle) and patient B (circle) were assessed by a FRETs-VWF73-based Bethesda-like assay. Both preparations showed a comparable profile over the entire concentration range.

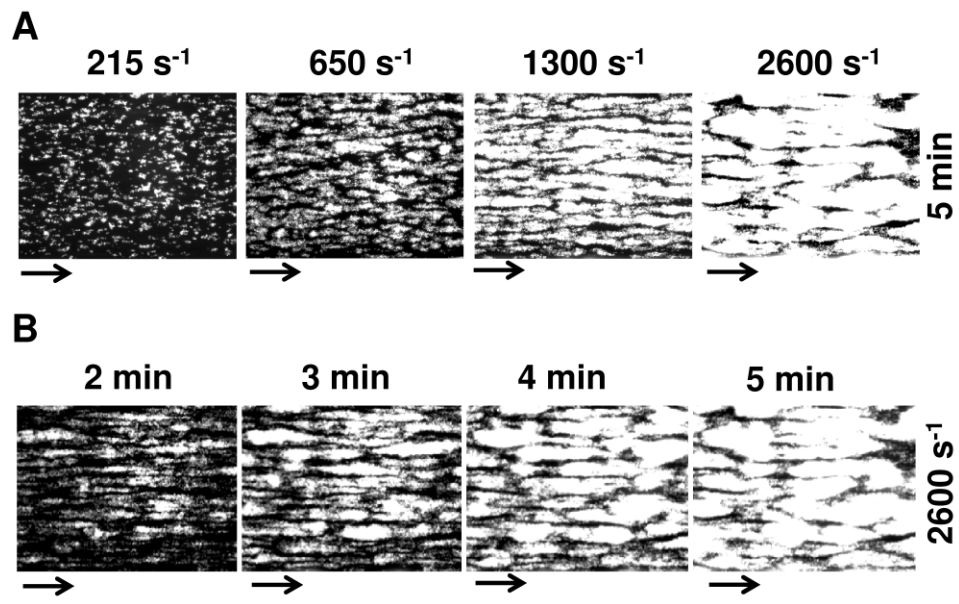


Figure 1.

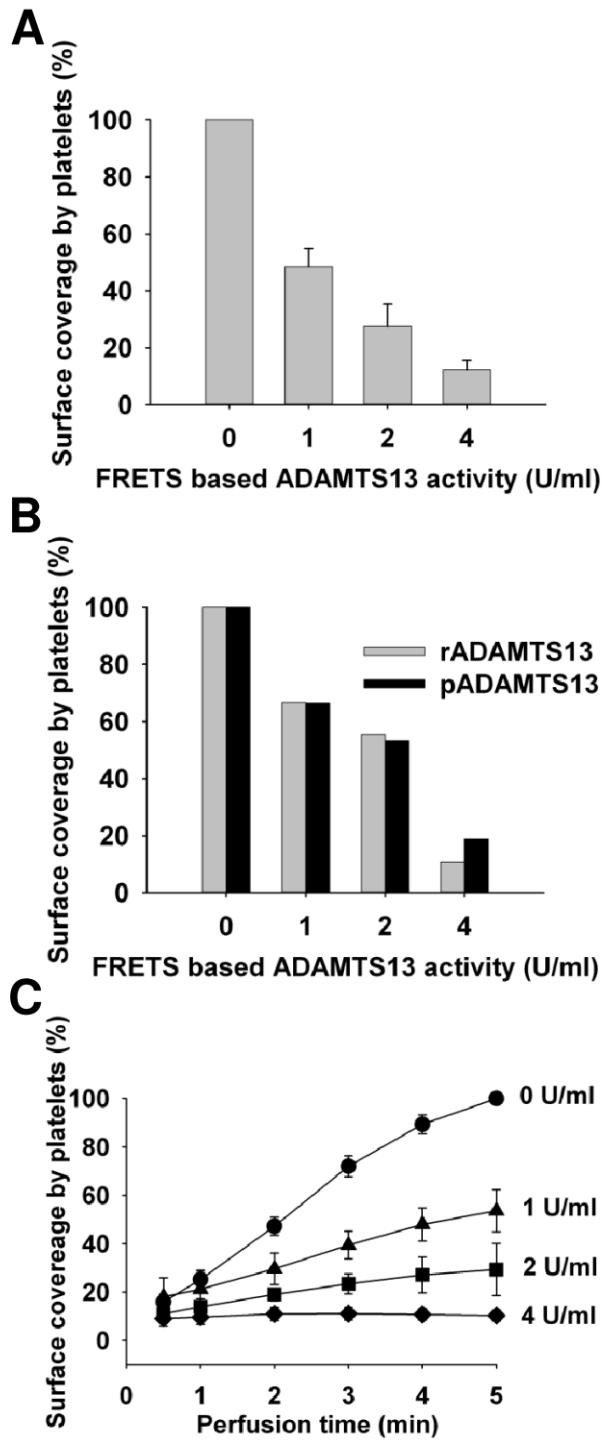


Figure 2.

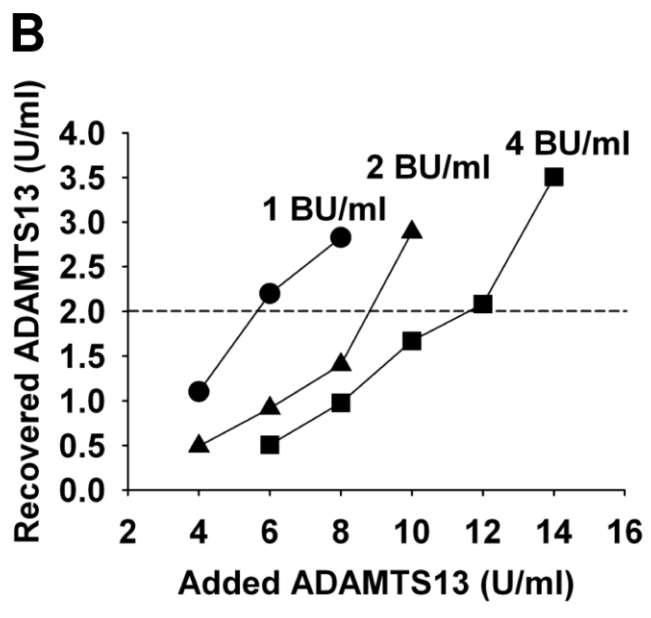
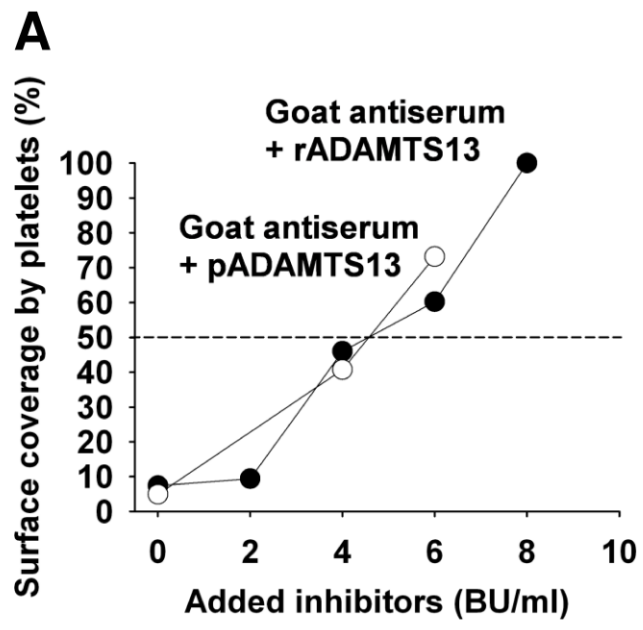


Figure 3.

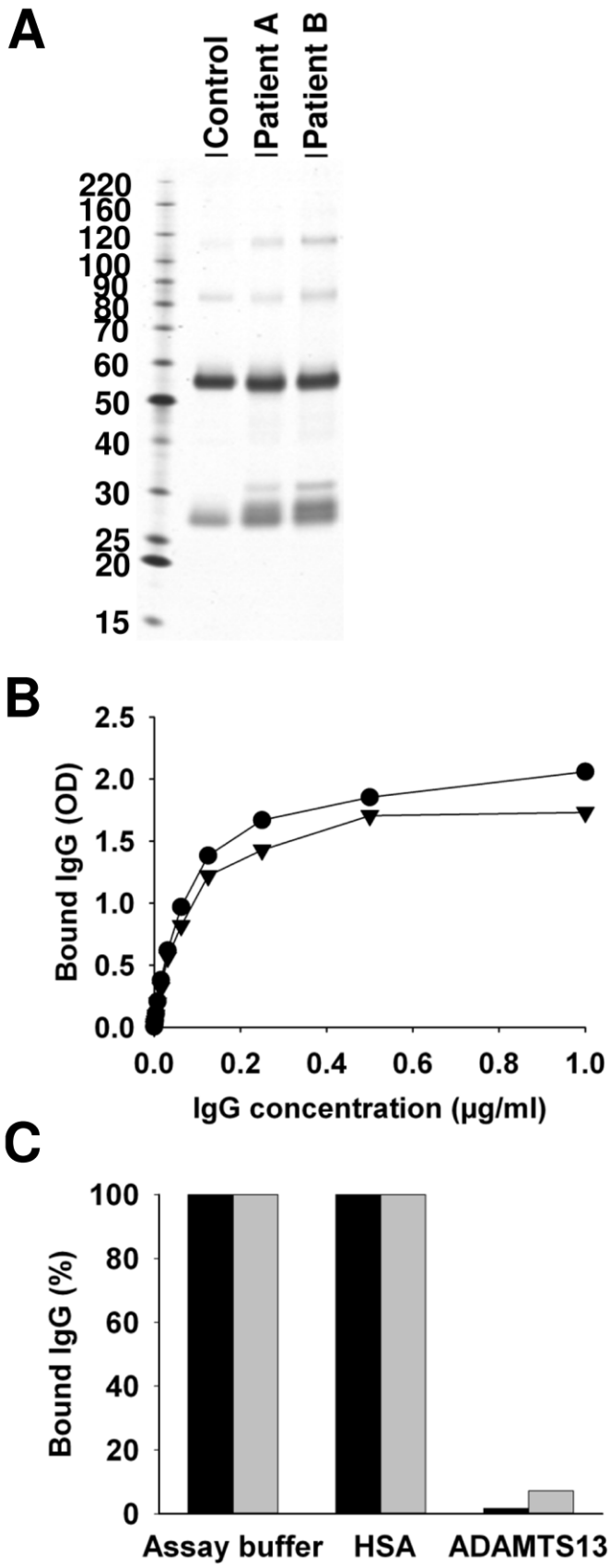


Figure 4.

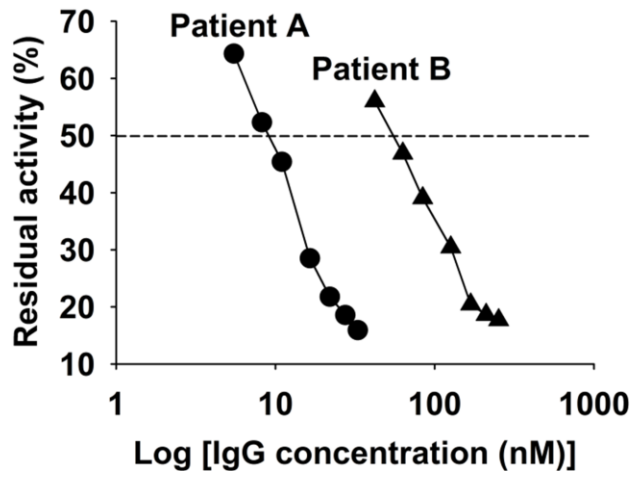


Figure 5.

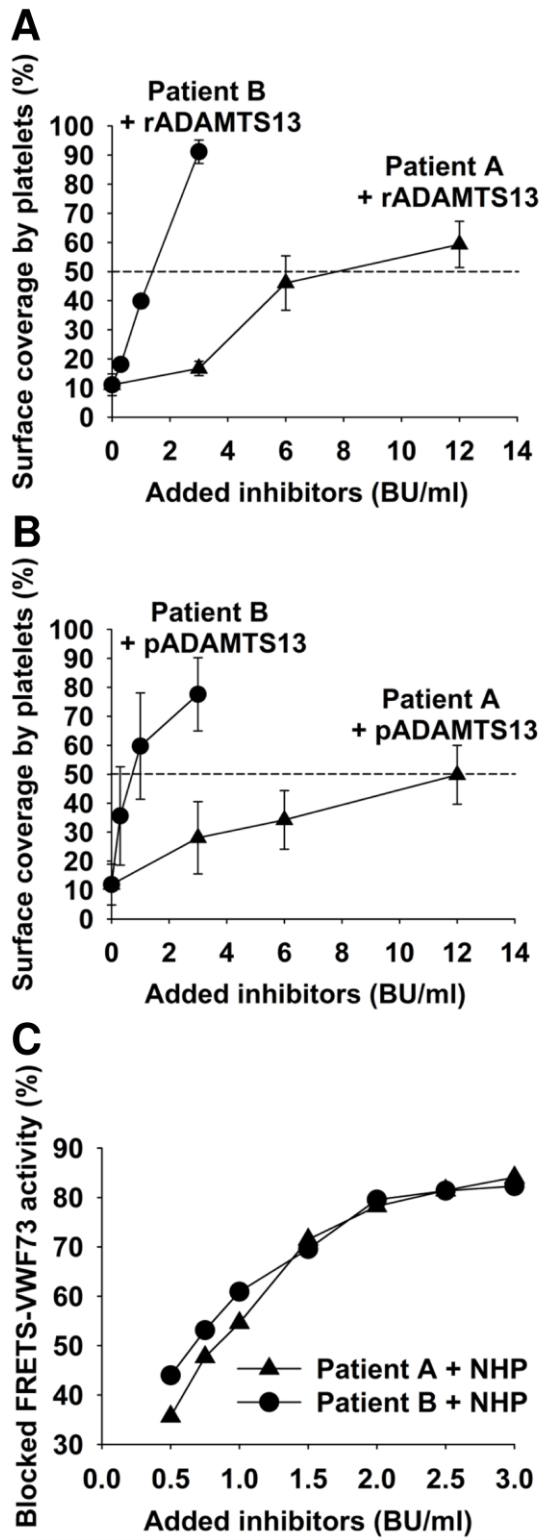
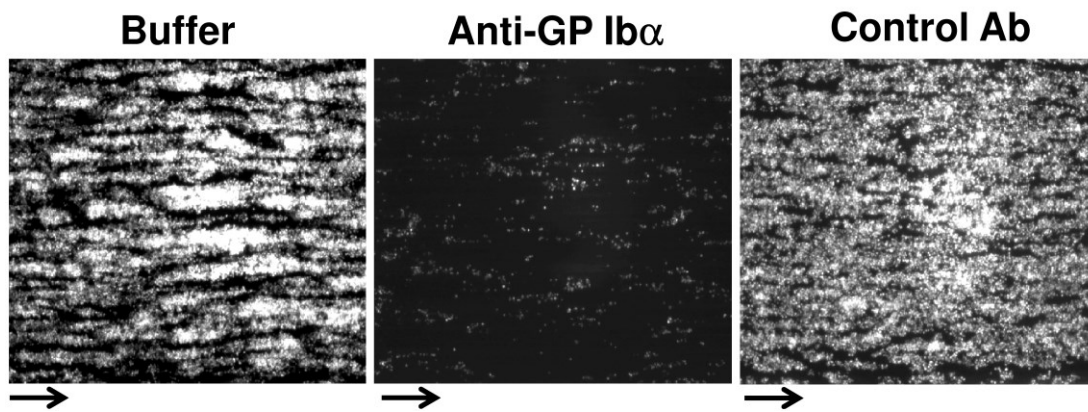


Figure 6.



**Supplementary Figure 1: Platelet aggregate formation is dependent on GP Ib $\alpha$ .** Cell suspensions of fluorescently labeled platelets ( $2.5 \times 10^8$  platelets/ml), erythrocytes (40% Hct) and rVWF (10  $\mu$ g/ml) were incubated for 15 min with a monoclonal antibody that blocks the interaction of platelet membrane glycoprotein GP Ib $\alpha$  with VWF (anti-GP Ib $\alpha$ ), a control monoclonal IgG1 antibody (Control Ab), or buffer and perfused over a surface coated with cellular fibronectin, collagen and rVWF at a wall shear rate of  $1500 \text{ s}^{-1}$ . This flow rate is above the  $1000 \text{ s}^{-1}$  threshold where platelet adhesion in human blood is entirely dependent on the VWF-GP Ib $\alpha$  interaction. Arrows indicate the direction of flow. Images selected were obtained after 5 min of perfusion and represent single frames from real time recordings. The anti-GP Ib $\alpha$  but not the control antibody significantly blocked the attachment of platelets to the channel and impaired the formation of aggregates, demonstrating that the adhesion of platelets to immobilized VWF was mediated by GP Ib $\alpha$ .

## REFERENCES

1. Zheng X, Chung D, Takayama TK et al. Structure of von Willebrand factor-cleaving protease (ADAMTS13), a metalloprotease involved in thrombotic thrombocytopenic purpura. *J Biol Chem* 2001; 276: 41059-41063.
2. Levy GG, Nichols WC, Lian EC et al. Mutations in a member of the ADAMTS gene family cause thrombotic thrombocytopenic purpura. *Nature* 2001; 413: 488-494.
3. Soejima K, Mimura N, Hirashima M et al. A novel human metalloprotease synthesized in the liver and secreted into the blood: possibly, the von Willebrand factor-cleaving protease? *J Biochem* 2001; 130: 475-480.
4. Dong JF, Moake JL, Nolasco L et al. ADAMTS-13 rapidly cleaves newly secreted ultralarge von Willebrand factor multimers on the endothelial surface under flowing conditions. *Blood* 2002; 100: 4033-4039.
5. Donadelli R, Orje JN, Capoferri C et al. Size regulation of von Willebrand factor-mediated platelet thrombi by ADAMTS13 in flowing blood. *Blood* 2006; 107: 1943-1950.
6. Moake JL. Thrombotic microangiopathies. *N Engl J Med* 2002; 347: 589-600.
7. Rieger M, Mannucci PM, Kremer Hovinga JA et al. ADAMTS13 autoantibodies in patients with thrombotic microangiopathies and other immunomediated diseases. *Blood* 2005; 106: 1262-1267.
8. Ferrari S, Scheiflinger F, Rieger M et al. Prognostic value of anti-ADAMTS 13 antibody features (Ig isotype, titer, and inhibitory effect) in a cohort of 35 adult French patients undergoing a first episode of thrombotic microangiopathy with undetectable ADAMTS 13 activity. *Blood* 2007; 109: 2815-2822.
9. Pos W, Sorvillo N, Fijnheer R et al. Residues Arg568 and Phe592 contribute to an antigenic surface for anti-ADAMTS13 antibodies in the spacer domain. *Haematologica* 2011; 96: 1670-1677.
10. Ferrari S, Mudde GC, Rieger M et al. IgG subclass distribution of anti-ADAMTS13 antibodies in patients with acquired thrombotic thrombocytopenic purpura. *J Thromb Haemost* 2009; 7: 1703-1710.
11. Scheiflinger F, Knobl P, Trattner B et al. Nonneutralizing IgM and IgG antibodies to von Willebrand factor-cleaving protease (ADAMTS-13) in a patient with thrombotic thrombocytopenic purpura. *Blood* 2003; 102: 3241-3243.
12. Kremer Hovinga JA, Vesely SK, Terrell DR et al. Survival and relapse in patients with thrombotic thrombocytopenic purpura. *Blood* 2010; 115: 1500-1511.
13. Klaus C, Plaimauer B, Studt JD et al. Epitope mapping of ADAMTS13 autoantibodies in acquired thrombotic thrombocytopenic purpura. *Blood* 2004; 103: 4514-4519.

14. Zheng XL, Wu HM, Shang D et al. Multiple domains of ADAMTS13 are targeted by autoantibodies against ADAMTS13 in patients with acquired idiopathic thrombotic thrombocytopenic purpura. *Haematologica* 2010; 95: 1555-1562.
15. Luken BM, Turenhout EA, Kaijen PH et al. Amino acid regions 572-579 and 657-666 of the spacer domain of ADAMTS13 provide a common antigenic core required for binding of antibodies in patients with acquired TTP. *Thromb Haemost* 2006; 96: 295-301.
16. Pos W, Crawley JT, Fijnheer R et al. An autoantibody epitope comprising residues R660, Y661, and Y665 in the ADAMTS13 spacer domain identifies a binding site for the A2 domain of VWF. *Blood* 2010; 115: 1640-1649.
17. Yamaguchi Y, Moriki T, Igari A et al. Epitope analysis of autoantibodies to ADAMTS13 in patients with acquired thrombotic thrombocytopenic purpura. *Thromb Res* 2011; 128: 169-173.
18. Luken BM, Kaijen PH, Turenhout EA et al. Multiple B-cell clones producing antibodies directed to the spacer and disintegrin/thrombospondin type-1 repeat 1 (TSP1) of ADAMTS13 in a patient with acquired thrombotic thrombocytopenic purpura. *J Thromb Haemost* 2006; 4: 2355-2364.
19. Grillberger R, Casina VC, Turecek PL et al. Anti-ADAMTS13 IgG autoantibodies present in healthy individuals share linear epitopes with those in patients with thrombotic thrombocytopenic purpura. *Haematologica* 2014; Feb 14. [Epub ahead of print]
20. Kokame K, Nobe Y, Kokubo Y et al. FRETs-VWF73, a first fluorogenic substrate for ADAMTS13 assay. *Br J Haematol* 2005; 129: 93-100.
21. Gerritsen HE, Turecek PL, Schwarz HP et al. Assay of von Willebrand factor (vWF)-cleaving protease based on decreased collagen binding affinity of degraded vWF: a tool for the diagnosis of thrombotic thrombocytopenic purpura (TTP). *Thromb Haemost* 1999; 82: 1386-1389.
22. Shenkman B, Inbal A, Tamarin I et al. Diagnosis of thrombotic thrombocytopenic purpura based on modulation by patient plasma of normal platelet adhesion under flow condition. *Br J Haematol* 2003; 120: 597-604.
23. Shim K, Anderson PJ, Tuley EA et al. Platelet-VWF complexes are preferred substrates of ADAMTS13 under fluid shear stress. *Blood* 2008; 111: 651-657.
24. Han Y, Xiao J, Falls E et al. A shear-based assay for assessing plasma ADAMTS13 activity and inhibitors in patients with thrombotic thrombocytopenic purpura. *Transfusion* 2011; 51: 1580-1591.
25. Froehlich-Zahnd R, George JN, Vesely SK et al. Evidence for a role of anti-ADAMTS13 autoantibodies despite normal ADAMTS13 activity in recurrent thrombotic thrombocytopenic purpura. *Haematologica* 2012; 97: 297-303.
26. Rieger M, Ferrari S, Kremer Hovinga JA et al. Relation between ADAMTS13 activity and ADAMTS13 antigen levels in healthy donors and patients with thrombotic microangiopathies (TMA). *Thromb Haemost* 2006; 95: 212-220.

27. Plaimauer B, Kremer Hovinga JA, Juno C et al. Recombinant ADAMTS13 normalizes von Willebrand factor-cleaving activity in plasma of acquired TTP patients by overriding inhibitory antibodies. *J Thromb Haemost* 2011; 9: 936-944.
28. Ferrari S, Palavra K, Gruber B et al. Persistence of circulating ADAMTS13-specific immune complexes in patients with acquired thrombotic thrombocytopenic purpura. *Haematologica* 2013; Nov 15. [Epub ahead of print]
29. Li Y, Choi H, Zhou Z et al. Covalent regulation of ULVWF string formation and elongation on endothelial cells under flow conditions. *J Thromb Haemost* 2008; 6: 1135-1143.
30. Nieswandt B and Watson SP. Platelet-collagen interaction: is GPVI the central receptor? *Blood* 2003; 102: 449-461.
31. Dong JF, Whitelock J, Bernardo A et al. Variations among normal individuals in the cleavage of endothelial-derived ultra-large von Willebrand factor under flow. *J Thromb Haemost* 2004; 2: 1460-1466.
32. Turner NA, Nolasco L, Ruggeri ZM et al. Endothelial cell ADAMTS-13 and VWF: production, release, and VWF string cleavage. *Blood* 2009; 114: 5102-5111.
33. Lotta LA, Valsecchi C, Pontiggia S et al. Measurement and prevalence of circulating ADAMTS13-specific immune complexes in autoimmune thrombotic thrombocytopenic purpura. *J Thromb Haemost* 2013;
34. Tao Z, Peng Y, Nolasco L et al. Recombinant CUB-1 domain polypeptide inhibits the cleavage of ULVWF strings by ADAMTS13 under flow conditions. *Blood* 2005; 106: 4139-4145.
35. Tao Z, Wang Y, Choi H et al. Cleavage of ultralarge multimers of von Willebrand factor by C-terminal-truncated mutants of ADAMTS-13 under flow. *Blood* 2005; 106: 141-143.
36. De MB, De Meyer SF, Feys HB et al. The distal carboxyterminal domains of murine ADAMTS13 influence proteolysis of platelet-decorated VWF strings in vivo. *J Thromb Haemost* 2010; 8: 2305-2312.
37. Muia J, Gao W, Haberichter SL et al. An optimized fluorogenic ADAMTS13 assay with increased sensitivity for the investigation of patients with thrombotic thrombocytopenic purpura. *J Thromb Haemost* 2013; 11: 1511-1518.